CORNELL AERONAUTICAL LABORATORY, INC.
BUFFALO, NEW YORK 14221

A DIGITAL COMPUTER SIMULATION OF BICYCLE DYNAMICS

CAL REPORT NO. YA-3063-K-1
JUNE 1971

Prepared For:

SCHWINN BICYCLE COMPANY
CHICAGO, ILLINOIS 60639

Prepared By: R. Douglas Roland, Jr.
R. Douglas Roland, Jr.
Assoc. Research Engineer
Vehicle Research Department

Approved By: F. Dell'Amico for K.D. Bird
K. D. Bird, Head
Vehicle Research Department

Daniel E. Massing
Daniel E. Massing
Engineering Assistant
Vehicle Research Department

FOREWORD

The work reported herein was performed by the Vehicle Research Department of the Cornell Aeronautical Laboratory, Inc. under Contract No. CC-182 for the Schwinn Bicycle Company. The period of performance was from 1 March 1971 to 31 May 1971. The dynamical analysis of the bicycle used in this program was developed at CAL prior to this program.

TABLE OF CONTENTS

TABLE OF CONTENTS (cont'd)

1.0 INTRODUCTION

The research discussed in this technical report includes the development, validation, and exercise of a free control bicycle-rider digital computer simulation program. This work is Phase I of a program whose overall objective is a comprehensive closed-loop simulation of a bicycle, stabilized and controlled by a path following rider logic model. This computer simulation program will be used for bicycle design and development with particular consideration being given to the effects of various design parameters and rider ability on bicycle maneuverability and stability.

This technical report includes the mathematical analysis of the bicycle which is the basis of the computer simulation program. The computer program, its required input, and various forms of output are described. An experimental program to obtain detailed measurements of the physical characteristics of a test bicycle and a typical rider is explained. This experimental program included the construction of an on-road bicycle tire tester and the measurement of the side force characteristics of two types of bicycle tires.

Full scale experiments with an instrumented bicycle were made to obtain time histories of motion variables from various maneuvers. A comparison of computer output with the data from the experimental tests was made to determine the validity of the simulation program.

A fifty-seven run simulation parameter study was performed as an exercise of the computer program and as a preliminary study of the effects of various design parameters on the free control stability of a riderless bicycle.

2.0 MATHEMATICAL ANALYSIS OF A BICYCLE AND RIDER

The mathematical analysis developed in this section is the basis of a digital computer simulation of a bicycle and rider. The bicycle-rider model is a system of three rigid masses with eight degrees of freedom: six rigid body degrees of freedom, a steer degree of freedom of the front wheel, and a rider roll degree of freedom. Included in the analysis are radial tire stiffness, tire side forces due to slip angle and inclination angle, the gyroscopic effects of the rotating wheels, as well as all inertial coupling terms between the rider, the front wheel and steering fork, and the rear wheel and frame.

2.1 Eight Degree of Freedom Bicycle Model

The bicycle-rider model is a system of three rigid masses with eight degrees of freedom. A rotating coordinate system (X, Y, Z) is defined as fixed in the rear wheel and frame structure and has three translational (u_o , v_o , w_o) and three rotational degrees (p, q, r) of freedom with respect to the space fixed coordinate system (X', Y', Z'), Figure 2.1. The front wheel and steering fork has a rotational degree of freedom ($\dot{\delta}$) about an inclined steer axis. The rider has a rotational degree of freedom ($\dot{\phi}_D$) about a horizontal roll axis, Figure 2.2. The origin of the vehicle coordinate system is at the intersection of the steering fork axis and an imaginary line which is perpendicular to the steering fork axis and passes through the rear wheel center. The X axis is along the longitudinal axis of the bicycle and is positive forward, the Y axis is positive to the right of the bicycle, and the Z axis is positive downward. The origin of the front fork coordinate system (X'', Y'', Z'') coincides with the origin of the vehicle coordinate system. The Z'' axis is coincident with the

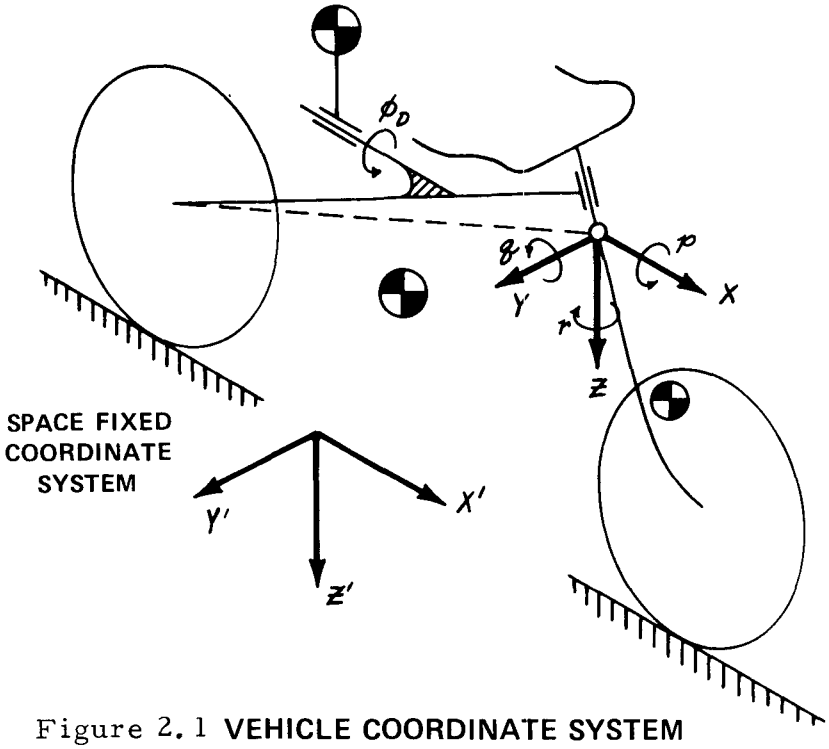

Figure 2.1 **VEHICLE COORDINATE SYSTEM**

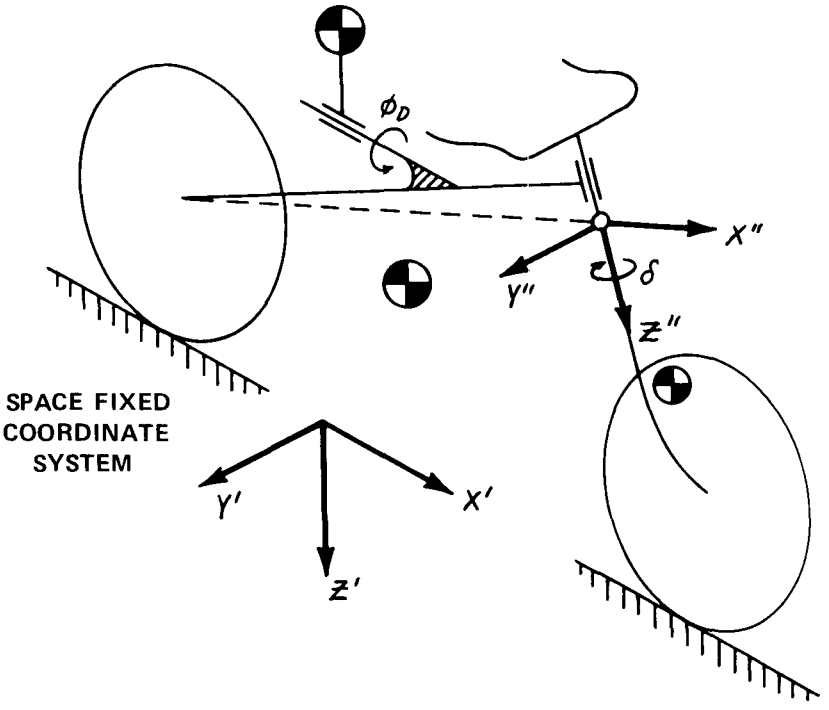

Figure 2.2 **FRONT FORK COORDINATE SYSTEM**

steering fork axis and positive downward, the X'' axis is positive forward, and the Y'' axis is positive to the right. The Y and Y'' axes are coincident at zero steer angle. The space fixed coordinate system is defined with the X'-Y' plane as the ground plane and with the Z' axis parallel to the gravity vector and positive downward.

The position of the bicycle in the space coordinate system is defined by the coordinates of the origin of the vehicle coordinate system (x_o' , y_o', z_o'). The angular orientation of the bicycle in the space coordinate system is defined by the Euler angles (ϕ, θ, ψ) about the X, Y, Z axes of the vehicle coordinate system taken in the order ψ, θ, ϕ .

The matrix for transforming coordinates in the vehicle coordinate system into coordinates in the space fixed coordinate system is given below.

$$[A] = \begin{bmatrix} \cos\theta\cos\psi & -\cos\phi\sin\psi+\sin\phi\sin\theta\cos\psi & \sin\phi\sin\psi+\cos\phi\sin\theta\cos\psi \\ \cos\theta\sin\psi & \cos\phi\cos\psi+\sin\phi\sin\theta\sin\psi & -\cos\psi\sin\phi+\cos\phi\sin\theta\sin\psi \\ -\sin\theta & \cos\theta\sin\phi & \cos\theta\cos\phi \end{bmatrix} \quad (2.1.1)$$

Figure 2.3 shows the parameters of the bicycle model which are included in the mathematical analysis. m_D, m_R, m_F are the masses of the rider, the rear wheel and frame, and the front wheel and steering fork assembly, respectively. The mass distribution of the bicycle is assumed to be symmetrical with respect to the vertical-longitudinal plane through its geometrical center. Thus the X-Y and Y-Z products of inertia

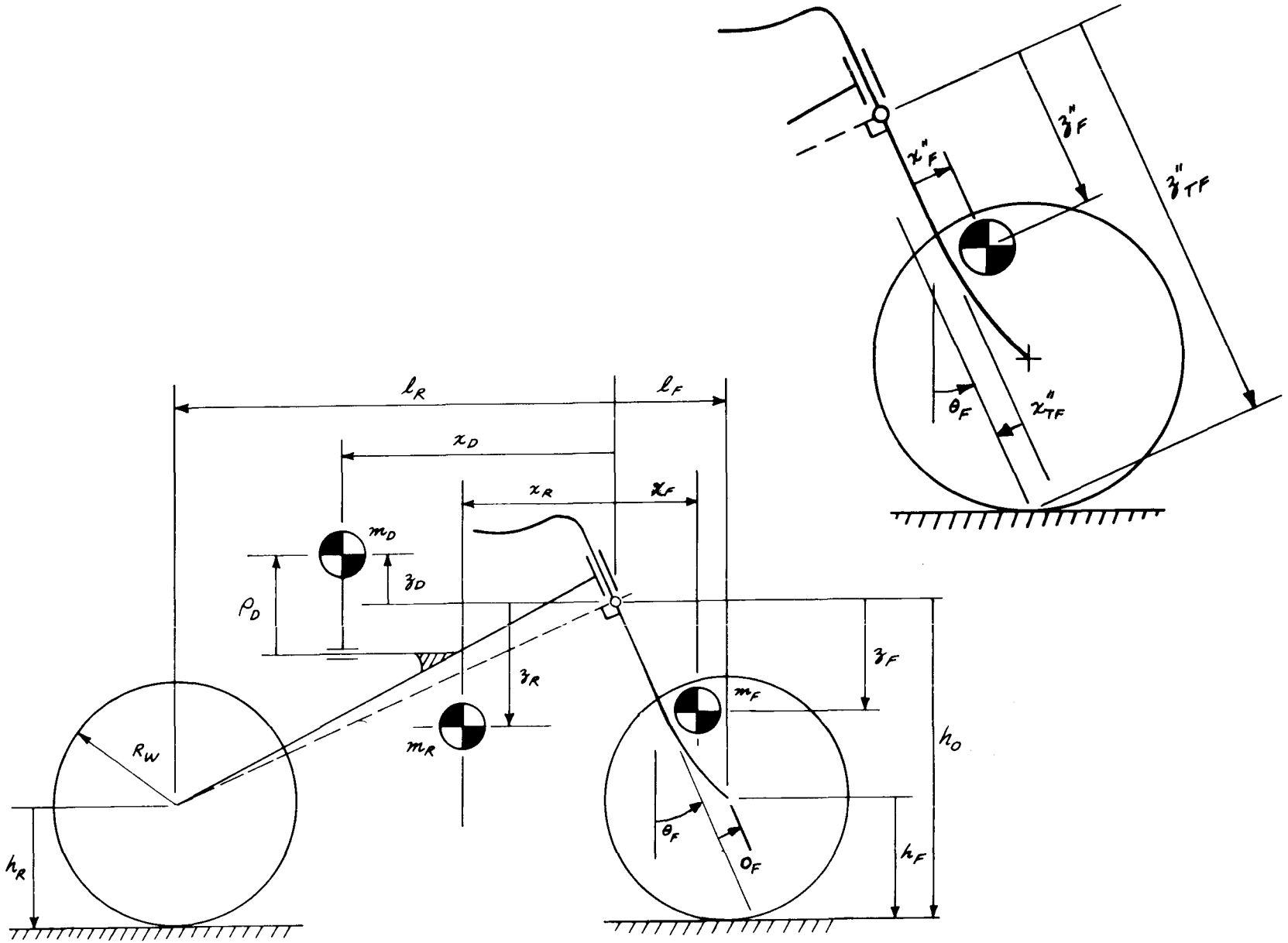

Figure 2.3 CHARACTERISTIC DIMENSIONS OF BICYCLE MODEL

of each rigid mass are zero. Θ_F is the caster angle of the steer axis. δ is the steer angle of the front wheel about the inclined steer axis. ω_F and ω_R are the spin velocities of the front and rear wheels. A no-slip condition is assumed between the wheels and the ground, therefore, the wheel spin velocities are equal to the forward velocity of the bicycle divided by the respective wheel rolling radius.

2.2 Rotational Degrees of Freedom of Wheels

The moment on the front wheel which reacts the gyroscopic effect of the spinning wheel is given below in matrix form. It is assumed that the moment of inertia about a diameter through the wheel is equal to one half the moment of inertia about the spin axis, I_{WF}.

$$\begin{bmatrix} N''_{XWF} \\ N''_{YWF} \\ N''_{ZWF} \end{bmatrix} = \begin{bmatrix} p'' \\ q'' \\ r'' + \dot{\delta} \end{bmatrix} \times \left(\begin{bmatrix} I_{WF}/2 & 0 & 0 \\ 0 & I_{WF} & 0 \\ 0 & 0 & I_{WF}/2 \end{bmatrix} \begin{bmatrix} p'' \\ q'' + \omega_F \\ r'' + \dot{\delta} \end{bmatrix} \right) \qquad (2.2.1)$$

where

$N''_{XWF}, N''_{YWF}, N''_{ZWF}$ are the X'', Y'', Z'' components of the moment on the front wheel which reacts the gyroscopic effect.

p'', q'', r'' are the X'', Y'', Z'' components of angular velocity vector of the vehicle coordinate system.

$$\begin{bmatrix} p'' \\ q'' \\ r'' \end{bmatrix} = [S]^T \begin{bmatrix} p \\ q \\ r \end{bmatrix} \qquad (2.2.2)$$

where $[S]$ is the transformation matrix from the front fork coordinate system to the vehicle coordinate system.

$$[S] = \left[\begin{array}{c|c|c} \cos\theta_F \cos\delta & -\cos\theta_F \sin\delta & \sin\theta_F \\ \hline \sin\delta & \cos\delta & 0 \\ \hline -\sin\theta_F \cos\delta & \sin\theta_F \sin\delta & \cos\theta_F \end{array}\right] \qquad (2.2.3)$$

Assuming that the velocity q'' is negligible compared to the wheel spin velocity, ω_F, the above equation reduces to the following.

$$N''_{xWF} = -(r'' + \dot{\delta})\,\omega_F\, I_{WF} \qquad (2.2.4)$$

$$N''_{yWF} = 0 \qquad (2.2.5)$$

$$N''_{zWF} = p''\,\omega_F\, I_{WF} \qquad (2.2.6)$$

The moment on the rear wheel which reacts the gyroscopic effect of the spinning wheel is given below in matrix form. It is assumed that the moment of inertia about a diameter through the wheel is equal to one half the moment of inertia about the spin axis, .

$$\begin{bmatrix} N_{xWR} \\ N_{yWR} \\ N_{zWR} \end{bmatrix} \begin{bmatrix} p \\ q \\ r \end{bmatrix} X \left(\begin{bmatrix} I_{WR}/2 & 0 & 0 \\ 0 & I_{WR} & 0 \\ 0 & 0 & I_{WR}/2 \end{bmatrix} \begin{bmatrix} p \\ q+\omega_R \\ r \end{bmatrix} \right) \qquad (2.2.7)$$

where

$N_{xWR}, N_{yWR}, N_{zWR}$ are the X, Y, Z components of the moment on the rear wheel which reacts the gyroscopic effect.

ω_R is the spin velocity of the rear wheel (assumed to be the forward velocity of the bicycle divided by the rolling radius of the wheel).

I_{WR} is the moment of inertia of the rear wheel about its spin axis.

Assuming that the pitch velocity, $\dot{\theta}''$, is negligible compared to the wheel spin velocity, ω_R, the above equation reduces to the following.

$$N_{XWR} = -r\omega_R I_{WR} \tag{2.2.8}$$

$$N_{YWR} = 0 \tag{2.2.9}$$

$$N_{ZWR} = p\omega_R I_{WR} \tag{2.2.10}$$

2.3 Rotational Degree of Freedom of Front Wheel Fork and Handlebar Assembly

The force balance equations for the front wheel and steering fork in the X, Y, Z directions are given below.

$$m_F \dot{u}_F = F_{XTF} + F_{XF} - m_F g \sin\theta \tag{2.3.1}$$

$$m_F \dot{v}_F = F_{YTF} + F_{YF} + m_F g \cos\theta \sin\phi \tag{2.3.2}$$

$$m_F \dot{w}_F = F_{ZTF} + F_{ZF} + m_F g \cos\theta \cos\phi \tag{2.3.3}$$

where

$F_{XTF}, F_{YTF}, F_{ZTF}$ are the X, Y, Z components of the tire force acting on the front wheel at the ground contact point.

F_{XF}, F_{YF}, F_{ZF} are the X, Y, Z components of the reaction force acting on the steering fork at the origin of the vehicle coordinate system.

The X, Y, Z components of the inertial acceleration of the c. g. of the front wheel fork and handlebar assembly are given below.

$$\dot{u}_F = \dot{u}_0 + q w_0 - r v_0 + z_F \dot{q} - y_F (\dot{r} + \ddot{\delta} \cos\theta_F) - x_F (q^2 + r^2)$$
$$+ y_F p q + z_F p r + z_F \cos\theta_F p \dot{\delta} + y_F \sin\theta_F q \dot{\delta} \qquad (2.3.4)$$
$$- (2 x_F \cos\theta_F - z_F \sin\theta_F) r \dot{\delta} - (x_F \cos^2\theta_F - z_F \sin\theta_F \cos\theta_F) \dot{\delta}^2$$

$$\dot{v}_F = \dot{v}_0 - p w_0 + r u_0 - z_F (\dot{p} + \ddot{\delta} \sin\theta_F) + x_F (\dot{r} + \ddot{\delta} \cos\theta_F) - y_F (p^2 + r^2)$$
$$+ x_F p q - y_F \sin\theta_F p \dot{\delta} + z_F q r + (x_F \sin\theta_F + z_F \cos\theta_F) q \dot{\delta} \qquad (2.3.5)$$
$$- 2 y_F \cos\theta_F r \dot{\delta} + (x_F \sin\theta_F \cos\theta_F - z_F \sin^2\theta_F) \dot{\delta}^2$$

$$\dot{w}_F = \dot{w}_0 + p v_0 - q u_0 + y_F (\dot{p} + \ddot{\delta} \sin\theta_F) - x_F \dot{q} - z_F (p^2 + q^2)$$
$$+ x_F p r + (x_F \cos\theta_F - 2 z_F \sin\theta_F) p \dot{\delta} + y_F \cos\theta_F q \dot{\delta} \qquad (2.3.6)$$
$$+ x_F \sin\theta_F r \dot{\delta} + (x_F \sin\theta_F \cos\theta_F - z_F \sin^2\theta_F) \dot{\delta}^2$$

where:

$$\begin{bmatrix} x_F \\ y_F \\ z_F \end{bmatrix} = [S] \begin{bmatrix} x_F'' \\ 0 \\ z_F'' \end{bmatrix} \qquad (2.3.7)$$

Thus the reaction forces acting on the front wheel fork and handlebar assembly are:

$$F_{XF} = m_F (\dot{u}_0 + z_F \dot{q} - y_F \dot{r} - y_F \cos\theta_F \ddot{\delta}) - \gamma_{12} - F_{XTF} \qquad (2.3.8)$$

$$F_{YF} = m_F (\dot{v}_0 - z_F \dot{p} + x_F \dot{r} + x_F'' \cos\delta \ddot{\delta}) - \gamma_{22} - F_{YTF} \qquad (2.3.9)$$

$$F_{ZF} = m_F (\dot{w}_0 + y_F \dot{p} - x_F \dot{q} + y_F \sin\theta_F \ddot{\delta}) - \gamma_{32} - F_{ZTF} \qquad (2.3.10)$$

where:

$$\gamma_{12} = m_F(-q w_0 + r v_0 - g \sin\theta + x_F\{q^2+r^2\} - y_F pq - z_F pr - z_F \cos\theta_F p\dot{\delta} - y_F \sin\theta_F q\dot{\delta} + \{x_F \cos\theta_F + x_F'' \cos\delta\} r\dot{\delta} + x_F'' \cos\theta_F \cos\delta\,\dot{\delta}^2) \quad (2.3.11)$$

$$\gamma_{22} = m_F(p w_0 - r u_0 + g \cos\theta \sin\phi + y_F\{p^2+r^2\} - x_F pq + y_F \sin\theta_F p\dot{\delta} - z_F qr - z_F'' q\dot{\delta} + 2 y_F \cos\theta_F r\dot{\delta} + y_F \cos^2\theta_F \dot{\delta}^2) \quad (2.3.12)$$

$$\gamma_{32} = m_F(-p v_0 + q u_0 + g \cos\theta \cos\phi + z_F\{p^2+q^2\} - x_F pr - \{x_F'' \cos\delta - z_F \sin\theta_F\} p\dot{\delta} - y_F qr - y_F \cos\theta_F q\dot{\delta} - x_F \sin\theta_F r\dot{\delta} - x_F'' \sin\theta_F \cos\delta\,\dot{\delta}^2) \quad (2.3.13)$$

The moment balance equation for the front wheel fork and handlebar assembly about the X'', Y'', Z'' axes of the front fork coordinate system is given below in matrix form.

$$[I_F''] = \begin{bmatrix} \dot{p}'' \\ \dot{q}'' \\ \dot{r}''+\ddot{\delta} \end{bmatrix} + \begin{bmatrix} p'' \\ q'' \\ r''+\dot{\delta} \end{bmatrix} \times \left([I_F''] \begin{bmatrix} p'' \\ q'' \\ r''+\dot{\delta} \end{bmatrix} \right) = [N_F''] \quad (2.3.14)$$

where

$$\begin{bmatrix} \dot{p}'' \\ \dot{q}'' \\ \dot{r}'' \end{bmatrix} = [S]^T \begin{bmatrix} \dot{p} \\ \dot{q} \\ \dot{r} \end{bmatrix} \quad (2.3.15)$$

$[I_F'']$ is the inertia tensor of the front wheel fork and handlebar assembly about its c.g. along a set of axes parallel to the X'', Y'', Z'' axes of the front fork coordinate system.

$$\left[I''_F\right] = \begin{bmatrix} I''_{FX} & 0 & -I''_{FXZ} \\ 0 & I''_{FY} & 0 \\ -I''_{FXZ} & 0 & I''_{FZ} \end{bmatrix} \qquad (2.3.16)$$

$\left[N''_F\right]$ is the moment acting on the front fork and handlebar assembly about a set of axes through its c. g. and parallel to the X'', Y'', Z'' axes of the front fork coordinate system.

$$\left[N''_F\right] = \begin{bmatrix} N''_{XF} - N''_{XWF} + F''_{YF}\,z''_F - F''_{YTF}(z''_{TF} - z''_F) + F''_{ZTF}\,y''_{TF} \\ N''_{YF} - N''_{YWF} - F''_{XF}\,z''_F + F''_{ZF}\,x''_F + F''_{XTF}(z''_{TF} - z''_F) - F''_{ZTF}(x''_{TF} - x''_F) \\ N''_{ZF} - N''_{ZWF} - F''_{YF}\,x''_F - F''_{XTF}\,y''_{TF} + F''_{YTF}(x''_{TF} - x''_F) \end{bmatrix} \qquad (2.3.17)$$

where

$x''_{TF}, y''_{TF}, z''_{TF}$ are the X'', Y'', Z'' coordinates of the tire-ground contact point.

N''_{XF}, N''_{YF} are the X'' and Y'' components of the reaction moment on the front wheel fork and handlebar assembly at the origin of the coordinate system.

The first two rows of the expansion of equation (2.3.14) are given below.

$$N''_{XF} = \dot{p}''I''_{FX} - (\dot{r}'' + \ddot{\delta})I''_{FXZ} - p''q''I''_{FXZ} - q''(r'' + \dot{\delta})(I''_{FY} - I''_{FZ}) + N''_{XWF} - F''_{YF}\,z''_F + F''_{YTF}(z''_{TF} - z''_F) - F''_{ZTF}\,y''_{TF} \qquad (2.3.18)$$

$$N''_{YF} = \dot{q}''I''_{FY} + \{p''^2 - (r'' + \dot{\delta})^2\}I''_{FXZ} + p''(r'' + \dot{\delta})(I''_{FX} - I''_{FZ}) + N''_{YWF} + F''_{XF}\,z''_F - F''_{ZF}\,x''_F - F''_{XTF}(z''_{TF} - z''_F) + F''_{ZTF}(x''_{TF} - x''_F) \qquad (2.3.19)$$

The third row of the expansion of equation (2.3.14) is the equation of motion for rotation of the front wheel fork and handlebar assembly about the steer axis.

$$-\dot{p}'' I''_{FXZ} + (\dot{r}'' + \ddot{\delta}) I''_{FZ} + q''(r'' + \dot{\delta}) I''_{FXZ} - p'' q'' (I''_{FX} - I''_{FY}) = N''_{ZF} - N''_{ZWF} - F''_{YF} x''_F - F''_{XTF} y''_{TF} + F''_{YTF} (x''_{TF} - x''_F) \quad (2.3.20)$$

or

$$-y_F \cos\theta_F m_F \dot{w}_0 + x''_F \cos\delta\, m_F \dot{v}_0 + y_F \sin\theta_F m_F \dot{w}_0 + \{\sin\theta_F (I''_{FZ} + x''^2_F m_F) - \cos\theta_F \cos\delta (I''_{FXZ} + x''_F z''_F m_F)\} \dot{p} - \sin\delta (I''_{FXZ} + x''_F z''_F m_F) \dot{q} + \{\cos\theta_F (I''_{FZ} + x''^2_F m_F) + \sin\theta_F \cos\delta (I''_{FXZ} + x''_F z''_F m_F)\} \dot{r} + (I''_{FZ} + x''^2_F m_F) \ddot{\delta} = q''(r'' + \dot{\delta}) I''_{FXZ} - p'' q'' (I''_{FX} - I''_{FY}) - x''_F (\cos\theta_F \sin\delta\, \gamma_{12} - \cos\delta\, \gamma_{22} - \sin\theta_F \sin\delta\, \gamma_{32}) + N''_{ZF} - N''_{ZWF} - F''_{XTF} y''_{TF} + F''_{YTF} (x''_{TF} - x''_F) \quad (2.3.21)$$

The X, Y, Z components of the reaction moment on the front wheel fork and handlebar assembly at the origin of the coordinate system are found below.

$$\begin{bmatrix} N_{XF} \\ N_{YF} \\ N_{ZF} \end{bmatrix} = [S] \begin{bmatrix} N''_{XF} \\ N''_{YF} \\ N''_{ZF} \end{bmatrix} \quad (2.3.22)$$

$$
\begin{aligned}
N_{XF} = {} & \sin\theta_F \cos\theta_F y_F m_F \ddot{u}_o - \cos\theta_F z_F'' m_F \ddot{w}_o + \cos^2\theta_F y_F m_F \ddot{w}_o \\
& + \left(\left\{\cos\theta_F z_F'' y_F + \cos^2\theta_F y_F^2\right\} m_F + \cos^2\theta_F \left\{\cos^2\delta I_{FX}'' + \sin^2\delta I_{FY}''\right\}\right. \\
& \left. - \sin\theta_F \cos\theta_F \cos\delta I_{FXZ}''\right)\dot{p} + \left(\left\{\sin\theta_F \cos\theta_F z_F - \cos^2\theta_F x_F\right\} y_F m_F\right. \\
& \left. - \cos\theta_F z_F'' x_F m_F + \cos\theta_F \sin\delta \cos\delta \left\{I_{FX}'' - I_{FY}''\right\}\right)\dot{q} - \left(\sin\theta_F \cos\theta_F\right. \\
& \left. y_F^2 m_F + \sin\theta_F \cos\theta_F \left\{\cos^2\delta I_{FX}'' + \sin^2\delta I_{FY}''\right\} + \cos^2\theta_F \cos\delta I_{FXZ}''\right)\dot{r} \qquad (2.3.23) \\
& - \cos\theta_F \cos\delta \left(x_F'' z_F'' m_F + I_{FXZ}''\right)\ddot{\delta} - \cos\theta_F \cos\delta \left(p'' q'' I_{FXZ}''\right. \\
& \left. + q'' \left\{r'' + \dot{\delta}\right\}\left\{I_{FY}'' - I_{FZ}''\right\} + \left\{r'' + \dot{\delta}\right\} \omega_F I_{WF}\right) - \cos\theta_F \sin\delta \left(\left\{p''^2\right.\right. \\
& \left.\left. - \left[r'' + \dot{\delta}\right]^2\right\} I_{FXZ}'' + p'' \left\{r'' + \dot{\delta}\right\}\left\{I_{FX}'' - I_{FZ}''\right\}\right) + \cos\theta_F z_F'' \gamma_{22} \\
& - \cos\theta_F y_F \left(\sin\theta_F \gamma_{12} + \cos\theta_F \gamma_{32}\right) + \sin\theta_F N_{ZF}''
\end{aligned}
$$

$$
\begin{aligned}
N_{YF} = {} & \left(\cos\theta_F z_F'' - \sin\theta_F \cos\delta x_F''\right) m_F \ddot{u}_o - \left(\sin\theta_F z_F'' + \cos\theta_F \cos\delta x_F''\right) m_F \ddot{w}_o \\
& - \left(\left\{\sin\theta_F z_F'' + \cos\theta_F \cos\delta x_F''\right\} y_F m_F - \cos\theta_F \sin\delta \cos\delta \left\{I_{FX}'' - I_{FY}''\right\}\right. \\
& \left. + \sin\theta_F \sin\delta I_{FXZ}''\right)\dot{p} + \left(\left\{\sin\theta_F x_F + \cos\theta_F y_F\right\} z_F'' m_F - \left\{\sin\theta_F y_F\right.\right. \\
& \left.\left. - \cos\theta_F x_F\right\} \cos\delta x_F'' m_F + \sin^2\delta I_{FX}'' + \cos^2\delta I_{FY}''\right)\dot{q} + \left(\left\{\sin\theta_F\right.\right. \\
& \left.\left. \cos\delta x_F'' - \cos\theta_F z_F''\right\} y_F m_F - \sin\theta_F \sin\delta \cos\delta \left\{I_{FX}'' - I_{FY}''\right\} - \cos\theta_F\right. \qquad (2.3.24) \\
& \left. \sin\delta I_{FXZ}''\right)\dot{r} - \left(z_F'' y_F m_F + \sin\delta I_{FXZ}''\right)\ddot{\delta} - \sin\delta \left(p'' q'' I_{FXZ}''\right. \\
& \left. + q'' \left\{r'' + \dot{\delta}\right\}\left\{I_{FY}'' - I_{FZ}''\right\} + \left\{r'' + \dot{\delta}\right\} \omega_F I_{WF}\right) + \cos\delta \left(\left\{p''^2 - \left[r'' + \dot{\delta}\right]^2\right\} I_{FXZ}''\right. \\
& \left. + p'' \left\{r'' + \dot{\delta}\right\}\left\{I_{FX}'' - I_{FZ}''\right\}\right) + \left(\sin\theta_F \cos\delta x_F'' - \cos\theta_F z_F''\right) \gamma_{12} \\
& + \left(\sin\theta_F z_F'' + \cos\theta_F \cos\delta x_F''\right) \gamma_{32}
\end{aligned}
$$

$$
\begin{aligned}
N_{ZF} = {} & -\sin^2\theta_F y_F m_F \ddot{u}_o + \sin\theta_F z_F'' m_F \ddot{v}_o - \sin\theta_F \cos\theta_F y_F m_F \ddot{w}_o \\
& - \left(\sin\theta_F z_F'' z_F m_F + \sin\theta_F \cos\theta_F y_F m_F + \sin\theta_F \cos\theta_F \left\{\cos^2\delta I_{FX}''\right.\right. \\
& \left.\left. + \sin^2\delta I_{FY}''\right\} - \sin^2\theta_F \cos\delta I_{FXZ}''\right)\dot{p} - \left(\sin\theta_F \left\{\sin\theta_F z_F - \cos\theta_F\right.\right. \\
& \left.\left. x_F\right\} y_F m_F + \sin\theta_F \sin\delta \cos\delta \left\{I_{FX}'' - I_{FY}''\right\}\right)\dot{q} + \left(\left\{\sin\theta_F z_F'' x_F\right.\right. \qquad (2.3.25) \\
& \left.\left. + \sin^2\theta_F y_F^2\right\} m_F + \sin^2\theta_F \left\{\cos^2\delta I_{FX}'' + \sin^2\delta I_{FY}''\right\} + \sin\theta_F \cos\theta_F\right. \\
& \left. \cos\delta I_{FXZ}''\right)\dot{r} + \sin\theta_F \cos\delta \left(z_F'' x_F'' m_F + I_{FXZ}''\right)\ddot{\delta} + \sin\theta_F \cos\delta \\
& \left(p'' q'' I_{FXZ}'' + q'' \left\{r'' + \dot{\delta}\right\}\left\{I_{FX}'' - I_{FZ}''\right\} + \left\{r'' + \dot{\delta}\right\} \omega_F I_{WF}\right) + \sin\theta_F \\
& \sin\delta \left(\left\{p''^2 - \left[r'' + \dot{\delta}\right]^2\right\} I_{FXZ}'' + p'' \left\{r'' + \dot{\delta}\right\}\left\{I_{FX}'' - I_{FZ}''\right\}\right) - \sin\theta_F \\
& z_F'' \gamma_{22} + \sin\theta_F y_F \left(\sin\theta_F \gamma_{12} + \cos\theta_F \gamma_{32}\right) + \cos\theta_F N_{ZF}''
\end{aligned}
$$

2.4 Rotational Degree of Freedom of the Rider

The force balance equations for the rider in the X, Y, Z directions are given below.

$$m_D \dot{u}_D = F_{xD} - m_D g \sin\theta \tag{2.4.1}$$

$$m_D \dot{v}_D = F_{yD} + m_D g \cos\theta \sin\phi \tag{2.4.2}$$

$$m_D \dot{w}_D = F_{zD} + m_D g \cos\theta \cos\phi \tag{2.4.3}$$

where

F_{xD}, F_{yD}, F_{zD} are the X, Y, Z components of the reaction force acting on the rider at the rider roll center.

The X, Y, Z components of the inertial acceleration of the c.g. of the rider are given below.

$$\dot{u}_D = \dot{u}_o + q w_o - r v_o + z_D \dot{q} - y_D \dot{r} - x_D (q^2 + r^2) - y_D p q + z_D p r + 2 y_D q \dot{\phi}_D + 2 \rho_D \cos\phi_D r \dot{\phi}_D \tag{2.4.4}$$

$$\dot{v}_D = \dot{v}_o - p w_o + r u_o - z_D \dot{p} + x_D \dot{r} - \rho_D \cos\phi_D \ddot{\phi}_D - y_D (p^2 + r^2) + x_D p q - 2 y_D p \dot{\phi}_D + z_D q r - y_D \dot{\phi}_D^2 \tag{2.4.5}$$

$$\dot{w}_D = \dot{w}_o + p v_o - q u_o - y_D \dot{p} - x_D \dot{q} + y_D \ddot{\phi}_D - z_D (p^2 + q^2) + x_D p r - 2 \rho_D \cos\phi_D p \dot{\phi}_D + y_D q r - \rho_D \cos\phi_D \dot{\phi}_D^2 \tag{2.4.6}$$

where:

$$y_D = -\rho_D \sin\phi_D \tag{2.4.7}$$

$$z_D = z'_D - \rho_D (1 - \cos\phi_D) \tag{2.4.8}$$

Thus the reaction forces acting on the rider may be written as follows.

$$F_{xD} = m_D(\dot{w}_o + \dot{q}\,z_D + \dot{r}\,\rho_D\phi_D) - \gamma_{13} \qquad (2.4.9)$$

$$F_{yD} = m_D(\dot{v}_o - \dot{p}\,z_D + \dot{r}\,x_D - \ddot{\phi}_D\rho_D) - \gamma_{23} \qquad (2.4.10)$$

$$F_{zD} = m_D(\dot{w}_o - \dot{p}\,\rho_D\phi_D - \dot{q}\,x_D - \ddot{\phi}_D\rho_D\phi_D) - \gamma_{33} \qquad (2.4.11)$$

where:

$$\gamma_{13} = m_D(-q\,w_o + r\,v_o - g\sin\theta + x_D\{q^2+r^2\} + y_D\,pq - z_D\,pr + y_D\,q\,\phi_D - 2\rho_D\cos\phi_D\,r\,\dot{\phi}_D) \qquad (2.4.12)$$

$$\gamma_{23} = m_D(p\,w_o - r\,u_o + g\cos\theta\sin\phi - y_D\{p^2+r^2\} - x_D\,pq + 2\,y_D\,p\,\phi_D - z_D\,qr + y_D\,\dot{\phi}_D^2) \qquad (2.4.13)$$

$$\gamma_{33} = m_D(-p\,v_o + q\,u_o + g\cos\theta\cos\phi + z_D\{p^2+q^2\} - x_D\,pr + 2\rho_D\cos\phi_D\,p\,\dot{\phi}_D - y_D\,qr + \rho_D\cos\phi_D\,\dot{\phi}_D^2) \qquad (2.4.14)$$

The moment balance equation for the rider about the axes of the X, Y, Z axes of the vehicle coordinate system are given below in matrix form.

$$[I_D]\begin{bmatrix}\dot{p}+\ddot{\phi}_D\\ \dot{q}\\ \dot{r}\end{bmatrix} + \left[\frac{\partial I_D}{\partial t}\right]\begin{bmatrix}p+\dot{\phi}_D\\ q\\ r\end{bmatrix} + \begin{bmatrix}p\\ q\\ r\end{bmatrix} \times \left([I_D]\begin{bmatrix}p+\dot{\phi}_D\\ q\\ r\end{bmatrix}\right) = [N_D] \qquad (2.4.15)$$

where $[I_D]$ is the inertia tensor of the rider through the rider c.g. with respect to the X, Y, Z axes of the vehicle coordinate system.

$$[I_D] = [D][I_D'][D]^T \qquad (2.4.16)$$

$[D]$ is the transformation matrix from the rider coordinate system to the vehicle coordinate system.

$$[D] = \begin{bmatrix} 1 & 0 & 0 \\ 0 & \cos\phi_D & -\sin\phi_D \\ 0 & \sin\phi_D & \cos\phi_D \end{bmatrix} \tag{2.4.17}$$

$[I''_D]$ is the inertia tensor of the rider about a set of axes through his c. g. and fixed with respect to the rider.

$$[I''_D] = \begin{bmatrix} I''_{Dx} & 0 & -I''_{Dxz} \\ 0 & I''_{Dy} & 0 \\ -I''_{Dxz} & 0 & I''_{Dz} \end{bmatrix} \tag{2.4.18}$$

and

$$\left[\frac{\partial I_D}{\partial t}\right] = \dot{\phi}_D \begin{bmatrix} 0 & \cos\phi_D I''_{Dxz} & \sin\phi_D I''_{Dxz} \\ \cos\phi_D I''_{Dxz} & 2\sin\phi_D\cos\phi_D(I''_{Dz}-I''_{Dy}) & (\cos\phi_D-\sin\phi_D)(I''_{Dy}-I''_{Dz}) \\ \sin\phi_D I''_{Dxz} & (\cos\phi_D-\sin\phi_D)(I''_{Dy}-I''_{Dz}) & 2\sin\phi_D\cos\phi_D(I''_{Dy}-I''_{Dz}) \end{bmatrix} \tag{2.4.19}$$

$[N_D]$ is the moment acting on rider about his c. g. with respect to a set of axes parallel to the X, Y, Z axes of the vehicle coordinate system.

$$[N_D] = \begin{bmatrix} N_{xD} + \rho_D \cos\phi_D F_{yD} - y_D F_{zD} \\ N_{yD} - \rho_D \cos\phi_D F_{xD} \\ N_{zD} + y_D F_{xD} \end{bmatrix} \tag{2.4.20}$$

The first row of the expansion of equation (2.4.15) yields the equation of motion for the rotation of the rider about his roll axis (the saddle).

$$
\begin{aligned}
&-\cos\phi_D \rho_D m_D \ddot{v}_o + y_D m_D \ddot{w}_o + (I_{Dx} + \cos\phi_D z_D \rho_D m_D + y_D^2 m_D)\dot{p} \\
&-(I_{Dxy} + x_D y_D m_D)\dot{q} - (I_{Dxz} + \cos\phi_D x_D \rho_D m_D)\dot{r} + (I_{Dx} + \rho_D^2 m_D)\ddot{\phi}_D \\
&= \cos\phi_D I''_{Dxz}\, q\dot{\phi}_D + \sin\phi_D I''_{Dxz}\, r\dot{\phi}_D - I_{Dxz}\, q(p+\dot{\phi}_D) - I_{Dyz}(q^2 - r^2) \\
&+ I_{Dxy}\, r(p+\dot{\phi}_D) + (I_{Dz} - I_{Dy})\, qr - \cos\phi_D \rho_D \gamma_{23} + y_D \gamma_{33} + N_{xD}
\end{aligned}
\tag{2.4.21}
$$

The Y and Z components of the reaction moment on the rider at the rider roll center are written below.

$$
\begin{aligned}
N_{yD} = &-I_{Dxy}(\dot{p}+\ddot{\phi}_D) + I_{Dy}\dot{q} - I_{Dyz}\dot{r} + \cos\phi_D I''_{Dxz}(p+\dot{\phi}_D)\dot{\phi}_D \\
&+ 2\sin\phi_D\cos\phi_D (I''_{Dz} - I''_{Dy})\, q\dot{\phi}_D + (\cos\phi_D - \sin\phi_D)(I''_{Dy} \\
&- I''_{Dz})\, r\dot{\phi}_D + I_{Dxz}(p\{p+\dot{\phi}_D\} - r^2) + I_{Dyz}\, pq - I_{Dz}\, pr \\
&- I_{Dx}\, r(p+\dot{\phi}_D) - I_{Dxy}\, qr + \rho_D \cos\phi_D (m_D\{\ddot{x}_o + z_D\dot{q} \\
&- y_D\dot{r}\} - \gamma_{13})
\end{aligned}
\tag{2.4.22}
$$

$$
\begin{aligned}
N_{zD} = &-I_{Dxz}(\dot{p}+\ddot{\phi}_D) - I_{Dyz}\dot{q} + I_{Dz}\dot{r} + \sin\phi_D I''_{Dxz}(p+\dot{\phi}_D)\dot{\phi}_D \\
&+ (\cos\phi_D - \sin\phi_D)(I''_{Dy} - I''_{Dz})\, q\dot{\phi}_D + 2\sin\phi_D\cos\phi_D (I''_{Dy} \\
&- I''_{Dz})\, r\dot{\phi}_D - I_{Dxy}(p\{p+\dot{\phi}_D\} - q^2) + I_{Dy}\, pq - I_{Dyz}\, pr \\
&- I_{Dx}\, q(p+\dot{\phi}_D) + I_{Dxz}\, qr - y_D(m_D\{\ddot{x}_o + z_D\dot{q} - y_D\dot{r}\} - \gamma_{13})
\end{aligned}
\tag{2.4.23}
$$

2.5 Translational and Rotational Degrees of Freedom of Rear Wheel and Frame Assembly

The external forces on the rear wheel and frame assembly are the rear tire force, the reaction forces of the front fork and of the rider, and the weight of the rear assembly. The force balance equations for the rear wheel and frame in the X, Y, Z directions are given below.

$$m_R \dot{u}_R = F_{XTR} - F_{XF} - F_{XD} - m_R g \sin\theta \qquad (2.5.1)$$

$$m_R \dot{v}_R = F_{YTR} - F_{YF} - F_{YD} + m_R g \cos\theta \sin\phi \qquad (2.5.2)$$

$$m_R \dot{w}_R = F_{ZTR} - F_{ZF} - F_{ZD} + m_R g \cos\theta \cos\phi \qquad (2.5.3)$$

where:

$F_{XTR}, F_{YTR}, F_{ZTR}$ are the X, Y, Z components of the tire forces acting on the rear wheel at the ground contact point.

The X, Y, Z components of the inertial acceleration of the c. g. of the rear wheel and frame assembly are given below.

$$\dot{u}_R = \dot{u}_0 + q w_0 - r v_0 + \dot{q} z_R - (q^2 + r^2) x_R + p r z_R \qquad (2.5.4)$$

$$\dot{v}_R = \dot{v}_0 - p w_0 + r u_0 - \dot{p} z_R + p q x_R + q r z_R \qquad (2.5.5)$$

$$\dot{w}_R = \dot{w}_0 + p v_0 - q u_0 - \dot{q} x_R + p r x_R - (p^2 + q^2) z_R \qquad (2.5.6)$$

The equations for the reaction forces from Sections 2.3 and 2.4 are substituted into equations (2.5.1), (2.5.2), and (2.5.3) which then yield the equations of translational motion of the rear wheel and frame assembly in the X, Y, Z directions as follows.

In the X direction

$$\Sigma m \dot{u}_o + \gamma_3 \dot{q} - \gamma_2 \dot{r} - m_F \cos\theta_F y_F \ddot{\delta} = \gamma_{11} + \gamma_{12} + \gamma_{13} + F_{XTF} + F_{XTR} \quad (2.5.7)$$

In the Y direction

$$\Sigma m \dot{v}_o - \gamma_3 \dot{p} + \gamma_1 \dot{r} + m_F x_F'' \cos\delta \ddot{\delta} - m_D \rho_D \cos\phi_D \ddot{\phi}_D = \gamma_{21} + \gamma_{22} + \gamma_{23} + F_{YTF} + F_{YTR} \quad (2.5.8)$$

In the Z direction

$$\Sigma m \dot{w}_o + \gamma_2 \dot{p} - \gamma_1 \dot{q} + m_F \sin\theta_F y_F \ddot{\delta} + m_D y_D \ddot{\phi}_D = \gamma_{31} + \gamma_{32} + \gamma_{33} + F_{ZTF} + F_{ZTR} \quad (2.5.9)$$

The following terms are defined to permit simplification of the equations of motion.

$$\Sigma m = m_F + m_R + m_D \quad (2.5.10)$$

$$\gamma_1 = m_F x_F + m_R x_R + m_D x_D \quad (2.5.11)$$

$$\gamma_2 = m_F y_F + m_D y_D \quad (2.5.12)$$

$$\gamma_3 = m_F z_F + m_R z_R + m_D z_D \quad (2.5.13)$$

$$\gamma_{11} = m_R (-q w_o + r v_o - g \sin\theta + x_R \{q^2 + r^2\} - z_R p r) \quad (2.5.14)$$

$$\gamma_{21} = m_R (p w_o - r u_o + g \cos\theta \sin\phi - x_R p q - z_R q r) \quad (2.5.15)$$

$$\gamma_{31} = m_R (-p v_o + q u_o + g \cos\theta \cos\phi - x_R p r + z_R \{p^2 + q^2\}) \quad (2.5.16)$$

The moment balance equation for the rear wheel and frame assembly about the X, Y, Z axes of the vehicle coordinate system is given below in matrix form.

$$[I_R]\begin{bmatrix}\dot{p}\\ \dot{q}\\ \dot{r}\end{bmatrix}+\begin{bmatrix}p\\ q\\ r\end{bmatrix}\times\left([I_R]\begin{bmatrix}p\\ q\\ r\end{bmatrix}\right)=[N_R] \qquad (2.5.17)$$

$[I_R]$ is the inertia tensor of the rear wheel and frame about the origin of the vehicle coordinate system.

$$[I_R]=\begin{bmatrix} I_{RX}+m_R z_R^2 & 0 & -I_{RXZ}-m_R x_R z_R \\ 0 & I_{RY}+m_R(x_R^2+z_R^2) & 0 \\ -I_{RXZ}-m_R x_R z_R & 0 & I_{RZ}+m_R x_R^2 \end{bmatrix} \qquad (2.5.18)$$

where:

I_{RX}, I_{RY}, I_{RZ} are the X, Y, Z moments of inertia of the rear wheel and frame about its c. g.

I_{RXZ} is the X-Z product of inertia of the rear wheel and frame about its c. g. (Since the vehicle is assumed to be symmetrical about the X-Z plane, its X-Y and Y-Z products of inertia are zero.

$[N_R]$ is the vector moment acting on the rear wheel and frame at the origin of the vehicle coordinate system.

$$[N_R]=\begin{bmatrix} -N_{XF}-N_{XD}-N_{XWR}+(z_D-\rho_D)F_{YD}-l_0F_{YTR}+m_R z_R(\dot{v}_0-pw_0+ru_0-g\cos\theta\sin\phi) \\ -N_{YF}-N_{YD}-N_{YWR}-(z_D-\rho_D)F_{XD}+x_DF_{ZD}+l_0F_{XTR}-l_RF_{ZTR} \\ +m_R x_R(\dot{w}_0+pv_0-qu_0-g\cos\theta\cos\phi)-m_R z_R(\dot{u}_0+qw_0-rv_0+g\sin\theta) \\ -N_{ZF}-N_{ZD}-N_{ZWR}-x_DF_{YD}+l_RF_{YTR}-m_R x_R(\dot{v}_0-pw_0+ru_0-g\cos\theta\sin\phi) \end{bmatrix} \qquad (2.5.19)$$

The expansion of equation (2.5.17) results in the following equations of motion for rotation of the rear wheel and frame assembly about the X, Y, Z axes of the vehicle coordinate system.

Equation of motion for rotation about the X axis:

$$\sin\theta_F \cos\theta_F y_F m_F \dot{u}_o - (z_R m_R + \cos\theta_F z''_F m_F + \{z_D - \rho_D\} m_D)\dot{v}_o + \cos^2\theta_F y_F m_F w_o + (I_{RX} + z_R^2 m_R + \cos^2\theta_F \{\cos^2\delta I''_{FX} + \sin^2\delta I''_{FY}\} - \sin\theta_F \cos\theta_F \cos\delta I''_{FXZ} + \{\cos\theta_F z''_F z_F + \cos^2\theta_F y_F^2\} m_F + z_D \{z_D - \rho_D\} m_D) p + (\cos\theta_F \sin\delta \cos\delta \{I''_{FX} - I''_{FY}\} + \{\sin\theta_F \cos\theta_F z_F - \cos^2\theta_F x_F\} y_F m_F - \cos\theta_F z''_F x_F m_F) q - (I_{RXZ} + x_R z_R m_R + \sin\theta_F \cos\theta_F \{\cos^2\delta I''_{FX} + \sin^2\delta I''_{FY}\} + \cos^2\theta_F \cos\delta I''_{FXZ} + \sin\theta_F \cos\theta_F y_F^2 m_F + x_D \{z_D - \rho_D\} m_D) r - \cos\theta_F \cos\delta (I''_{FXZ} + x''_F z''_F m_F) \ddot{\delta} + \cos\phi_D \rho_D (z_D - \rho_D) m_D = pq I_{RXZ} + qr (I_{RY} - I_{RZ}) + \cos\theta_F \cos\delta \beta_1 + \cos\theta_F \sin\delta \beta_2 + r\omega_R I_{WR} - z_R \gamma_{21} - \cos\theta_F z''_F \gamma_{22} - \cos\theta_F y_F (\sin\theta_F \gamma_{12} + \cos\theta_F \gamma_{32}) - (z_D - \rho_D)\gamma_{23} - l_o F_{YTR} + \cos\theta_F \cos\delta (y''_{TF} F''_{ZTF} - z''_{TF} F''_{YTF}) - \cos\theta_F \sin\delta (z''_{TF} F''_{XTF} - x''_{TF} F''_{ZTF}) - \sin\theta_F N''_{ZF} - N_{XD} \qquad (2.5.20)$$

Equation of motion for rotation about the Y axis:

$$\gamma_3 \dot{u}_o - \gamma_1 \dot{v}_o + (\cos\theta_F \sin\delta \cos\delta \{I''_{FX} - I''_{FY}\} - \sin\theta_F \sin\delta I''_{FXZ} - x_F y_F m_F - I_{DXY} - x_D \rho_D m_D) p + (I_{RY} + \{x_R^2 + z_R^2\} m_R + \sin^2\delta I''_{FX} + \cos^2\delta I''_{FY} + \{\sin\theta_F x_F + \cos\theta_F y_F\} z''_F m_F - \{\sin\theta_F y_F - \cos\theta_F x_F\} \cos\delta x''_F m_F + I_{DY} + x_D^2 m_D + z_D \{z_D - \rho_D [1 - \cos\phi_D]\} m_D) q - (\sin\theta_F \sin\delta \cos\delta \{I''_{FX} - I''_{FY}\} + \cos\theta_F \sin\delta I''_{FXZ} + z_F y_F m_F + I_{DYZ} + y_D \{z_D - \rho_D [1 - \cos\phi_D]\} m_D) r - (\sin\delta I''_{FXZ} + z''_F y_F m_F) \ddot{\delta} - (I_{DXY} + x_D y_D m_D) \ddot{\phi}_D = -(p^2 - r^2) I_{RXZ} - pr (I_{RX} - I_{RZ}) + \sin\delta \beta_1 - \cos\delta \beta_2 - \cos\phi_D (p + \dot{\phi}_D) \phi_D I''_{DXZ} + 2 \sin\phi_D \cos\phi_D q \phi_D (I^*_{DY} - I^*_{DZ}) - (\cos\phi_D - \sin\phi_D) r \phi_D (I^*_{DY} - I^*_{DZ}) - (p \{p + \phi_D\} - r^2) I_{DXZ} - pq I_{DYZ} - pr I_{DZ} - r (p + \phi_D) I_{DX} + qr I_{DXY} - x_R \gamma_{31} + z_R \gamma_{11} - x_F \gamma_{32} + z_F \gamma_{12} - x_D \gamma_{33} + (z_D - \rho_D \{1 - \cos\phi_D\}) \gamma_{13} + h_o F_{XTR} - l_R F_{ZTR} + \sin\delta (y''_{TF} F''_{ZTF} - z''_{TF} F''_{YTF}) + \cos\delta (z''_{TF} F''_{XTF} - x''_{TF} F''_{ZTF}) \qquad (2.5.21)$$

Equation of motion for rotation about the Z axis:

$$
\begin{aligned}
&-(\sin^2\theta_F\, y_F\, m_F + y_D\, m_D)\,\dot{u}_0 + (x_R\, m_R + \sin\theta_F\, z''_F\, m_F + x_D\, m_D)\,\dot{v}_0 \\
&- \sin\theta_F \cos\theta_F\, y_F\, m_F\, \dot{w}_0 - (I_{RXZ} + x_R\, z_R\, m_R - \sin^2\theta_F \cos\delta\, I''_{FXZ} + \sin\theta_F \cos\theta_F \\
&\{\cos^2\delta\, I''_{FX} + \sin^2\delta\, I''_{FY}\} + \sin\theta_F\, z''_F\, y_F\, m_F + \sin\theta_F \cos\theta_F\, y_F\, m_F + I_{DXZ} \\
&+ x_D\, z_D\, m_D)\,\dot{p} - (\sin\theta_F \sin\delta \cos\delta \{I''_{FX} - I''_{FY}\} + \sin\theta_F \{\sin\theta_F\, z_F - \cos\theta_F\, x_F\} \\
&y_F\, m_F + I_{DYZ} + y_D\, z_D\, m_D)\,\dot{q} + (I_{RZ} + x_R^2\, m_R + \sin^2\theta_F \{\cos^2\delta\, I''_{FX} + \sin^2\delta \\
&I''_{FY}\} + \sin\theta_F \cos\theta_F\, I''_{FXZ} + \{\sin\theta_F\, z''_F\, x_F + \sin^2\theta_F\, y_F^2\}\, m_F + I_{DZ} \\
&+ \{x_D^2 + y_D^2\}\, m_D)\,\dot{r} + \sin\theta_F \cos\delta\,(I''_{FXZ} + x''_F\, z''_F\, m_F)\,\ddot{\delta} - (I_{DXZ} + \cos\phi_D \\
&x_D\, \rho_D\, m_D)\,\ddot{\phi}_D = -q\, r\, I_{RXZ} + p\, q\,(I_{RX} - I_{RY}) - \sin\theta_F \cos\delta\, \beta_1 - \sin\theta_F \\
&\sin\delta\, \beta_2 - \sin\phi_D\,(p + \dot{\phi}_D)\,\dot{\phi}_D\, I''_{DXZ} - (\cos\phi_D - \sin\phi_D)\, q\, \dot{\phi}_D\,(I''_{DY} - I''_{DZ}) \\
&- 2\sin\phi_D \cos\phi_D\, r\, \dot{\phi}_D\,(I''_{DY} - I''_{DZ}) + (p\{p + \dot{\phi}_D\} - q^2) - p\, q\, I_{DY} + p\, r\, I_{DYZ} \\
&+ q\,(p + \dot{\phi}_D)\, I_{DX} - q\, r\, I_{DXZ} - p\, \omega_R\, I_{WR} + x_R\, \gamma_{21} + \sin\theta_F\, z''_F\, \gamma_{22} - \sin\theta_F \\
&y_F\,(\sin\theta_F\, \gamma_{12} + \cos\theta_F\, \gamma_{32}) + x_D\, \gamma_{23} - y_D\, \gamma_{13} + l_R\, F_{YTR} - \sin\theta_F \cos\delta\,(y''_{TF}\, F''_{ZTF} \\
&- z''_{TF}\, F''_{YTF}) + \sin\theta_F \sin\delta\,(z''_{TF}\, F''_{XTF} - x''_{TF}\, F''_{ZTF}) - \cos\theta_F\, N''_{ZF}
\end{aligned}
\tag{2.5.22}
$$

where:

$$\beta_1 = p''\, q''\, I''_{FXZ} + q''(r'' + \dot{\delta})(I''_{FY} - I''_{FZ}) + (r'' + \dot{\delta})\,\omega_F\, I_{WF} \tag{2.5.23}$$

$$\beta_2 = (p''^2 - \{r'' + \dot{\delta}\}^2)\, I''_{FXZ} + p''(r'' + \dot{\delta})(I''_{FX} - I''_{FZ}) \tag{2.5.24}$$

2.6 Tire Forces

The inclination angles and slip angles of the front and rear wheels are determined so that tire forces and moments at the ground contact points may be calculated, Figure 2.4.

The direction cosines in the space fixed coordinate system of the normal to the front wheel plane are found below. The elements of the right-most matrix represent the direction cosines of the normal to the wheel plane in vehicle coordinate system.

$$\begin{bmatrix} \cos\alpha_{YWF} \\ \cos\beta_{YWF} \\ \cos\gamma_{YWF} \end{bmatrix} = [A] \begin{bmatrix} -\sin\delta\cos\theta_F \\ \cos\delta \\ \sin\delta\sin\theta_F \end{bmatrix} \qquad (2.6.1)$$

where:

$\cos\alpha_{YWF}, \cos\beta_{YWF}, \cos\gamma_{YWF}$ are the direction cosines of the normal to the front wheel plane with respect to the X', Y', Z' axes of the space fixed coordinate system.

The inclination angle of the front wheel with respect to the ground, ϕ_F, is the angle between the wheel plane and a plane perpendicular to the ground plane and having the same line of intersection with the ground plane as the wheel plane.

$$\phi_F = \arcsin\left(\cos\alpha_{YWF}\cos\alpha_G + \cos\beta_{YWF}\cos\beta_G + \cos\gamma_{YWF}\cos\gamma_G\right) \qquad (2.6.2)$$

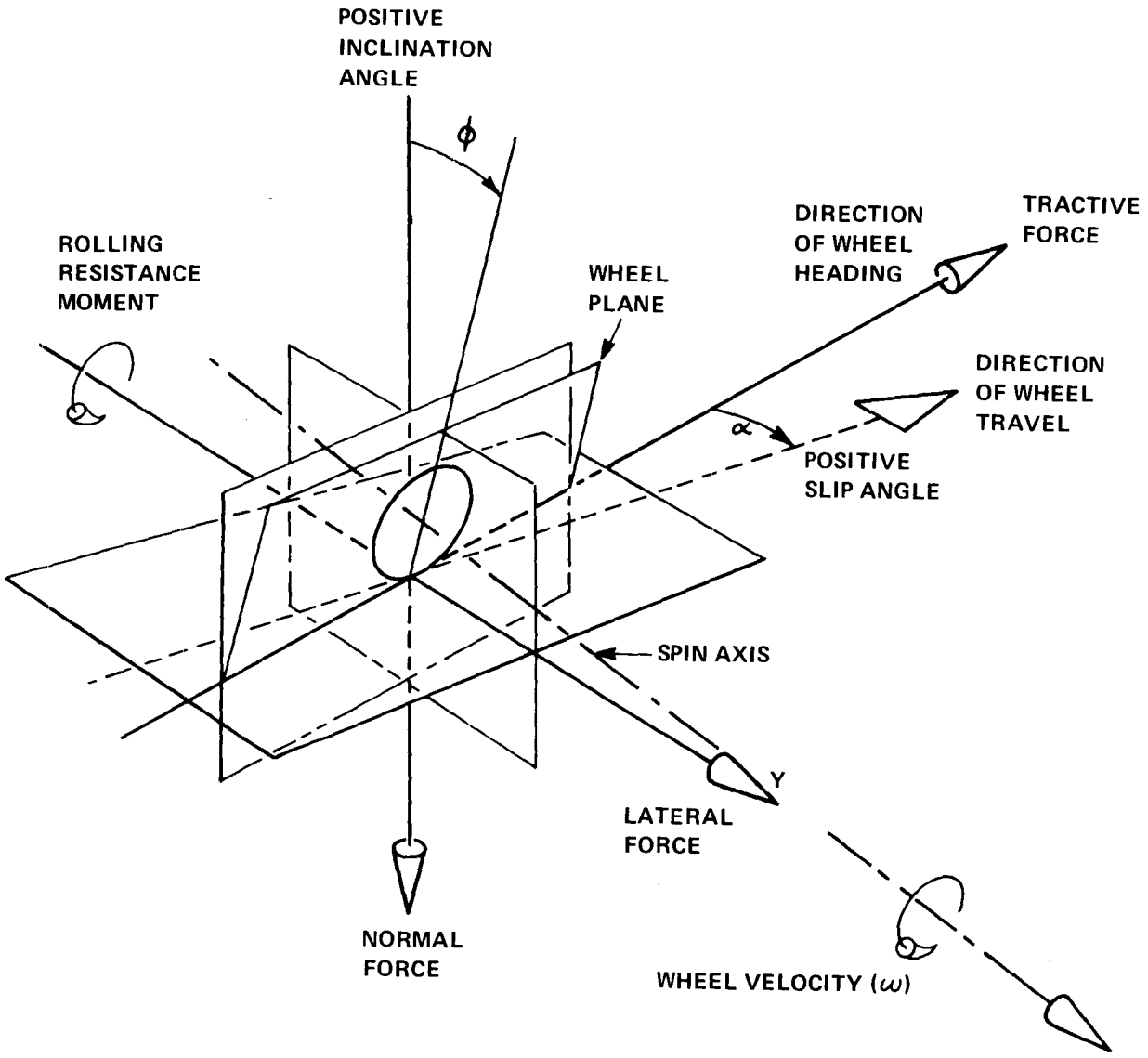

Figure 2.4 SIGN CONVENTION OF TIRE FORCES, MOMENTS AND GEOMETRY

where:

$\cos\alpha_G, \cos\beta_G, \cos\gamma_G$ are the direction cosines of the normal to the ground plane with respect to the X', Y', Z' axes of the space fixed coordinate system.

Since flat level ground is assumed, the normal to the ground plane is vertical and $\cos\alpha_G = 0, \cos\beta_G = 0, \cos\gamma_G = 1.$

therefore $$\phi_F = \arcsin(\cos\gamma_{YWF}) \tag{2.6.3}$$

The direction cosines in the space fixed coordinate system of the normal to the rear wheel plane are found below.

$$\begin{bmatrix}\cos\alpha_{YWR}\\ \cos\beta_{YWR}\\ \cos\gamma_{YWR}\end{bmatrix} = [A]\begin{bmatrix}0\\1\\0\end{bmatrix} \tag{2.6.4}$$

Again assuming flat level ground, the inclination angle of the rear wheel with respect to the ground, ϕ_R, may be expressed as follows.

$$\phi_R = \arcsin(\cos\gamma_{YWR}) \tag{2.6.5}$$

The slip angle is the angle in the ground plane between the heading vector of the wheel and the velocity vector of the ground contact point. Since the ground plane is parallel to the X'-Y' plane of the space fixed coordinate system, the heading angle is the angle between the X' axis and the line of intersection of wheel plane and the ground plane.

Thus the front and rear wheel heading angles, ψ_F and ψ_R, are as follows.

$$\psi_F = \arctan\left(-\cos\alpha_{ywF} / \cos\beta_{ywF}\right) \tag{2.6.6}$$

$$\psi_R = \arctan\left(-\cos\alpha_{ywR} / \cos\beta_{ywR}\right) \tag{2.6.7}$$

Assuming that changes in the rolling radii of the front and rear wheels are negligible, the velocity components (u_F, v_F, w_F and u_R, v_R, w_R) along the X, Y, Z axes of points located at the front and rear wheel ground contact points, but fixed in the vehicle coordinate system, are given below.

$$u_F = u_0 + q h_0 \tag{2.6.8}$$

$$u_R = u_0 + q h_0 \tag{2.6.9}$$

$$v_F = v_0 - p h_0 + r l_F \tag{2.6.10}$$

$$v_R = v_0 - p h_0 + r l_R \tag{2.6.11}$$

$$w_F = w_0 - q l_F \tag{2.6.12}$$

$$w_R = w_0 - q l_R \tag{2.6.13}$$

The components in the space fixed coordinate system of the velocity vectors of the front and rear wheel ground contact points are found below.

$$\begin{bmatrix} u_F' \\ v_F' \\ w_F' \end{bmatrix} = [A] \begin{bmatrix} u_F \\ v_F \\ w_F \end{bmatrix} \tag{2.6.14}$$

$$\begin{bmatrix} u'_R \\ v'_R \\ w'_R \end{bmatrix} = [A] \begin{bmatrix} u_R \\ v_R \\ w_R \end{bmatrix} \qquad (2.6.15)$$

Since the ground plane is parallel to the X'-Y' plane of the space fixed coordinate system, the angle between the X' axis and the velocity vectors of the front and rear wheel ground contact points in the ground plane may be found as follows.

$$\psi_{VF} = \arctan\left(v'_F / u'_F\right) \qquad (2.6.16)$$

$$\psi_{VR} = \arctan\left(v'_R / u'_R\right) \qquad (2.6.17)$$

The front and rear wheel slip angles may now be expressed as follows.

$$\alpha_F = \psi_F - \psi_{VF} \qquad (2.6.18)$$

$$\alpha_R = \psi_R - \psi_{VR} \qquad (2.6.19)$$

The normal load on a tire is assumed to be equal to the radial stiffness of the tire times the deflection of the tire section in the direction normal to the ground, Figure 2.5.

The elevation of the front wheel center above the ground, z'_{WF}, is given by the following equation.

$$\begin{bmatrix} x'_{WF} \\ y'_{WF} \\ z'_{WF} \end{bmatrix} = \begin{bmatrix} x'_0 \\ y'_0 \\ z'_0 \end{bmatrix} + [A] \begin{bmatrix} x_{WF} \\ y_{WF} \\ z_{WF} \end{bmatrix} \qquad (2.6.20)$$

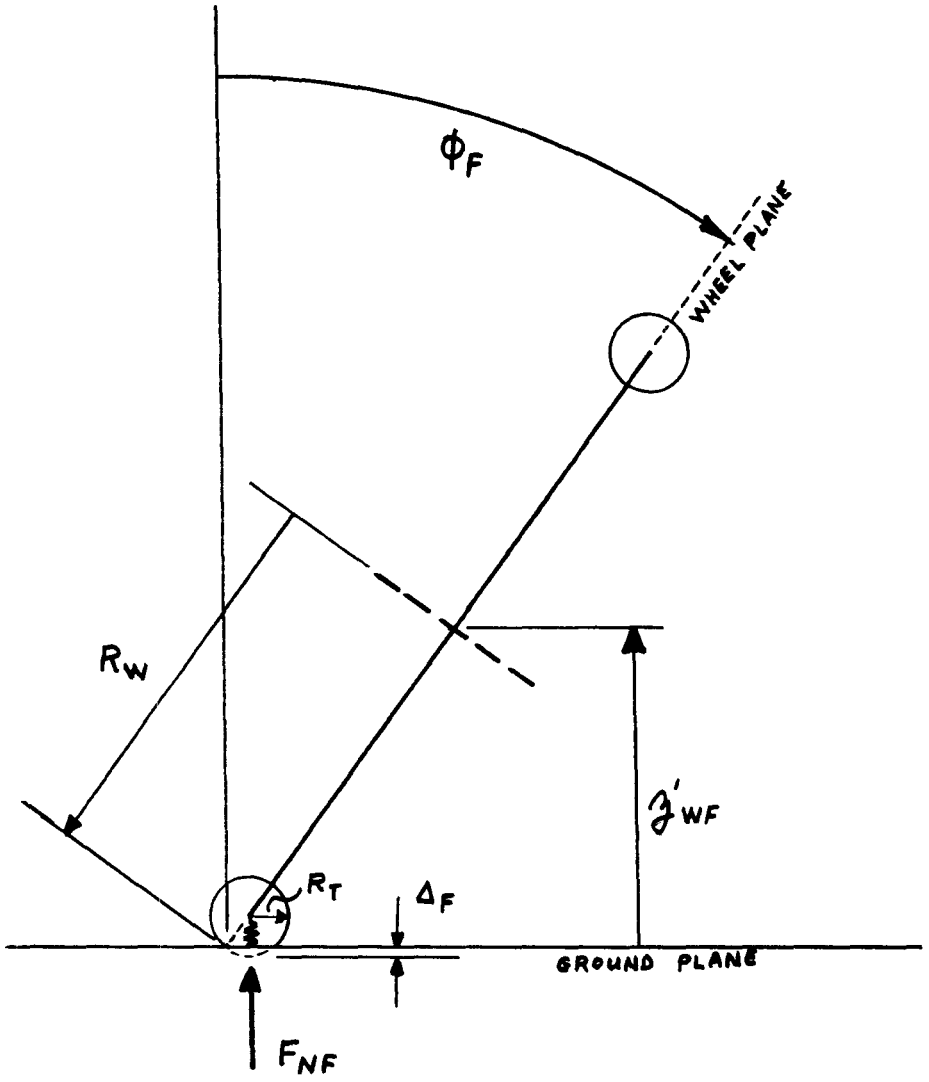

Figure 2.5 TIRE STIFFNESS MODEL FOR COMPUTATION OF NORMAL FORCE

where

x'_o, y'_o, z'_o are X', Y', Z' coordinates of the origin of the bicycle coordinate system.

x_{WF}, y_{WF}, z_{WF} are the location of the front wheel center in the bicycle coordinate system.

$$\begin{bmatrix} x_{WF} \\ y_{WF} \\ z_{WF} \end{bmatrix} = [S] \begin{bmatrix} x'_{WF} \\ y'_{WF} \\ z'_{WF} \end{bmatrix} \tag{2.6.21}$$

Thus from Figure 2.5 it can be seen that the deflection of the tire section is:

$$\Delta_F = R_T + z'_{WF} + (R_W - R_T) \cos \phi_F \tag{2.6.22}$$

The elevation of the rear wheel center above the ground, z'_{WR}, is given by the following equation.

$$\begin{bmatrix} x'_{WR} \\ y'_{WR} \\ z'_{WR} \end{bmatrix} = \begin{bmatrix} x'_o \\ y'_o \\ z'_o \end{bmatrix} + [A] \begin{bmatrix} \ell_R \\ 0 \\ \ell_0 - R_W \end{bmatrix} \tag{2.6.23}$$

and

$$\Delta_R = R_T + z'_{WR} + (R_W - R_T) \cos \phi_R \tag{2.6.24}$$

The normal forces (normal to the ground plane) on the front and rear tires are given below.

$$F_{NF} = - K_T \Delta_F \tag{2.6.25}$$

$$F_{NR} = - K_T \Delta_R \tag{2.6.26}$$

If a wheel is not in contact with the ground (Δ_F or Δ_R is zero or negative), the normal force is zero; thus all the tire forces and moments are zero for that wheel.

The tire rolling resistance force is assumed to be proportional to tire normal load. Thus the circumferential force on the front and rear tires is as follows.

$$F_{cF} = K_{RR} F_{NF} \qquad (2.6.27)$$

$$F_{cR} = K_{RR} F_{NR} \qquad (2.6.28)$$

These circumferential force vectors lie along the line of intersection of the ground plane and the corresponding wheel plane.

The side forces on the front and rear tires are expressed by the following approximate relationships.

$$F_{SF} = F_{NF}\left(K_{\alpha 1}\alpha_F + K_{\alpha 2}\alpha_F^2\, SGN\alpha_F + K_{\phi 1}\phi_F + K_{\phi 2}\phi_F^2\, SGN\phi_F\right) \qquad (2.6.29)$$

$$F_{SR} = F_{NR}\left(K_{\alpha 1}\alpha_R + K_{\alpha 2}\alpha_R^2\, SGN\alpha_R + K_{\phi 1}\phi_R + K_{\phi 2}\phi_R^2\, SGN\phi_R\right) \qquad (2.6.30)$$

where

$K_{\alpha 1}, K_{\alpha 2}$ are tire characteristics relating side force and slip angle.

$K_{\phi 1}, K_{\phi 2}$ are tire characteristics relating side force and inclination angle.

$SGN\alpha_F$ indicates the term has the sign of α_F or other corresponding angle.

The side force vectors lie in the ground plane and are perpendicular to the circumferential force vectors.

In order to transform the front tire force components into the bicycle coordinate system and the front fork coordinate system, the direction cosines of these force vectors must be mathematically defined. The direction components in the space fixed coordinate system of the line of intersection of the front wheel plane (direction cosines: $\cos\alpha_{ywF}$, $\cos\beta_{ywF}$, $\cos\gamma_{ywF}$) and the ground plane (direction cosines: 0, 0, 1) are found by taking the vector cross-product of the normals to these two planes.

$$a_{cF} = \cos\beta_{ywF} \tag{2.6.31}$$

$$b_{cF} = -\cos\alpha_{ywF} \tag{2.6.32}$$

$$c_{cF} = 0 \tag{2.6.33}$$

The direction cosines in the space fixed coordinate system of the front circumferential force are:

$$\cos\alpha_{cF} = \frac{\cos\beta_{ywF}}{\sqrt{\cos^2\alpha_{ywF} + \cos^2\beta_{ywF}}} \tag{2.6.34}$$

$$\cos\beta_{cF} = \frac{-\cos\alpha_{ywF}}{\sqrt{\cos^2\alpha_{ywF} + \cos^2\beta_{ywF}}} \tag{2.6.35}$$

$$\cos\gamma_{cF} = 0 \tag{2.6.36}$$

The direction components in the space fixed coordinate system of front side force vector (a_{sF}, b_{sF}, c_{sF}) are given by taking the vector cross-product of the normal to the ground plane and the unit vector in the direction of the front circumferential force vector.

$$a_{SF} = -\cos\beta_{CF} \tag{2.6.37}$$

$$b_{SF} = \cos\alpha_{CF} \tag{2.6.38}$$

$$c_{SF} = 0 \tag{2.6.39}$$

The direction cosines of the front side force vector in the space fixed coordinate system are:

$$\cos\alpha_{SF} = \frac{\cos\alpha_{YWF}}{\sqrt{\cos^2\alpha_{YWF} + \cos^2\beta_{YWF}}} \tag{2.6.40}$$

$$\cos\beta_{SF} = \frac{\cos\beta_{YWF}}{\sqrt{\cos^2\alpha_{YWF} + \cos^2\beta_{YWF}}} \tag{2.6.41}$$

$$\cos\gamma_{SF} = 0 \tag{2.6.42}$$

Thus the front tire force components in the X, Y, Z directions of the bicycle coordinate system are:

$$\begin{bmatrix} F_{XTF} \\ F_{YTF} \\ F_{ZTF} \end{bmatrix} = [A]^T \begin{bmatrix} F_{CF}\cos\alpha_{CF} + F_{SF}\cos\alpha_{SF} \\ F_{CF}\cos\beta_{CF} + F_{SF}\cos\beta_{SF} \\ F_{NF} \end{bmatrix} \tag{2.6.43}$$

The components in the X'', Y'', Z'' directions of the front fork coordinate system are:

$$\begin{bmatrix} F''_{XTF} \\ F''_{YTF} \\ F''_{ZTF} \end{bmatrix} = [S]^T \begin{bmatrix} F_{XTF} \\ F_{YTF} \\ F_{ZTF} \end{bmatrix} \tag{2.6.44}$$

The components of the rear tire forces in the bicycle coordinate system are simply expressed by the following equations.

$$F_{XTR} = F_{CR} \tag{2.6.45}$$

$$F_{YTR} = F_{SR} \cos \phi_R + F_{NR} \sin \phi_R \tag{2.6.46}$$

$$F_{ZTR} = -F_{SR} \sin \phi_R + F_{NR} \cos \phi_R \tag{2.6.47}$$

In order to accurately compute the moment of the front tire forces about the steer axis, it is necessary to determine the location of the ground contact point in the front fork coordinate system.

The ground contact point is defined as the point of intersection of the wheel plane, the ground plane, and the plane passing through the wheel center which is perpendicular to the ground plane and wheel plane.

The equations for these three planes in the front fork coordinate system are respectively:

$$y'' = h_F \cos \beta_{GZ''} \tag{2.6.48}$$

$$x'' \cos \alpha_{GZ''} + y'' \cos \beta_{GZ''} + z'' \cos \gamma_{GZ''} = -z_0' \tag{2.6.49}$$

$$x'' \cos \alpha_{C''} + z'' \cos \gamma_{C''} = x''_{WF} \cos \alpha_{C''} + z''_{WF} \cos \gamma_{C''} \tag{2.6.50}$$

where:

$\cos \alpha_{GZ''}$, $\cos \beta_{GZ''}$, $\cos \gamma_{GZ''}$ are the direction cosines of the normal to the ground plane with respect to the X'', Y'', Z'' axes of the front fork coordinate system.

$$\begin{bmatrix} \cos\alpha_{GZ''} \\ \cos\beta_{GZ''} \\ \cos\gamma_{GZ''} \end{bmatrix} = [S]^T \begin{bmatrix} \sin\phi\sin\psi + \cos\phi\sin\theta\cos\psi \\ -\cos\psi\sin\phi + \cos\phi\sin\phi\sin\psi \\ \cos\theta\cos\phi \end{bmatrix} \qquad (2.6.51)$$

Where the right matrix represents the direction cosines of the normal to the ground plane with respect to the X, Y, Z axes of the vehicle coordinate system, from Equation (2.1.1).

$\cos\alpha_{C''}$, $\cos\beta_{C''}$, $\cos\gamma_{C''}$ are the direction cosines of the line of intersection of the wheel plane and the ground plane with respect to the X'', Y'', Z'' axes.

$$\cos\alpha_{C''} = \frac{\cos\gamma_{GZ''}}{\sqrt{\cos^2\alpha_{GZ''} + \cos^2\gamma_{GZ''}}} \qquad (2.6.52)$$

$$\cos\beta_{C''} = 0 \qquad (2.6.53)$$

$$\cos\gamma_{C''} = \frac{-\cos\alpha_{GZ''}}{\sqrt{\cos^2\alpha_{GZ''} + \cos^2\gamma_{GZ''}}} \qquad (2.6.54)$$

Thus the coordinates of the ground contact point in the front fork coordinate system ($x''_{TF}, y''_{TF}, z''_{TF}$) are given by the following equation.

$$\begin{bmatrix} x''_{TF} \\ y''_{TF} \\ z''_{TF} \end{bmatrix} = \begin{bmatrix} 0 & 1 & 0 \\ \cos\alpha_{GZ''} & \cos\beta_{GZ''} & \cos\gamma_{GZ''} \\ \cos\alpha_{C''} & 0 & \cos\beta_{C''} \end{bmatrix}^{-1} \begin{bmatrix} R_F\cos\beta_{GZ''} \\ -z'_0 \\ x''_{WF}\cos\alpha_{C''} + z''_{WF}\cos\gamma_{C''} \end{bmatrix} \qquad (2.6.55)$$

2.7 Matrix Equation of Motion

Figure 2.6 shows the equations of motion which have been developed in Sections 2.1 through 2.6 as a single matrix equation of motion for the eight coupled degrees of freedom of the bicycle model.

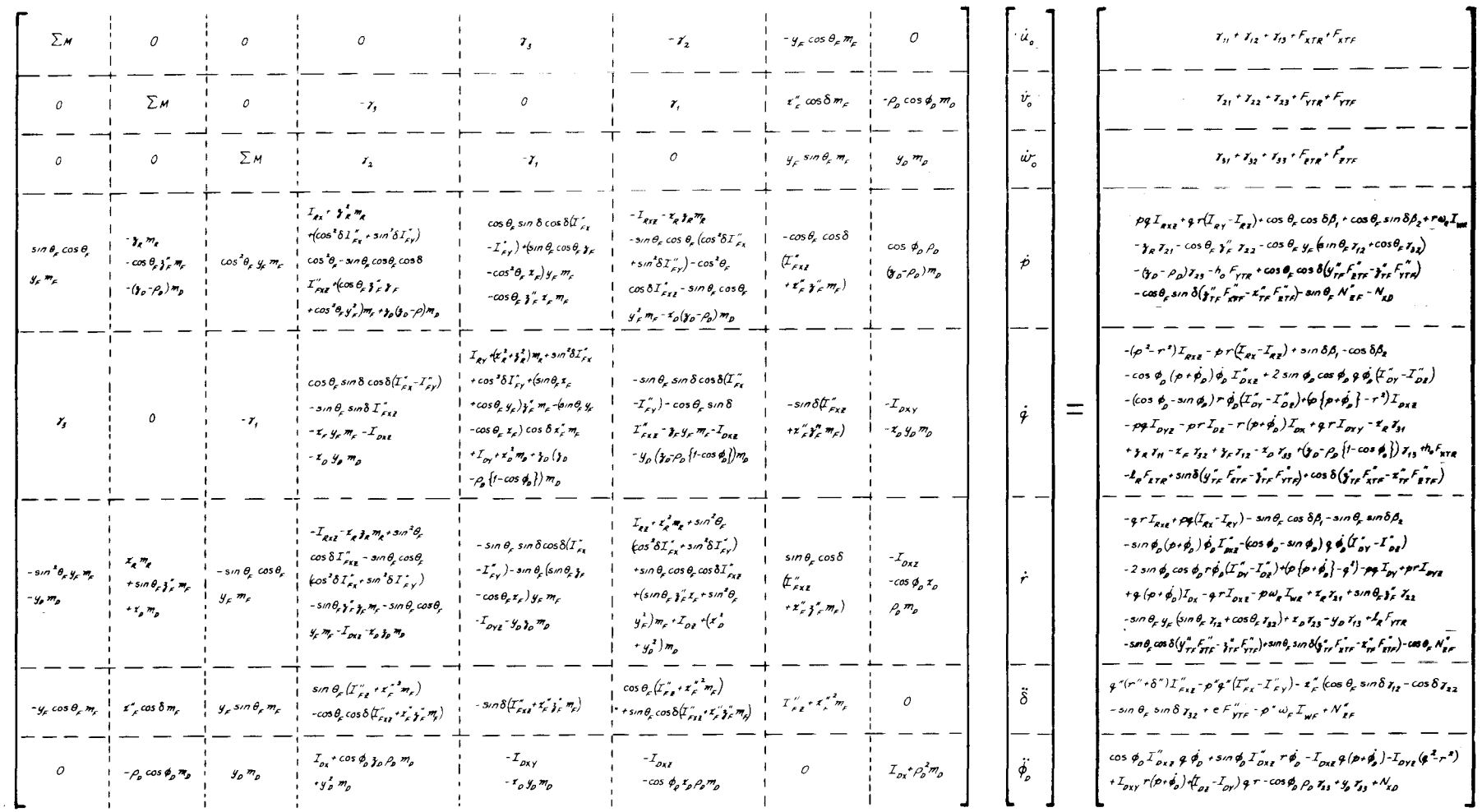

Figure 2.6 MATRIX EQUATION OF MOTION

3.0 DIGITAL COMPUTER SIMULATION PROGRAM

The simulation program, consisting of seven subroutines, uses approximately 110 K bytes of core storage and requires about 6 seconds of CPU time per second of problem time when run on an IBM 360-65 computer. The output processor program uses approximately 160 K bytes of core storage and requires about 5 seconds of CPU time per run. The total cost of both the simulation and output processor programs is approximately seven dollars per problem.

Forty-four input data are required by the simulation program. These data include dimensions, weights, moments of inertia, tire side force coefficient, initial conditions, etc. Figure 3.1 is a listing of typical input data.

The digital computer bicycle simulation program basically consists of the application of a modified Runge-Kutta step-by-step procedure to integrate equations of motion developed in Section 2. The integration step size is variable although a value of 0.01 second is generally used. With a step size of 0.01 second, solutions up to 10 seconds duration (problem time) may be obtained. Solution output is obtained from a separate output processor program which can produce time histories of as many as 36 variables (bicycle translational and angular positions, velocities, accelerations, and tire force components, etc.) in both printed and plotted format.

The characteristic dimensions of the bicycle for simulation program input are shown in Figure 3.2 and defined in Table 3.1.

SIMULATION STUDY OF BICYCLE DESIGN PARAMETER CHANGES 27JUN'71
STANDARD BICYCLE WITH 102 LB. RIDER SPEED = 15 MPH (57)

WHEELBASE (IN)	41.50
TOTAL WEIGHT OF BICYCLE (LB)	40.80
LOCATION OF TOTAL BICYCLE C.G. FORWARD OF REAR WHEEL CENTER (IN)	18.05
LOCATION OF TOTAL BICYCLE C.G. ABOVE GROUND (IN)	20.76
ROLL MOMENT OF INERTIA OF THE TOTAL BICYCLE ABOUT AXIS THROUGH TOTAL C.G. (LB-IN-SEC SQ)	12.64
PITCH MOMENT OF INERTIA OF THE TOTAL BICYCLE ABOUT AXIS THROUGH TOTAL C.G. (LB-IN-SEC SQ)	35.95
YAW MOMENT OF INERTIA OF THE TOTAL BICYCLE ABOUT AXIS THROUGH TOTAL C.G. (LB-IN-SEC SQ)	25.70
ROLL-YAW PRODUCT OF INERTIA OF THE TOTAL BICYCLE ABOUT AXIS THROUGH TOTAL C.G. (LB-IN-SEC SQ)	-1.62

WEIGHT OF RIDER (LB)	102.00
LOCATION OF RIDER C.G. FORWARD OF REAR WHEEL CENTER (IN)	11.30
HEIGHT OF RIDER C.G. ABOVE GROUND (IN)	46.60
HEIGHT OF SADDLE ABOVE GROUND (IN)	38.20
ROLL MOMENT OF INERTIA OF RIDER ABOUT AN AXIS THROUGH HIS C.G. (LB-IN-SEC SQ)	27.80
PITCH MOMENT OF INERTIA OF RIDER ABOUT AN AXIS THROUGH HIS C.G. (LB-IN-SEC SQ)	39.90
YAW MOMENT OF INERTIA OF RIDER ABOUT AN AXIS THROUGH HIS C.G. (LB-IN-SEC SQ)	18.40
ROLL-YAW PRODUCT OF INERTIA OF RIDER ABOUT AN AXIS THROUGH HIS C.G. (LB-IN-SEC SQ)	0.0

WEIGHT OF FRONT FORK ASSEMBLY (FORK,WHEEL,AND HANDLE BARS),(LB)	11.40
PERPENDICULAR DISTANCE FROM C.G. OF FRONT FORK ASSEMBLY TO STEER AXIS (IN)	1.50
DISTANCE PARALLEL TO STEER AXIS FROM C.G. OF FRONT FORK ASSEMBLY TO FRONT WHEEL CENTER (IN)	9.50
ROLL MOMENT OF INERTIA OF FRONT FORK ASSEMBLY ABOUT AN AXIS PERPENDICULAR TO THE STEER AXIS THROUGH C.G. OF ASSEMBLY (LB-IN-SEC SQ)	4.59
PITCH MOMENT OF INERTIA OF FRONT FORK ASSEMBLY ABOUT AN AXIS THROUGH THE C.G. OF THE ASSEMBLY (LB-IN-SEC SQ)	5.56
YAW MOMENT OF INERTIA OF FRONT FORK ASSEMBLY ABOUT THE STEER AXIS (LB-IN-SEC SQ)	1.86
ROLL-YAW PRODUCT OF INERTIA OF FRONT FORK ASSEMBLY ABOUT AN AXIS THROUGH THE C.G. OF THE ASSEMBLY (LB-IN-SEC SQ)	-0.32

CASTER ANGLE OF THE STEER AXIS (DEG)	21.00
FORK OFFSET (IN)	1.87
UNDEFLECTED WHEEL ROLLING RADIUS (IN)	13.62
TIRE SECTION WIDTH (IN)	1.60
RADIAL STIFFNESS OF TIRE (LB/IN)	710.00
SPIN MOMENT OF INERTIA OF THE FRONT WHEEL (LB-IN-SEC SQ)	1.76
SPIN MOMENT OF INERTIA OF THE REAR WHEEL (LB-IN-SEC SQ)	1.76
FIRST AND SECOND ORDER COEFFICIENTS RELATING TIRE SIDE FORCE AND SLIP ANGLE	0.32 0.02
FIRST AND SECOND ORDER COEFFICIENTS RELATING TIRE SIDE FORCE AND INCLINATION ANGLE	0.01 0.0
COEFFICIENT OF ROLLING RESISTANCE (LB/LB)	0.0
AERODYNAMIC DRAG COEFFICIENT (LB/MPH-SQ)	0.0

INITIAL X LOCATION (FT)	0.0
INITIAL Y LOCATION (FT)	0.0
INITIAL YAW ANGLE (DEG)	0.0
INITIAL FORWARD VELOCITY (MPH)	15.00
MAXIMUM ROLL ANGLE (DEG)	60.00
MAXIMUM PATH DISTANCE (FT)	70.00
MAXIMUM SIMULATION TIME (SEC)	0.50
INTEGRATION TIME INCREMENT (SEC)	0.01

MAXIMUM SIMULATION TIME EXCEEDED, COMPUTATION TERMINATED

TOTAL SIMULATION TIME = 0.510

Figure 3.1 TYPICAL INPUT DATA FOR COMPUTER SIMULATION PROGRAM

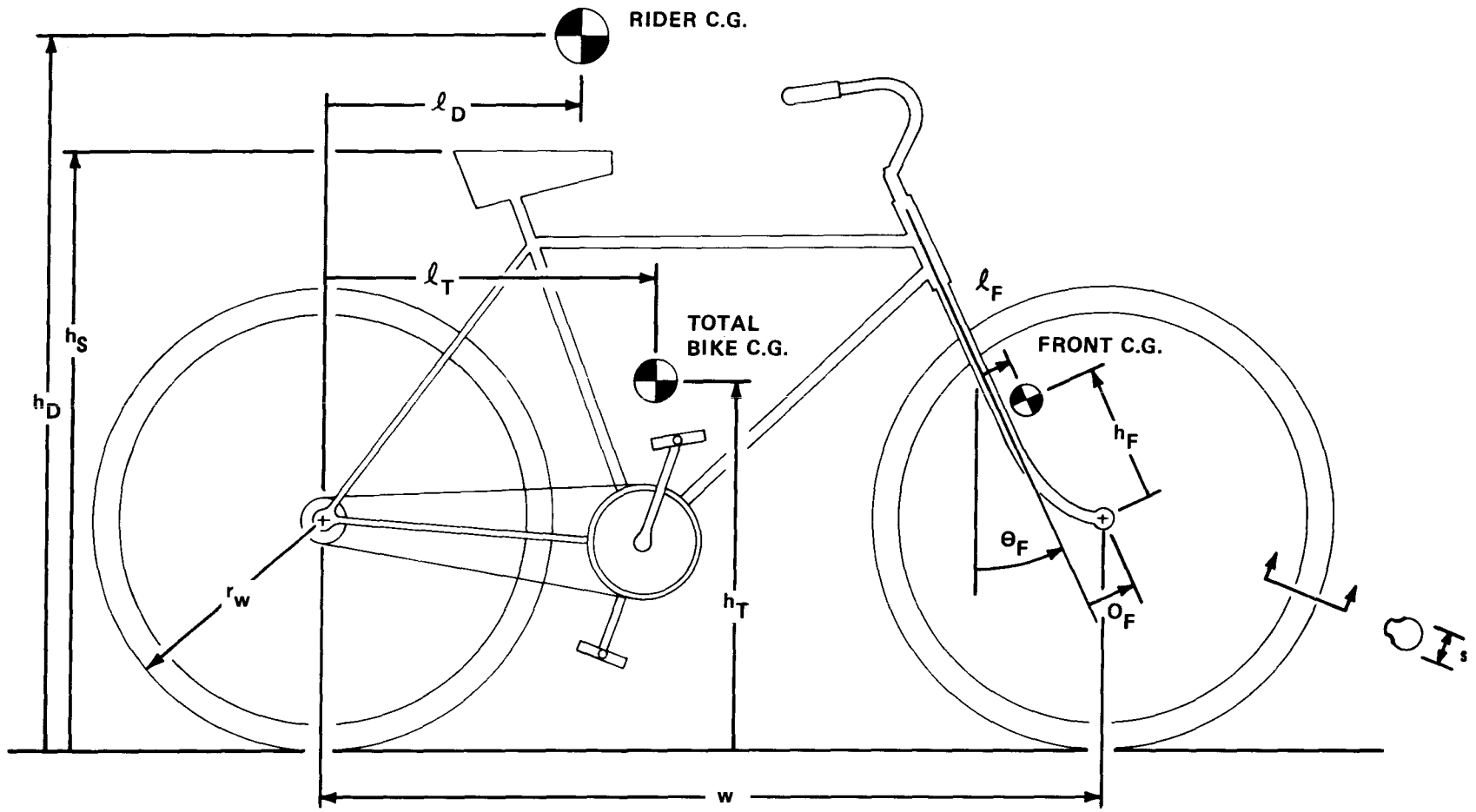

Figure 3.2 CHARACTERISTIC DIMENSIONS OF BICYCLE FOR COMPUTER SIMULATION INPUT

Table 3.1

Characteristic Dimensions of Bicycle for Computer Simulation Input

w	=	wheelbase
ℓ_T	=	location of total bicycle c.g. forward of rear wheel center
h_T	=	height of total bicycle c.g. above ground
ℓ_D	=	location of rider c.g. forward of rear wheel center
h_D	=	height of rider c.g. above ground
h_S	=	height of saddle above ground
ℓ_F	=	perpendicular distance from c.g. of front fork assembly to steer axis
h_F	=	distance parallel to steer axis from c.g. of front fork assembly to front wheel center
Θ_F	=	caster angle of the steer axis
o_F	=	fork offset
r_W	=	undeflected wheel rolling radius
s	=	tire section width

Figures 3.3, 3.4, and 3.5 are typical printed lists of the 36 output variables. The order in which these output variables is presented is determined by input control data to the output processor program. Plotted output variables and scale factors are also controlled by the output processor program, Figure 3.6. Abbreviations and definitions of output variables are given in Table 3.2.

SIMULATION STUDY OF BICYCLE DESIGN PARAMETER CHANGES 27JUN'71
STANDARD BICYCLE WITH 102 LB. RIDER SPEED = 15 MPH (57)

TIME SEC.	DISTANCE FT.	STR ANG DEG.	RDR ROLL DEG.	STR TORQ LB.IN.	RDR TORQ LB.IN.	X FT.	Y FT.	VELOCITY MPH	ROLL DEG.	VEH SLIP DEG.	YAW VEL DEG/SEC	LAT ACC G'S
0.000	0.0	0.0	0.0	0.0	0.0	0.0	0.0	15.00	0.0	0.0	0.0	0.00
0.010	0.22	0.00	0.00	2.00	-0.27	0.22	-0.00	15.00	-0.00	-0.00	-0.02	-0.00
0.020	0.44	0.01	0.00	4.00	-1.22	0.44	-0.00	15.00	-0.00	-0.00	-0.05	-0.00
0.030	0.66	0.03	0.00	6.00	-4.37	0.66	-0.00	15.00	-0.00	-0.00	-0.08	-0.00
0.040	0.88	0.06	-0.00	8.00	-15.65	0.88	-0.00	15.00	0.00	0.00	-0.13	-0.00
0.050	1.10	0.10	-0.00	10.00	-57.43	1.10	-0.00	15.00	0.00	0.04	-0.35	-0.02
0.060	1.32	0.15	-0.03	12.00	-171.04	1.32	-0.00	15.00	0.02	0.12	-0.95	-0.08
0.070	1.54	0.24	-0.07	14.00	-241.75	1.54	-0.00	15.00	0.05	0.15	-0.66	-0.11
0.080	1.76	0.35	-0.10	16.00	-255.16	1.76	-0.00	15.00	0.09	0.12	-0.08	-0.08
0.090	1.98	0.48	-0.11	18.00	-277.16	1.98	-0.00	15.00	0.12	0.12	0.39	-0.05
0.100	2.20	0.64	-0.11	20.00	-293.51	2.20	-0.00	15.00	0.14	0.13	0.94	-0.02
0.110	2.42	0.81	-0.10	22.00	-307.78	2.42	-0.00	14.99	0.15	0.16	1.60	0.02
0.120	2.64	1.01	-0.09	24.00	-319.74	2.64	0.00	14.99	0.17	0.20	2.40	0.05
0.130	2.86	1.21	-0.07	26.00	-329.93	2.86	0.00	14.99	0.17	0.25	3.31	0.08
0.140	3.08	1.43	-0.05	28.00	-338.66	3.08	0.00	14.99	0.17	0.31	4.32	0.10
0.150	3.30	1.65	-0.02	30.00	-346.28	3.30	0.00	14.99	0.16	0.38	5.41	0.12
0.160	3.52	1.88	0.00	30.00	-352.88	3.52	0.01	14.99	0.14	0.44	6.59	0.14
0.170	3.74	2.11	0.03	30.00	-358.64	3.74	0.01	14.99	0.12	0.51	7.86	0.16
0.180	3.96	2.33	0.05	30.00	-363.56	3.96	0.01	14.99	0.08	0.58	9.18	0.17
0.190	4.18	2.55	0.08	30.00	-367.75	4.18	0.02	14.99	0.04	0.64	10.53	0.18
0.200	4.40	2.76	0.10	30.00	-371.25	4.40	0.02	14.99	-0.02	0.69	11.87	0.18
0.210	4.62	2.95	0.12	24.00	-373.69	4.62	0.03	14.98	-0.09	0.73	13.24	0.19
0.220	4.84	3.11	0.14	18.00	-374.75	4.84	0.03	14.98	-0.17	0.78	14.65	0.18
0.230	5.06	3.23	0.16	12.00	-374.17	5.06	0.04	14.98	-0.26	0.80	16.02	0.16
0.240	5.28	3.29	0.18	6.00	-371.62	5.28	0.05	14.98	-0.36	0.81	17.24	0.12
0.250	5.50	3.28	0.19	0.00	-367.10	5.50	0.06	14.98	-0.48	0.79	18.24	0.08
0.260	5.72	3.22	0.19	0.0	-361.12	5.72	0.07	14.97	-0.60	0.73	18.88	0.02
0.270	5.94	3.10	0.20	0.0	-354.29	5.94	0.08	14.97	-0.74	0.63	19.09	-0.04
0.280	6.16	2.96	0.19	0.0	-347.10	6.15	0.09	14.97	-0.89	0.50	18.93	-0.09
0.290	6.38	2.79	0.19	0.0	-340.09	6.37	0.10	14.96	-1.05	0.33	18.45	-0.13
0.300	6.59	2.61	0.18	0.0	-333.58	6.59	0.11	14.96	-1.22	0.14	17.74	-0.16
0.310	6.81	2.43	0.17	0.0	-327.74	6.81	0.12	14.96	-1.40	-0.06	16.86	-0.19
0.320	7.03	2.25	0.16	0.0	-322.44	7.03	0.13	14.95	-1.58	-0.27	15.87	-0.20
0.330	7.25	2.07	0.15	0.0	-317.63	7.25	0.13	14.95	-1.78	-0.48	14.81	-0.20
0.340	7.47	1.90	0.14	0.0	-313.27	7.47	0.14	14.95	-1.98	-0.69	13.73	-0.21
0.350	7.69	1.73	0.12	0.0	-309.15	7.69	0.15	14.94	-2.20	-0.90	12.63	-0.20
0.360	7.91	1.56	0.11	0.0	-305.31	7.91	0.16	14.94	-2.42	-1.10	11.55	-0.20
0.370	8.13	1.39	0.10	0.0	-301.62	8.13	0.17	14.94	-2.64	-1.29	10.47	-0.20
0.380	8.35	1.22	0.09	0.0	-298.21	8.35	0.18	14.94	-2.88	-1.48	9.40	-0.20
0.390	8.57	1.05	0.08	0.0	-294.93	8.56	0.19	14.93	-3.12	-1.67	8.34	-0.21
0.400	8.79	0.88	0.07	0.0	-291.76	8.78	0.20	14.93	-3.37	-1.85	7.28	-0.21
0.410	9.01	0.71	0.06	0.0	-288.77	9.00	0.20	14.93	-3.62	-2.02	6.22	-0.20
0.420	9.22	0.54	0.05	0.0	-285.75	9.22	0.21	14.93	-3.88	-2.20	5.16	-0.20
0.430	9.44	0.37	0.04	0.0	-282.79	9.44	0.22	14.93	-4.14	-2.37	4.10	-0.20
0.440	9.66	0.19	0.03	0.0	-279.83	9.66	0.23	14.93	-4.41	-2.53	3.04	-0.20
0.450	9.88	0.02	0.02	0.0	-276.77	9.88	0.23	14.93	-4.68	-2.69	1.98	-0.20
0.460	10.10	-0.15	0.01	0.0	-273.65	10.10	0.24	14.93	-4.96	-2.84	0.91	-0.21
0.470	10.32	-0.32	-0.00	0.0	-270.50	10.32	0.24	14.93	-5.23	-3.00	-0.17	-0.21
0.480	10.54	-0.49	-0.01	0.0	-267.39	10.54	0.25	14.93	-5.52	-3.14	-1.25	-0.21
0.490	10.76	-0.66	-0.02	0.0	-264.23	10.76	0.25	14.93	-5.80	-3.29	-2.34	-0.21

Figure 3.3 TYPICAL PRINTOUT FROM COMPUTER SIMULATION PROGRAM

STIMULATION STUDY OF BICYCLE DESIGN PARAMETER CHANGES 27JUN'71
STANDARD BICYCLE WITH 102 LB. RIDER SPEED = 15 MPH (57)

TIME SEC.	PATH RAD FT.	Z IN.	PITCH DEG.	YAW DEG.	ROLL VEL DEG/SEC	PTCH VEL DEG/SEC	YAW VEL DEG/SEC	YAW MOM LB.FT.	FNF/TNF	TSF/TNF	TSFP/TNF	TTFP/TNF
0.000	*********	-26.76	0.10	0.0	0.0	0.0	0.0	0.0	0.32	0.0	0.0	0.0
0.010	51752.44	-26.76	0.10	-0.00	-0.01	0.01	-0.02	0.19	0.32	0.00	0.00	0.00
0.020	35686.56	-26.76	0.10	-0.00	-0.05	0.01	-0.05	0.77	0.32	0.00	0.00	0.00
0.030	21135.98	-26.76	0.10	-0.00	-0.19	0.01	-0.08	2.41	0.32	0.00	0.00	0.00
0.040	5435.92	-26.76	0.10	-0.00	-0.71	0.00	-0.13	8.16	0.32	0.02	0.02	0.00
0.050	1272.39	-26.76	0.10	-0.00	-2.68	-0.01	-0.35	29.23	0.32	0.10	0.10	0.00
0.060	408.79	-26.76	0.10	0.00	-7.95	-0.01	-0.96	81.01	0.32	0.28	0.28	0.00
0.070	312.06	-26.76	0.10	0.01	-10.57	-0.01	-0.67	98.86	0.32	0.35	0.35	0.00
0.080	341.40	-26.76	0.10	0.03	-10.42	-0.01	-0.10	91.08	0.32	0.32	0.32	0.00
0.090	358.03	-26.76	0.10	0.05	-10.93	-0.02	0.37	90.76	0.32	0.31	0.31	0.00
0.100	385.29	-26.76	0.10	0.07	-11.35	-0.03	0.92	89.87	0.32	0.30	0.30	0.00
0.110	412.80	-26.76	0.10	0.10	-11.84	-0.04	1.58	89.67	0.32	0.29	0.29	0.00
0.120	438.84	-26.76	0.10	0.14	-12.39	-0.05	2.37	89.57	0.32	0.29	0.29	0.00
0.130	460.07	-26.76	0.10	0.18	-12.99	-0.06	3.28	89.56	0.32	0.28	0.28	0.00
0.140	478.89	-26.76	0.10	0.24	-13.66	-0.05	4.29	89.58	0.32	0.28	0.28	0.00
0.150	492.68	-26.76	0.10	0.31	-14.40	-0.04	5.38	89.62	0.32	0.27	0.27	0.00
0.160	507.72	-26.76	0.10	0.38	-15.20	-0.03	6.57	89.53	0.32	0.27	0.27	0.00
0.170	514.06	-26.76	0.10	0.47	-16.08	-0.02	7.83	89.25	0.32	0.26	0.26	0.00
0.180	513.74	-26.76	0.10	0.58	-17.04	-0.03	9.15	88.72	0.32	0.26	0.26	0.00
0.190	498.67	-26.76	0.10	0.70	-18.06	-0.05	10.50	88.02	0.32	0.26	0.26	0.00
0.200	480.53	-26.76	0.10	0.83	-19.14	-0.08	11.84	87.15	0.32	0.26	0.26	0.00
0.210	467.53	-26.76	0.10	0.97	-20.29	-0.10	13.21	85.78	0.32	0.25	0.25	0.01
0.220	442.96	-26.76	0.10	1.13	-21.45	-0.11	14.61	83.70	0.32	0.25	0.25	0.01
0.230	404.36	-26.76	0.10	1.30	-22.64	-0.12	15.98	81.04	0.32	0.26	0.26	0.01
0.240	362.27	-26.76	0.10	1.48	-23.82	-0.13	17.20	77.96	0.32	0.26	0.26	0.01
0.250	323.08	-26.76	0.10	1.67	-24.97	-0.14	18.19	74.67	0.32	0.27	0.27	0.01
0.260	285.36	-26.76	0.10	1.87	-26.09	-0.17	18.83	71.77	0.32	0.28	0.28	0.01
0.270	258.72	-26.76	0.10	2.08	-27.17	-0.23	19.04	69.71	0.31	0.28	0.28	0.01
0.280	240.93	-26.76	0.10	2.28	-28.20	-0.30	18.87	68.40	0.31	0.29	0.29	0.01
0.290	229.14	-26.75	0.10	2.48	-29.18	-0.38	18.39	67.79	0.31	0.30	0.30	0.01
0.300	221.75	-26.75	0.11	2.68	-30.12	-0.46	17.67	67.70	0.31	0.30	0.30	0.01
0.310	217.74	-26.75	0.11	2.87	-31.03	-0.51	16.79	68.07	0.31	0.31	0.31	0.00
0.320	216.61	-26.75	0.11	3.04	-31.90	-0.55	15.80	68.73	0.31	0.31	0.31	0.00
0.330	217.51	-26.75	0.11	3.21	-32.73	-0.58	14.74	69.64	0.32	0.32	0.32	0.00
0.340	219.87	-26.75	0.10	3.37	-33.52	-0.60	13.65	70.78	0.32	0.32	0.32	0.00
0.350	222.94	-26.74	0.10	3.51	-34.28	-0.62	12.56	72.04	0.32	0.33	0.33	0.00
0.360	225.80	-26.74	0.10	3.65	-35.00	-0.64	11.47	73.42	0.32	0.33	0.33	0.00
0.370	228.34	-26.73	0.10	3.77	-35.69	-0.65	10.38	74.80	0.32	0.34	0.34	0.00
0.380	230.36	-26.73	0.10	3.88	-36.32	-0.64	9.31	76.26	0.32	0.34	0.34	0.01
0.390	232.40	-26.72	0.10	3.98	-36.92	-0.62	8.25	77.67	0.32	0.35	0.35	0.01
0.400	234.81	-26.72	0.10	4.08	-37.47	-0.58	7.19	79.08	0.32	0.35	0.35	0.01
0.410	237.71	-26.71	0.10	4.16	-37.98	-0.55	6.13	80.52	0.32	0.36	0.36	0.01
0.420	241.10	-26.70	0.10	4.23	-38.45	-0.53	5.07	81.89	0.32	0.36	0.36	0.01
0.430	244.36	-26.69	0.10	4.29	-38.87	-0.52	4.01	83.23	0.32	0.37	0.37	0.01
0.440	247.21	-26.68	0.10	4.34	-39.27	-0.51	2.94	84.51	0.32	0.37	0.37	0.02
0.450	249.71	-26.67	0.10	4.38	-39.62	-0.48	1.87	85.71	0.32	0.38	0.38	0.02
0.460	252.06	-26.66	0.10	4.40	-39.93	-0.42	0.80	86.89	0.32	0.38	0.38	0.02
0.470	254.60	-26.65	0.10	4.42	-40.21	-0.33	-0.27	88.15	0.32	0.39	0.39	0.02
0.480	257.83	-26.64	0.09	4.43	-40.45	-0.21	-1.35	89.58	0.32	0.39	0.39	0.02
0.490	261.62	-26.62	0.09	4.42	-40.65	-0.07	-2.42	91.14	0.33	0.40	0.40	0.02

Figure 3.4 TYPICAL PRINTOUT FROM COMPUTER SIMULATION PROGRAM

SIMULATION STUDY OF BICYCLE DESIGN PARAMETER CHANGES 27JUN'71
STANDARD BICYCLE WITH 102 LB. RIDER SPEED = 15 MPH (57)

TIME SEC.	FT SLIP DEG.	FT INCL DEG.	FT NF LB.	FT SF LB.	FT SFP LB.	FT TFP LB.	RR SLIP DEG.	RR INCL DEG.	RR NF LB.	RR SF LB.	RR SFP LB.	RR TFP LB.
0.000	0.0	0.0	-45.52	0.0	0.0	0.0	0.0	0.0	-97.28	0.0	0.0	0.0
0.010	0.00	0.00	-45.50	0.02	0.02	0.00	-0.00	-0.00	-97.29	-0.06	-0.06	-0.00
0.020	0.01	0.01	-45.46	0.12	0.12	-0.00	-0.01	-0.00	-97.32	-0.24	-0.24	-0.00
0.030	0.01	0.01	-45.42	0.17	0.17	-0.00	-0.03	-0.00	-97.33	-0.81	-0.81	-0.00
0.040	-0.02	0.02	-45.41	-0.28	-0.28	0.00	-0.09	0.00	-97.36	-2.90	-2.90	0.00
0.050	-0.20	0.04	-45.45	-2.90	-2.90	0.01	-0.35	0.00	-97.37	-10.79	-10.79	0.01
0.060	-0.75	0.08	-45.49	-10.28	-10.28	0.05	-1.05	0.02	-97.38	-30.35	-30.35	0.06
0.070	-0.98	0.14	-45.52	-13.27	-13.27	0.09	-1.31	0.05	-97.40	-37.19	-37.19	0.10
0.080	-0.86	0.21	-45.51	-11.68	-11.68	0.10	-1.20	0.09	-97.42	-34.15	-34.15	0.07
0.090	-0.80	0.29	-45.45	-10.86	-10.86	0.11	-1.19	0.12	-97.40	-33.87	-33.87	0.07
0.100	-0.72	0.37	-45.38	-9.80	-9.80	0.13	-1.17	0.14	-97.34	-33.34	-33.34	0.08
0.110	-0.65	0.45	-45.35	-8.85	-8.85	0.15	-1.16	0.15	-97.26	-33.08	-33.08	0.09
0.120	-0.59	0.53	-45.35	-8.01	-9.00	0.17	-1.15	0.17	-97.16	-32.87	-32.87	0.12
0.130	-0.53	0.61	-45.41	-7.28	-7.27	0.19	-1.15	0.17	-97.08	-32.71	-32.71	0.14
0.140	-0.49	0.68	-45.49	-6.64	-6.64	0.20	-1.14	0.17	-97.05	-32.59	-32.59	0.18
0.150	-0.45	0.75	-45.54	-6.07	-6.06	0.21	-1.14	0.16	-97.06	-32.49	-32.49	0.21
0.160	-0.41	0.82	-45.52	-5.58	-5.57	0.23	-1.13	0.14	-97.11	-32.35	-32.35	0.25
0.170	-0.39	0.88	-45.51	-5.23	-5.23	0.24	-1.12	0.12	-97.18	-32.19	-32.18	0.29
0.180	-0.37	0.92	-45.48	-5.04	-5.03	0.26	-1.11	0.08	-97.24	-31.96	-31.96	0.32
0.190	-0.37	0.95	-45.44	-4.99	-4.98	0.28	-1.10	0.04	-97.29	-31.70	-31.70	0.35
0.200	-0.38	0.97	-45.44	-5.04	-5.03	0.30	-1.09	-0.02	-97.29	-31.42	-31.41	0.38
0.210	-0.40	0.97	-45.47	-5.30	-5.29	0.34	-1.07	-0.09	-97.25	-30.99	-30.99	0.40
0.220	-0.44	0.95	-45.47	-5.96	-5.95	0.40	-1.05	-0.17	-97.18	-30.40	-30.40	0.41
0.230	-0.52	0.90	-45.41	-7.03	-7.01	0.49	-1.02	-0.26	-97.10	-29.69	-29.69	0.42
0.240	-0.63	0.82	-45.28	-8.44	-8.42	0.60	-0.99	-0.36	-97.05	-28.91	-28.91	0.41
0.250	-0.75	0.71	-45.07	-10.10	-10.08	0.72	-0.96	-0.48	-97.04	-28.10	-28.10	0.39
0.260	-0.89	0.55	-44.83	-11.82	-11.79	0.81	-0.93	-0.60	-97.08	-27.44	-27.44	0.35
0.270	-1.01	0.38	-44.60	-13.32	-13.30	0.87	-0.91	-0.74	-97.17	-27.03	-27.03	0.30
0.280	-1.11	0.17	-44.44	-14.55	-14.52	0.88	-0.90	-0.89	-97.28	-26.83	-26.83	0.23
0.290	-1.19	-0.04	-44.42	-15.52	-15.50	0.84	-0.89	-1.05	-97.38	-26.82	-26.82	0.15
0.300	-1.24	-0.28	-44.51	-16.26	-16.24	0.78	-0.89	-1.22	-97.39	-26.94	-26.94	0.06
0.310	-1.28	-0.52	-44.62	-16.79	-16.77	0.69	-0.90	-1.40	-97.34	-27.18	-27.18	-0.03
0.320	-1.30	-0.77	-44.69	-17.13	-17.12	0.59	-0.91	-1.58	-97.21	-27.48	-27.48	-0.13
0.330	-1.31	-1.03	-44.71	-17.34	-17.33	0.48	-0.92	-1.78	-97.00	-27.84	-27.84	-0.24
0.340	-1.31	-1.30	-44.64	-17.45	-17.45	0.37	-0.93	-1.98	-96.75	-28.26	-28.26	-0.34
0.350	-1.32	-1.57	-44.57	-17.55	-17.54	0.25	-0.95	-2.20	-96.50	-28.72	-28.72	-0.45
0.360	-1.32	-1.85	-44.54	-17.66	-17.66	0.14	-0.96	-2.42	-96.29	-29.22	-29.22	-0.56
0.370	-1.33	-2.14	-44.61	-17.82	-17.82	0.03	-0.98	-2.64	-96.14	-29.74	-29.73	-0.67
0.380	-1.33	-2.44	-44.79	-18.04	-18.04	-0.08	-0.99	-2.88	-96.11	-30.29	-30.28	-0.78
0.390	-1.34	-2.74	-44.97	-18.26	-18.26	-0.20	-1.01	-3.12	-96.16	-30.83	-30.82	-0.90
0.400	-1.34	-3.05	-45.13	-18.46	-18.46	-0.31	-1.02	-3.37	-96.28	-31.36	-31.34	-1.01
0.410	-1.34	-3.37	-45.20	-18.64	-18.63	-0.43	-1.03	-3.62	-96.41	-31.90	-31.88	-1.13
0.420	-1.35	-3.69	-45.22	-18.79	-18.78	-0.54	-1.05	-3.88	-96.51	-32.41	-32.38	-1.24
0.430	-1.35	-4.01	-45.24	-18.95	-18.94	-0.66	-1.06	-4.14	-96.53	-32.91	-32.88	-1.36
0.440	-1.36	-4.34	-45.32	-19.16	-19.14	-0.78	-1.07	-4.41	-96.44	-33.40	-33.36	-1.47
0.450	-1.37	-4.67	-45.49	-19.39	-19.37	-0.90	-1.09	-4.68	-96.26	-33.86	-33.82	-1.59
0.460	-1.37	-5.01	-45.69	-19.64	-19.62	-1.03	-1.10	-4.96	-96.03	-34.33	-34.28	-1.70
0.470	-1.38	-5.35	-45.92	-19.90	-19.87	-1.15	-1.11	-5.23	-95.82	-34.82	-34.77	-1.82
0.480	-1.38	-5.69	-46.06	-20.12	-20.08	-1.27	-1.13	-5.52	-95.67	-35.36	-35.31	-1.94
0.490	-1.38	-6.04	-46.16	-20.32	-20.27	-1.40	-1.15	-5.80	-95.64	-35.95	-35.89	-2.06

Figure 3.5 TYPICAL PRINTOUT FROM COMPUTER SIMULATION PROGRAM

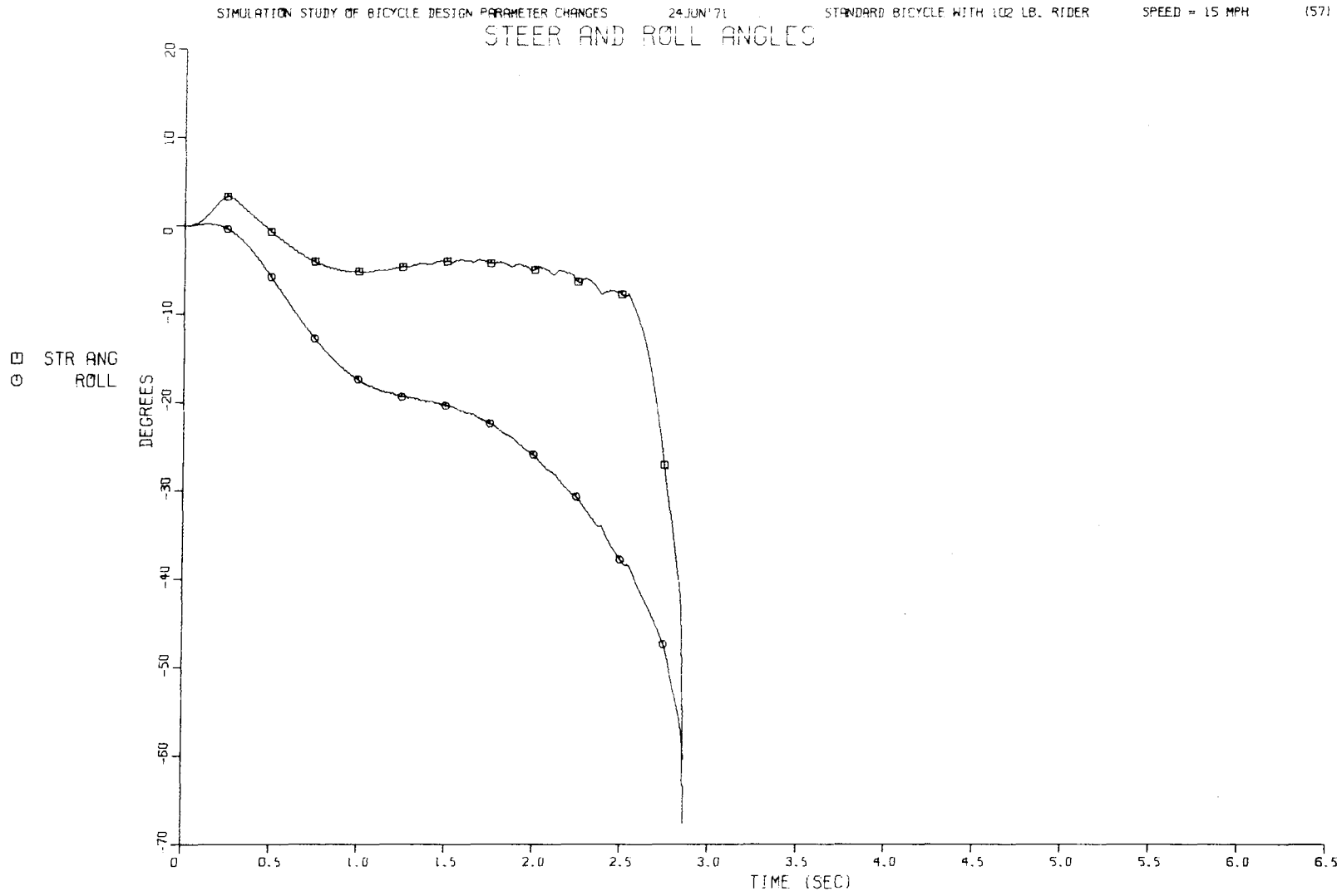

Figure 3.6 TYPICAL PLOTTED OUTPUT FROM COMPUTER SIMULATION PROGRAM

TABLE 3.2

OUTPUT VARIABLE CODE NUMBERS, DEFINITIONS, ABBREVIATIONS AND UNITS

Number	Variable Definition	Abbreviation	Unit
1	Simulation Time	TIME	sec.
2	Path Distance	DISTANCE	ft.
3	Steer Angle	STR ANG	deg.
4	Rider Roll Angle	RDR ROLL	deg.
5	Steer Torque	STR TORQ	lb. in.
6	Rider Roll Torque	RDR TORQ	lb. in.
7	Space X Coordinate of Origin	X	ft.
8	Space Y Coordinate of Origin	Y	ft.
9	Total Bike Velocity	VELOCITY	mph.
10	Roll Angle	ROLL	deg.
11	Vehicle Slip Angle	VEH SLIP	deg.
12	Yaw Velocity Relative to Vertical	YAW VEL	deg./sec.
13	Lateral Acceleration	LAT ACC	g's
14	Path Radius	PAT RAD	ft.
15	Space Z Coordinate of Origin	Z	in.
16	Pitch Angle	PITCH	deg.
17	Yaw Angle	YAW	deg.
18	Roll Velocity	ROLL VEL	deg./sec.
19	Pitch Velocity	PTCH VEL	deg./sec.
20	Yaw Velocity Relative to Bike	YAW VEL	deg./sec.
21	Yaw Moment on Bike	YAW MOM	lb. in.
22	Ratio of Front Normal Force to Total Normal Force	FNF/TNF	
23	Ratio of Total Side Force to Total Normal Force	TSF/TNF	
24	Ratio of Total Side Force Relative to Path to Total Normal Force	TSFP/TNF	
25	Ratio of Total Tractive Force Relative to Path to Total Normal Force	TTF/TNF	
26	Front Wheel Slip Angle	FT SLIP	deg.
27	Front Wheel Inclination Angle	FT INCL	deg.
28	Front Normal Force	FT NF	lb.
29	Front Side Force	FT SF	lb.
30	Front Side Force Relative to Path	FT SFP	lb.
31	Front Tractive Force Relative to Path	FT TFP	lb.
32	Rear Wheel Slip Angle	RR SLIP	deg.
33	Rear Wheel Inclination Angle	RR INCL	deg.
34	Rear Normal Force	RR NF	lb.
35	Rear Side Force	RR SF	lb.
36	Rear Side Force Relative to Path	RR SFP	lb.
37	Rear Tractive Force Relative to Path	RR RFP	lb.

4.0 MEASUREMENT OF PHYSICAL CHARACTERISTICS OF BICYCLE AND RIDER

Experimental measurements were made to determine the physical characteristics of the bicycle and rider necessary for mechanization of the computer simulation. Three basic groups of data were obtained: (1) weights, dimensions, and mass moments and products of inertia of the major bicycle components (frame, front fork, and wheels), (2) bicycle tire side force characteristics as functions of normal load, slip angle, and inclination angle, (3) dimensions and mass moments of inertia of a typical (102 pound) rider.

4.1 Physical Characteristics of Bicycle Components

The experimental bicycle was a special 22 inch single speed Schwinn Suburban with coaster brakes. The resultant measurements of this bicycle are given in Table 2.1. Weight measurements were obtained with the use of a platform scale having a resolution of $\pm$ 0.1 lb. Linear dimensions were measured with scales having a resolution of $\pm$ 0.05 inch while angular measurements were obtained with a vernier inclinometer having $\pm$ 1/2^{o} resolution. In some cases, specific dimensions were obtained by calculation using other measured parameters. The longitudinal center of gravity (C.G.) position of the total bicycle was calculated from measurements of the front/rear wheel weight distribution and the wheelbase dimension, while the vertical C.G. position was located by determining the intersection between the longitudinal C.G. axis and a line projected from a point suspending the bicycle. The bike was suspended from several single points such that a measurement accuracy of $\pm$ 1/8 inch was obtained. A measurement of the C.G. position of the front fork assembly was developed

by suspending the assembly from a wire and determining its gravitational balance point. The caster trail dimension was developed from computations involving the measured geometry describing the ground plane projections of the steer axis and the vertical axis of the front wheel.

The moment of inertia parameters of the total bicycle, the front fork assembly, and the tire/rim assembly were experimentally determined using a torsional pendulum. The theory of the measurement technique and the resulting errors developed by the process are discussed below.

Each test inertia was attached to a long slender steel rod and set into angular oscillation. A measurement of the period of oscillation was converted to the moment of inertia by appropriate calculation. A single oscillatory degree of freedom was maintained by placing a bearing just above the test inertia to prevent radial movement of the torsion bar. The test component was balanced at its C.G. so that negligible side force existed at the bearing.

The majority of the bike components were easily attached to the rod but in a few cases, fixtures of significant inertia had to be fabricated to secure the more awkward components. In such cases, appropriate corrections were applied to the experimental data to account for fixture inertia.

A fundamental test method for obtaining the mass moment of inertia of any body is by the use of a torsional pendulum. The combination of the inertia coupled to a torsional spring simulates a second order system with negligible damping. Bearing restrictions should be minimal in that the system is free to oscillate without decay. In addition, it is essential that the test object be oriented with its C.G. on the rotational axis of the pendulum to eliminate any bending moments that might contaminate the angular oscillation of the system. Figures 4.1 thru 4.7 demonstrate several examples of bicycle and component arrangements and test apparatus.

It can be shown that an expression for the natural frequency of oscillation of an undamped second order system can be written as:

$$f_n = \frac{1}{2\pi}\sqrt{\frac{K_\theta}{I}}$$

Since the period of oscillation (T) is the reciprocal of the natural frequency (f_n), this expression can be solved for the moment of inertia as a function of the measured period of oscillation as follows.

$$I = \frac{K_\theta T^2}{4\pi^2} \text{ (LB.-IN.-SEC.}^2\text{)}$$

It is customary to use a long slender rod of such dimension that an easily measured period of oscillation is obtained, approximately one second. In addition, use of a long rod minimizes end effects at the attachments

FIGURE 4.1

Measuring the roll moment of inertia of the entire bicycle with a seven foot torsional spring.

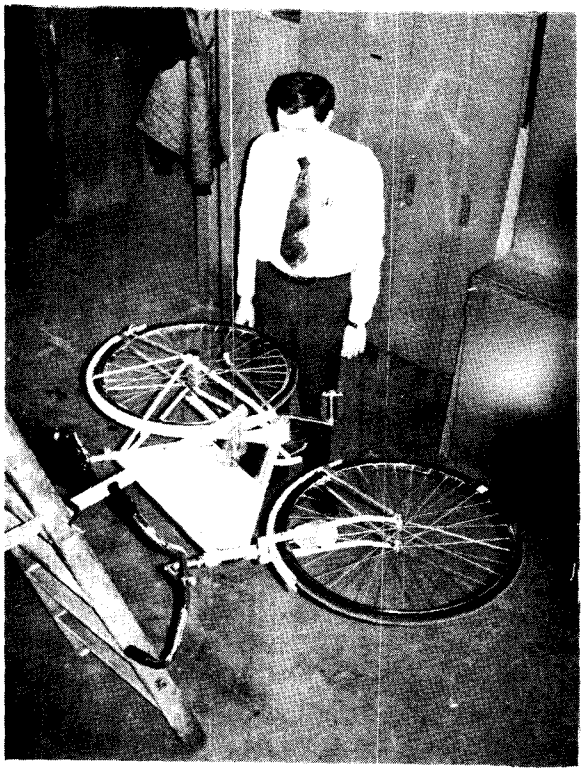

FIGURE 4.2

Measuring the pitch moment of inertia of the entire bicycle with a ten foot torsional spring.

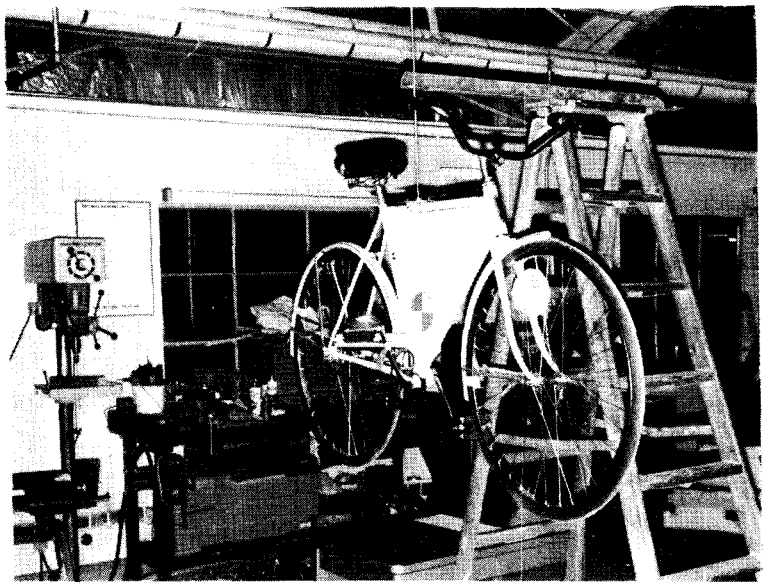

FIGURE 4.3

Measuring the yaw moment of inertia of the entire bicycle with a seven foot torsional spring.

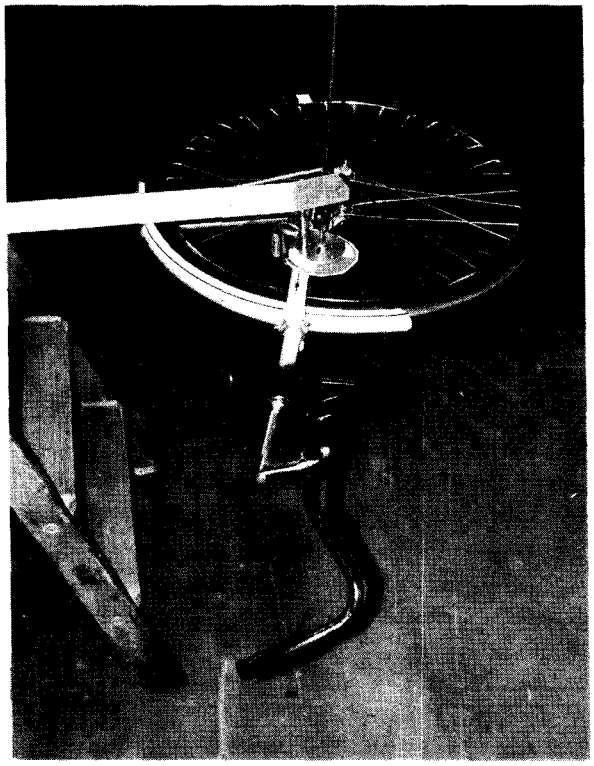

FIGURE 4.4

Measuring the pitch moment of inertia of the front fork assembly with a ten foot torsional spring.

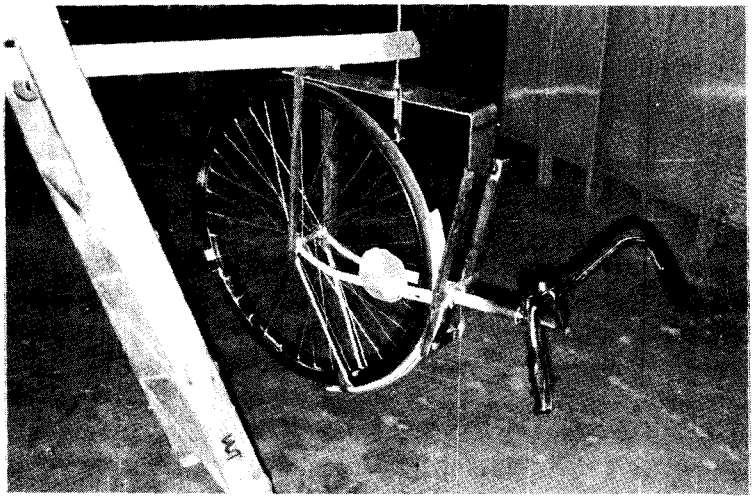

FIGURE 4.5

Measuring the roll moment of inertia of the front fork assembly about an axis through its c.g. perpendicular to the steer axis.

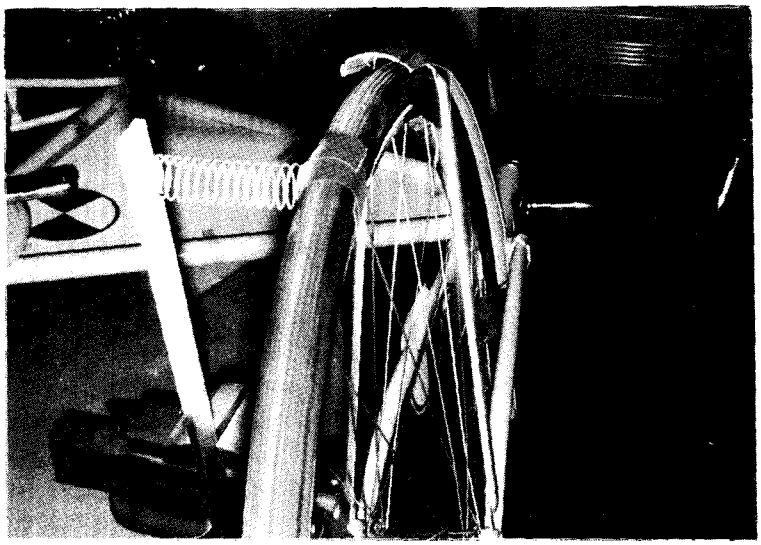

FIGURE 4.6

Measuring the moment of inertia of front fork assembly and handle bars about steer axis with calibrated coil spring.

FIGURE 4.7

Measuring the spin moment of inertia of a wheel with a ten foot torsional spring.

where non-uniform shear stress distributions can exist. The "spring rate" (K_θ) of the torsion bar can be calculated using an expression relating the moment (M_t)-angular deflection (θ) conditions in a cylinder of homogeneous composition. This expression is derived in the following manner.

$$M_t = \frac{\theta \pi d^4 G}{32 l}$$

Therefore:

$$K_\theta = \frac{M_t}{\theta} = \frac{\pi d^4 G}{32 l} \qquad \text{(IN. LB. / RADIAN)}$$

Where (d) is the diameter and (l) is the length of the rod and (G) is the shear modulus of elasticity of the rod material (usually steel, $G = 1.2 \times 10^7$ PSI). It is essential that the angular deflection of the pendulum be small so that K_θ remains a linear parameter. The maximum deflection based on material yield stress can be computed from the expression derived below.

Given the maximum shear stress (τ) expression;

$$\tau = \frac{M_t d}{2J} = \frac{16 M_t}{\pi d^3} \qquad (J = \text{polar moment of inertia})$$

and substituting the previous moment expression yields a result relating the maximum angular deflection in terms of shear stress.

$$\theta_{max} = \frac{2 \tau l}{dG} \qquad \text{(RADIAN)}$$

As a practical matter it is desirable to keep the angular deflections small, say 1/10 θ_{max}, thus insuring that the system oscillates in a strain region that corresponds to the linear elastic region of the rod material.

Occasionally, it is necessary to attach the unknown inertia to the torsion bar with a fixture that contributes significantly to the combined inertia of the system, Fig. 4.5. Assuming that the fixture and the unknown inertia have their centers of gravity on the axis of rotation, the test inertia can be computed, knowing the period of oscillation of the fixture (T_f) and the combined assembly (T), using the following.

Since $$f_n = \frac{1}{2\pi}\sqrt{\frac{K_\theta}{I + I_f}}$$

this yields an expression for the test inertia,

$$I = \frac{K_\theta}{4\pi^2}(T + T_f)(T - T_f)$$

The period of oscillation can be timed with a stopwatch having a resolution of .01 second. Several periods should be timed consecutively so that start-stop timing errors are minimized.

The product moments of inertia were obtained from computations involving the moments about the fixed bike coordinates and another moment value obtained from a rotated position of the coordinate system. A rotational transformation expression for the coordinate system shown in Figure 4.8 was employed in calculating the product moments from computed values of the appropriate inertias and the measured angle of rotation. The expression, given in Reference 13 and solved for the product moment of inertia, is as follows.

$$I_{xy} = \frac{-I_{x'y'} + I_{yy}\sin^2(\alpha + \pi/2) + I_{xx}\cos^2(\alpha + \pi/2)}{2\sin(\alpha + \pi/2)\cos(\alpha + \pi/2)}$$

Where I_{xx} and I_{yy} are the roll and yaw moments of inertia of the total bicycle with respect to the ground plane and $I_{z'z'}$ is the moment about an axis of the rotated coordinate system. A similar technique was employed in obtaining the product moment I_{xz} of the fork assembly.

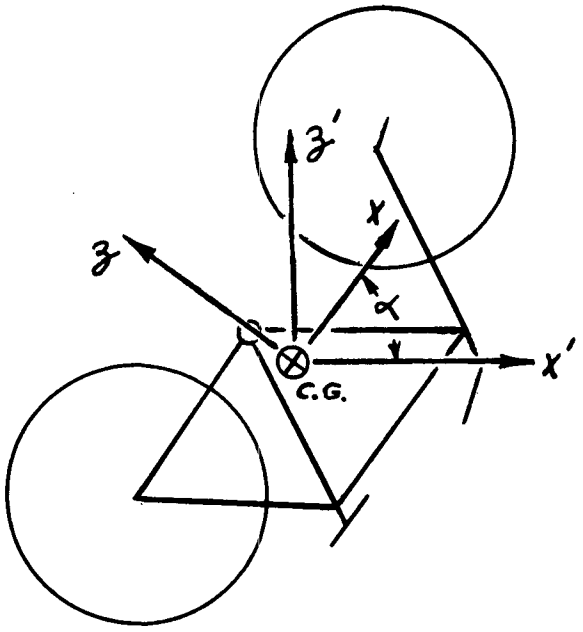

FIGURE 4.8

Results of the indirect measurement techniques used to compute moments of inertia can be analyzed to determine their influence on the accuracy of the calculated values. Table 4.1 is a summary of the analysis. The number of observations represents the number of independent time intervals where a consecutive number of oscillations were timed, usually 5, 10, 15 or 20 periods. Total time divided by the cycle count produced an average period for that observation. The number of periods timed represents the cumulative total of all observations. The mean period is a mean average of the average periods for all observations. Computed values of each inertia are developed from the expression given previously using the mean period and in some instances are not corrected to eliminate fixture inertia. Standard deviations calculated for each moment of inertia are based on theory developed in Reference 5 to approximate the standard deviation of computed results. Briefly, the development of the analysis is as follows.

Given a function relating the moment of inertia to measured variables T, the period of oscillation, and K_θ the torsional spring constant, the standard deviation of the computed result can be calculated using the expression developed as follows:

$$\sigma_I \approx \left[\left(\frac{\partial I}{\partial T}\Big|_{\bar{T},\bar{K}_\theta} \sigma_T \right)^2 + \left(\frac{\partial I}{\partial K_\theta}\Big|_{\bar{T},\bar{K}_\theta} \sigma_{K_\theta} \right)^2 \right]^{1/2}$$

since $$I = f(T, K_\theta) = \frac{K_\theta T^2}{4\pi^2}$$

then $$\sigma_I \approx \left[\left(\frac{\bar{T}\bar{K}_\theta}{2\pi^2} \sigma_T \right)^2 + \left(\frac{\bar{T}^2}{4\pi^2} \sigma_{K_\theta} \right)^2 \right]^{1/2}$$

Table 4.1

BICYCLE INERTIA PARAMETERS
- MEASUREMENT SUMMARY -

	Test Condition	No. of Observations	Total No. Periods Timed	Test Method	Period of Oscillation (Sec.) Mean	Period of Oscillation (Sec.) Standard Deviation	Moments of Inertia (Lb. In. Sec.^{2}) Computed Value	Moments of Inertia (Lb. In. Sec.^{2}) Corrected Value	Moments of Inertia (Lb. In. Sec.^{2}) Computed Std. Deviation
Total Bike	I_{xx}	13	155	1	3.04	.0248	12.76*	11.31	.2138
	I_{yy}	10	56	2	5.97	.0157	34.50		.2638
	I_{zz}	11	96	1	4.28	.0219	25.10		.2771
Fork Assy.	I_{xx}	11	115	2	2.47	.0112	5.91*	4.59	.0627
	I_{yy}	9	90	2	2.40	.0102	5.56		.0563
	I_{zz}	16	230	3	0.73	.0135	1.81**	1.86	.0673
Std. Tire & Rim	I_{xx}	8	105	2	0.99	.0072	0.94		.0147
	I_{yy}	10	150	2	1.35	.0060	1.76		.0185
Total Bike	I_{xz} ($\alpha = 47.5^\circ$)	10	56	2	4.47	.0302	-1.62		.330
Fork Assy.	I_{xz} ($\alpha = 30^\circ$)	7	85	2	2.26	.0115	-0.27	-0.32 (Avg.)	.066
	($\alpha = -45^\circ$)	9	90	2	2.07	.0105	-0.37		.087

Test Method 1 - 0.25 in. dia., 7 ft. lg. torsion bar, K_θ = 54.45 in. lb. / rad.

2 - 0.25 in. dia., 10 ft. lg. torsion bar, K_θ = 38.05 in. lb. / rad.

3 - Linear spring (K = 0.69 lb. / in.) at 14 in. radius

$K_\theta = Kr^2 =$ 135 in. lb. / rad.

* Values not corrected for fixture inertia.

** Corrected for bent fork.

Approximate values of the standard deviation of the computed moments of inertia were obtained by substituting the appropriate mean values ($\bar{T}$, $\bar{K}_\theta$), and the standard deviations of their means (σ_T , σ_{K_θ}).

A similar analysis was used to determine the standard deviation of the computed product moments of inertia. The expression relating the product moment to other measured inertia values given previously can be used to derive an expression for standard deviation in the following manner.

since $$I_{xz} = f\left(I_{z'z'}, I_{zz}, I_{xx}\right)$$

The function can be simplified by assigning coefficients that are functions of the coordinate system rotation (α).

$$I_{xz} = - C_1 I_{z'z'} + C_2 I_{zz} + C_3 I_{xx}$$

Where $$C_1 = \frac{1}{SIN\,(2\alpha + \pi)}$$

$$C_2 = \frac{SIN^2\,(\alpha + \pi/2)}{SIN\,(2\alpha + \pi)}$$

$$C_3 = \frac{COS^2(\alpha + \pi/2)}{SIN\,(2\alpha + \pi)}$$

Then $$\sigma_{I_{xz}} \approx \left[\left(\frac{\partial I_{xz}}{\partial I_{z'z'}} \sigma_{I_{z'z'}}\right)^2 + \left(\frac{\partial I_{xz}}{\partial I_{zz}} \sigma_{I_{zz}}\right)^2 + \left(\frac{\partial I_{xz}}{\partial I_{xx}} \sigma_{I_{xx}}\right)^2\right]^{1/2}$$

and

$$\frac{\partial I_{xz}}{\partial I_{z'z'}} = - C_1 \;;\; \frac{\partial I_{xz}}{\partial I_{zz}} = C_2 \;;\; \frac{\partial I_{xz}}{\partial I_{xx}} = C_3$$

Therefore

$$\sigma_{I_{xz}} \approx \left[\left(-C_1 \sigma_{I_{z'z'}}\right)^2 + \left(C_2 \sigma_{I_{zz}}\right)^2 + \left(C_3 \sigma_{I_{xx}}\right)^2\right]^{1/2}$$

In all cases, the average torsional spring constant used was obtained by averaging the results of calibrations of the rod, calculated values, and values computed from tests of known (calculated) inertias. A value of σ_{K_θ} = 0.21 IN. LB./RAD. was obtained for both the 7 and 10 ft. rods.

Considering the standard deviations computed for the moments of inertia, a 2σ deviation represents a range of 1.6 to 7.4 percent spread in the results obtained by this test method. As would be expected, the standard deviations of the product moments are large by comparison since they rely on the combined effects of the moment measurements themselves. Much of the error in determining product moments arises from the analytical technique involving small differences between large quantities.

Improved accuracy could be realized by the addition of a more sophisticated means of timing the period of oscillation since timing errors contribute the major influence in the data spread. An electronic counter gated by a light beam interrupter serves as an example of more accurate timing.

4.2 Bicycle Tire Tester and Measurement of Tire Side Force Characteristics

A thorough review of the published literature on bicycle research revealed no knowledge of the side force characteristics of bicycle tires. Having given consideration to the significance of this data in developing a simulation of the dynamic performance of bicycles, an on-road bicycle tire tester was designed and constructed. The tire tester was designed to be towed behind an automobile and to have the capability of measuring bicycle tires of all sizes. Tire normal load, slip angle, and inclination angle are variable with ranges of 35 to 150 pounds, -3 to +10 degrees and -6 to +45 degrees, respectively.

The tire tester uses a strain gage bridge, Figure 4.13, mounted on a cantilever beam and an on-board strip-chart recorder to measure side force. The beam is rigidly attached to the rear structure of the tester which supports the bicycle wheel. This rear structure is attached to the triangular box-shaped front section, Figure 4.11, by a bearing which allows only rotation about a vertical axis. The tire side force produces a moment about the bearing axis which is reacted by the indexing block, Figure 4.14, at the end of the cantilever beam. The strain in the beam is measured and converted into tire side force.

The triangular box-shaped front section is hinged to the back of the tow vehicle, Figure 4.12, where screw brackets are used to zero the pitch and camber angles of the test rig. Tire slip angle is changed by moving the indexing block which constrains the end of the cantilever beam. Inclination angle is changed by disassembling the rear structure and bolting it back together in a new location, Figure 4.10. Normal load is changed by placing barbell weights on a support rod directly above the bearing.

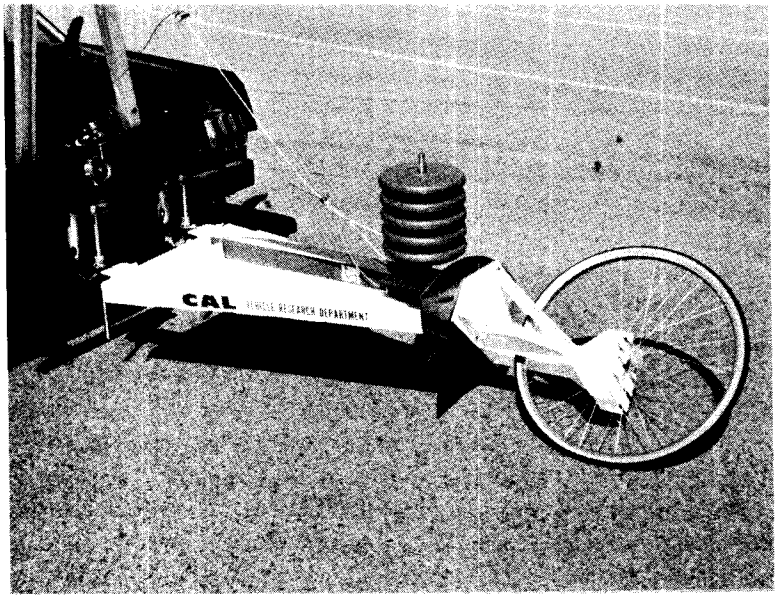

FIGURE 4.9

Bicycle tire tester with wheel set at 45 degrees inclination angle.

FIGURE 4.10

Rear view of bicycle tire tester showing tow vehicle and crane for lifting test rig.

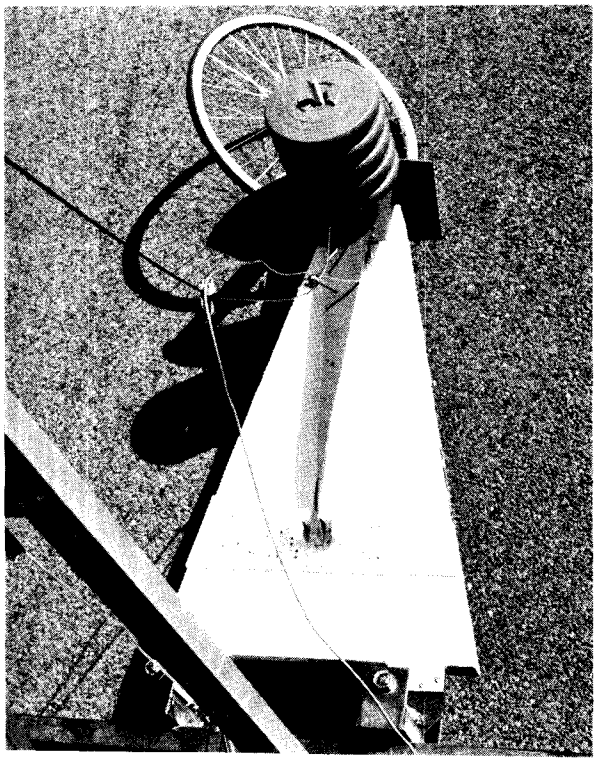

FIGURE 4.11

Top view of bicycle tire tester.

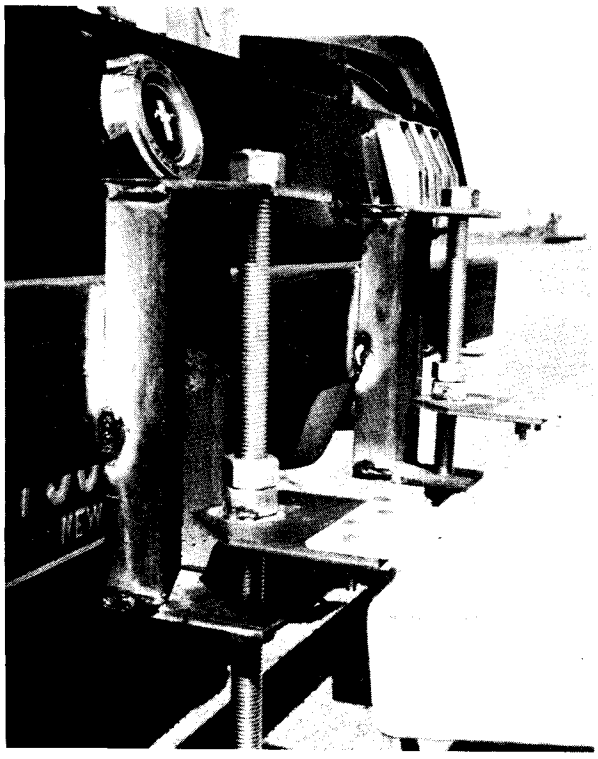

FIGURE 4.12

Screw brackets for adjusting pitch and camber angle of test rig.

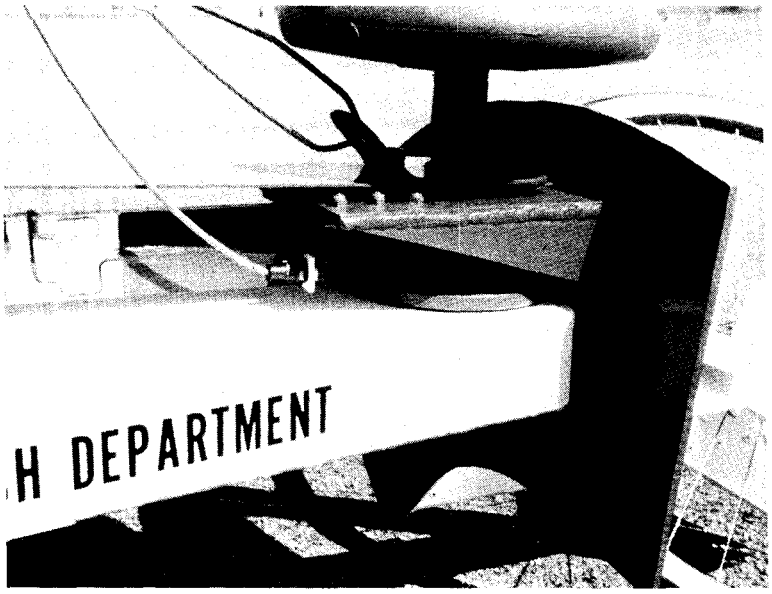

FIGURE 4.13

Strain gage bridge for measuring side force.

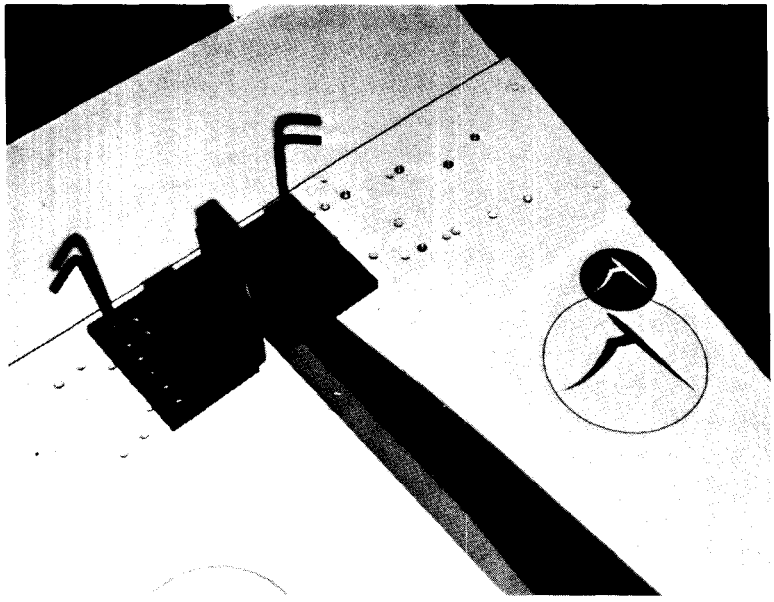

FIGURE 4.14

Indexing block for wheel steer angle.

The tire test rig was towed approximately five miles per hour over a sealed asphalt surface. The order of changing the test conditions was: first, normal load; second, slip angle; last, camber angle. This order was chosen because of the relative difficulty in varying the three parameters. The filtered signal from the strain gage bridge was recorded on a strip chart recorder and the side force was taken as the measured average of the recorded data. A digital voltmeter was also used for immediate visual readout of the side force.

The Puff High Pressure Road Racer and Breeze Sports Touring tires were tested. Plots of the reduced data show significant differences in the side force characteristics of the two types of tires. Both tires were tested at actual normal loads of 36.4, 73.4, and 105.5 pounds. The first tire tested was the Puff at inclination angles of 0, 6, 15, 25 and 35 degrees for a slip angle range of 0 to 4 degrees. After having observed the plotting data for the Puff tire, the range of measurement for the Breeze was increased to inclination angles of 0, 10, 20, 30 and 40 degrees for an increased slip angle range of 0 to 6 degrees.

The following corrections were made to the measured data:

(a) Because of the bending of the cantilever beam on which the strain gage bridge is mounted, the true slip angle of the tire is less than the nominal slip angle of the test rig. The steer compliance correction is 0.033 degrees of slip angle per pound of side force.

(b) Because of coupling in the test rig, the strain gage bridge indicates a side force when the inclination angle and slip angle are non-zero although the true slip angle is actually zero.

This side force correction is a nonlinear function of indicated slip angle, inclination angle, and normal load. The maximum correction for this coupling effect is approximately 5 pounds occurring at the 40 degree inclination angle, 8 degree indicated slip angle, 36.4 pound normal load test condition.

(c) It is practically impossible to align the tire in the test rig precisely at zero slip angle. To account for this inherent error in the zero slip angle, the plotted data is offset by an amount equal to the corrected slip angle at which the corrected side force is zero.

Measured and corrected numerical data are given in Appendix I and carpet plots of the final curves of side force versus slip angle and inclination angle are shown in Figures 4.15 through 4.20.

The "vertical" curves of the side force versus slip angle with inclination angle held constant are third order polynominal fits (least mean squared error criterion) to the corrected data for that specific normal load.

The "horizontal" curves of side force versus inclination angle with slip angle held constant are higher order "computer faired" curves and do not represent a statistical fit to the data.

It is apparent from the plotted data that there is a fundamental difference in the side force characteristics of these two tires. The camber thrust of the Puff tire is highly nonlinear with inclination angle, thus accounting for the overlapping curves. The camber stiffness (change in camber thrust per degree of inclination angle) of the Breeze tire, however, is not greatly changed by increasing the inclination angle (up to 40 degrees).

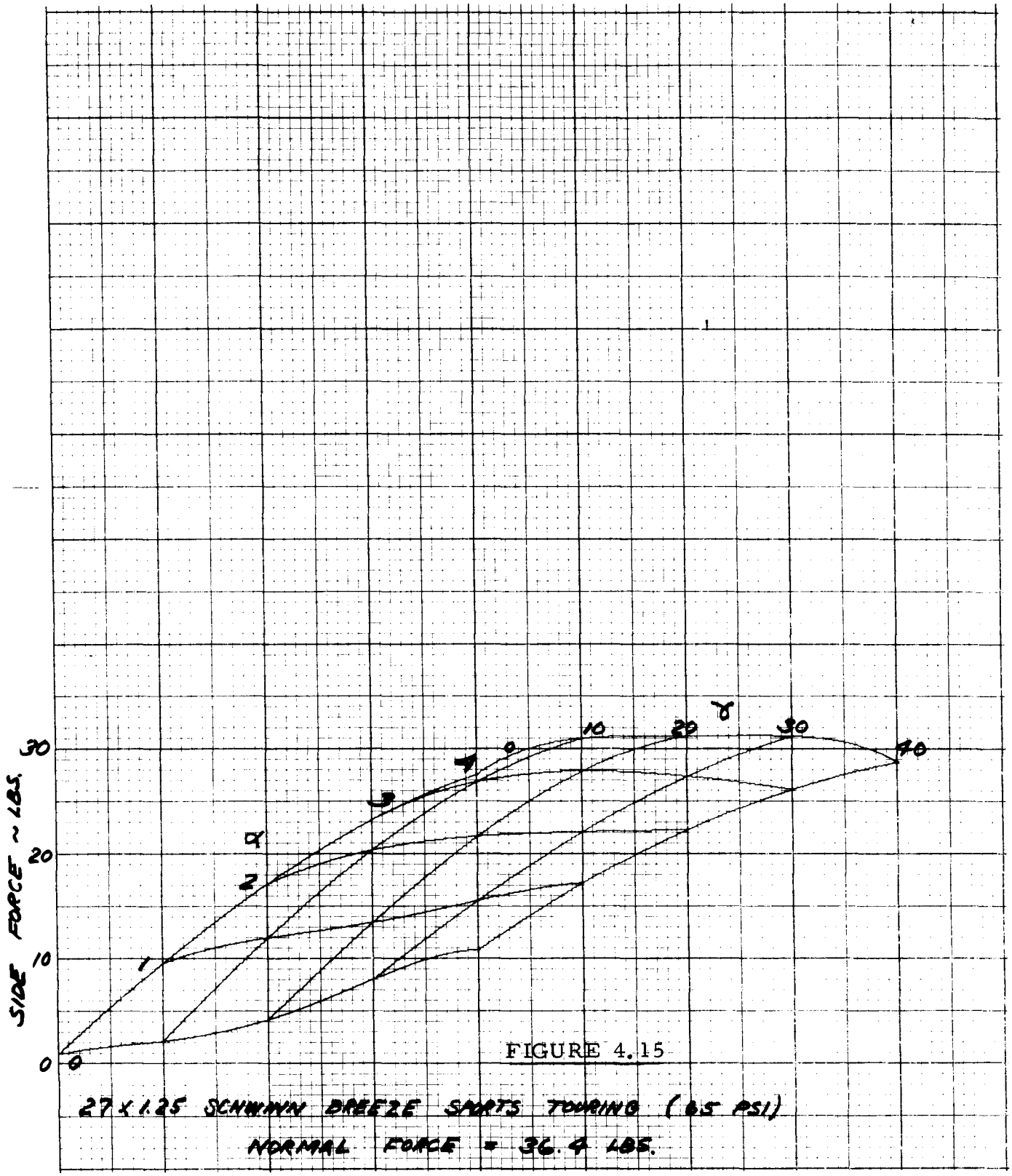

FIGURE 4.15

27 x 1.25 SCHWINN BREEZE SPORTS TOURING (65 PSI)
NORMAL FORCE = 36.4 LBS.

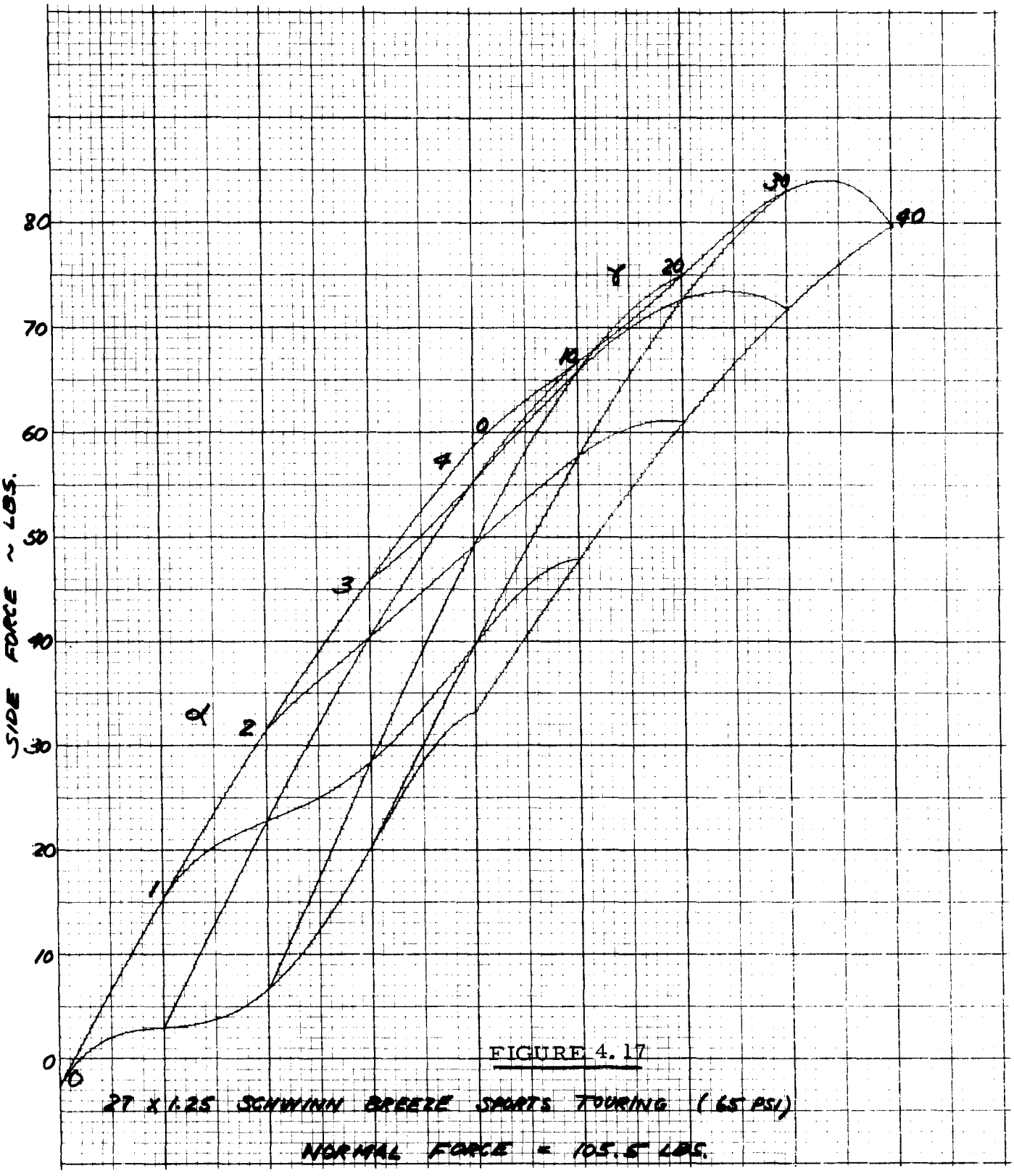

FIGURE 4.17

27 x 1.25 SCHWINN BREEZE SPORTS TOURING (65 PSI)

NORMAL FORCE = 105.5 LBS.

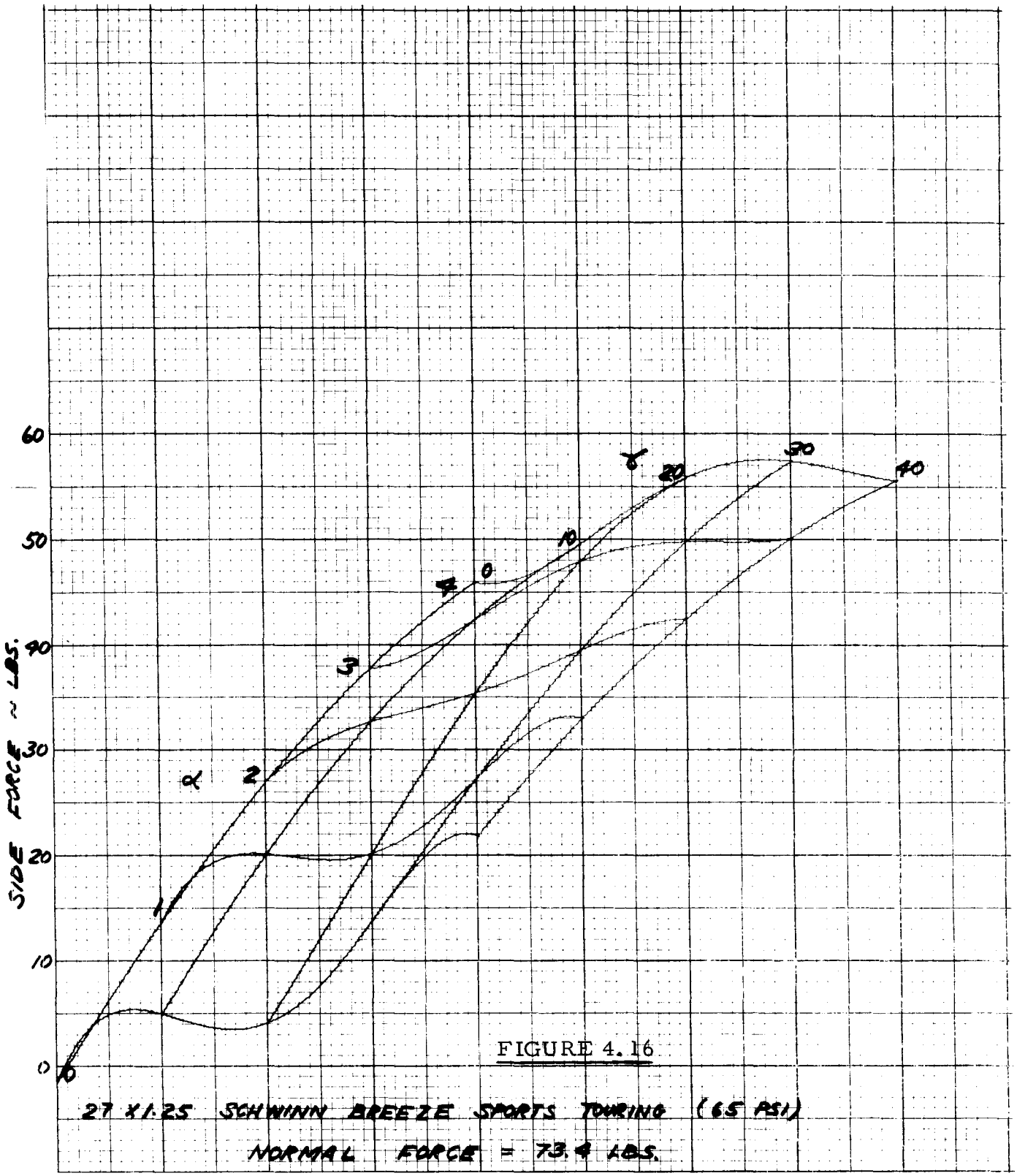

FIGURE 4.16

27 X 1.25 SCHWINN BREEZE SPORTS TOURING (65 PSI)

NORMAL FORCE = 73.4 LBS.

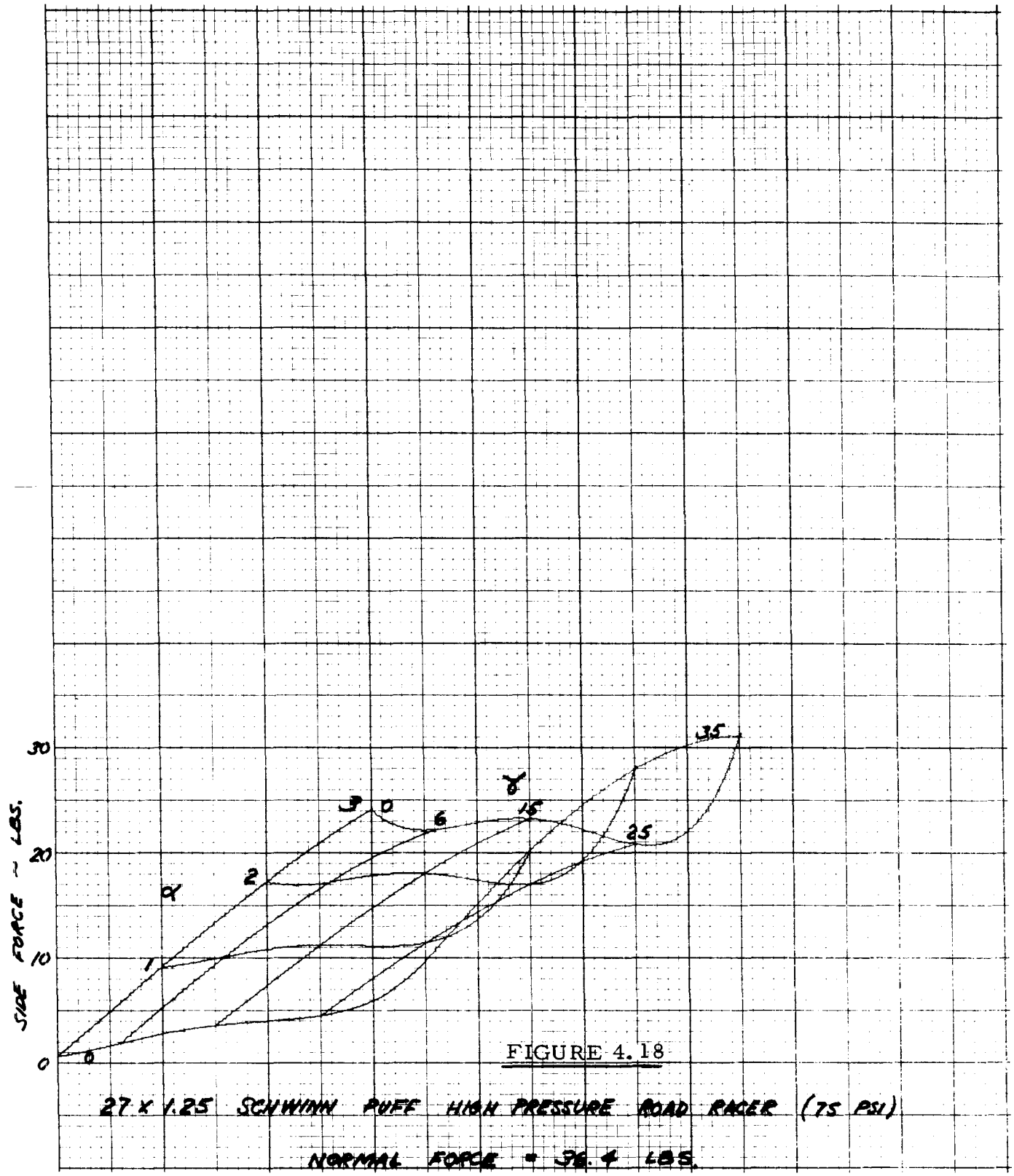

FIGURE 4.18

27 x 1.25 SCHWINN PUFF HIGH PRESSURE ROAD RACER (75 PSI)

NORMAL FORCE = 36.4 LBS.

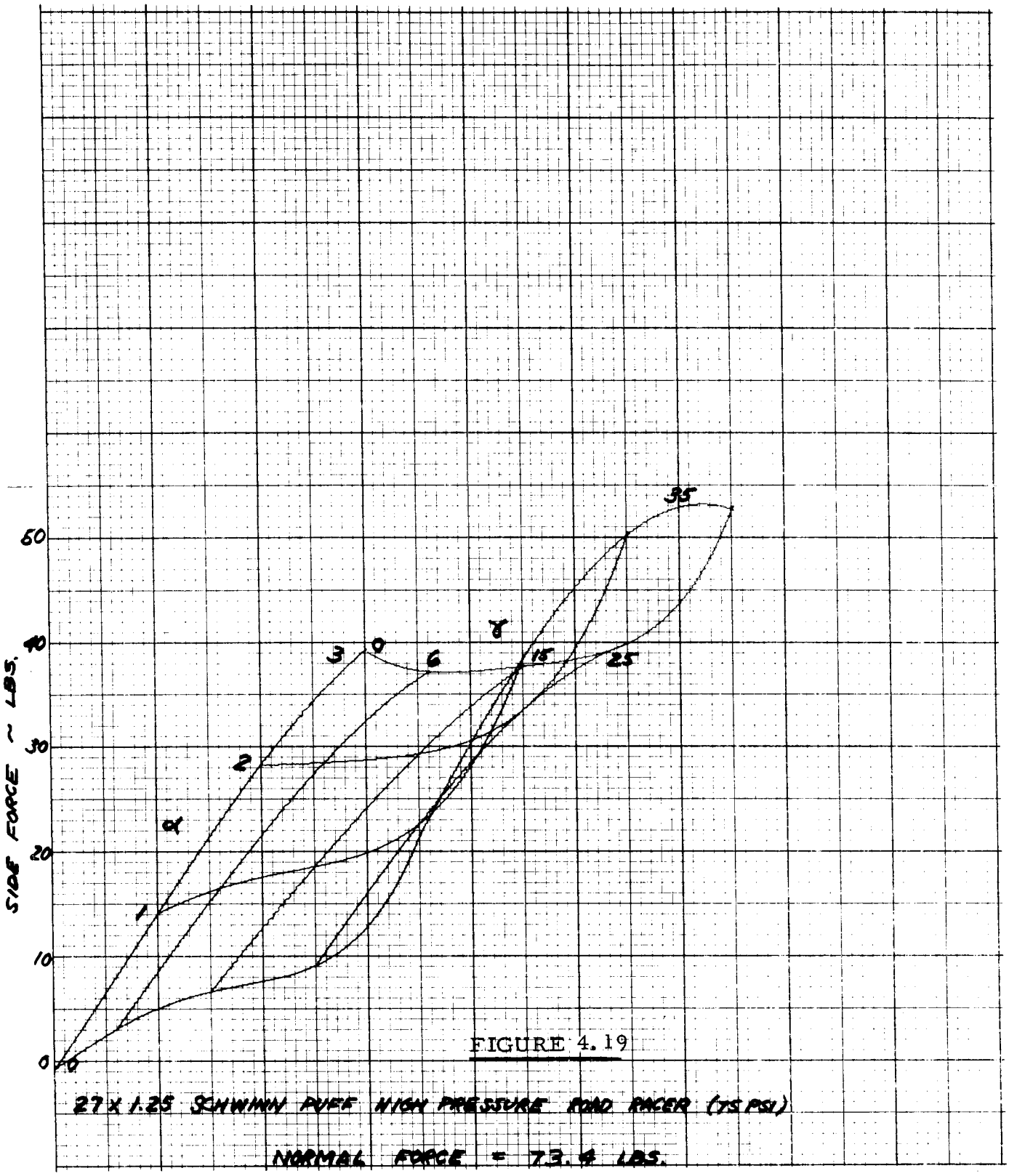

FIGURE 4.19

27 x 1.25 SCHWINN PUFF HIGH PRESSURE ROAD RACER (75 PSI)

NORMAL FORCE = 73.4 LBS.

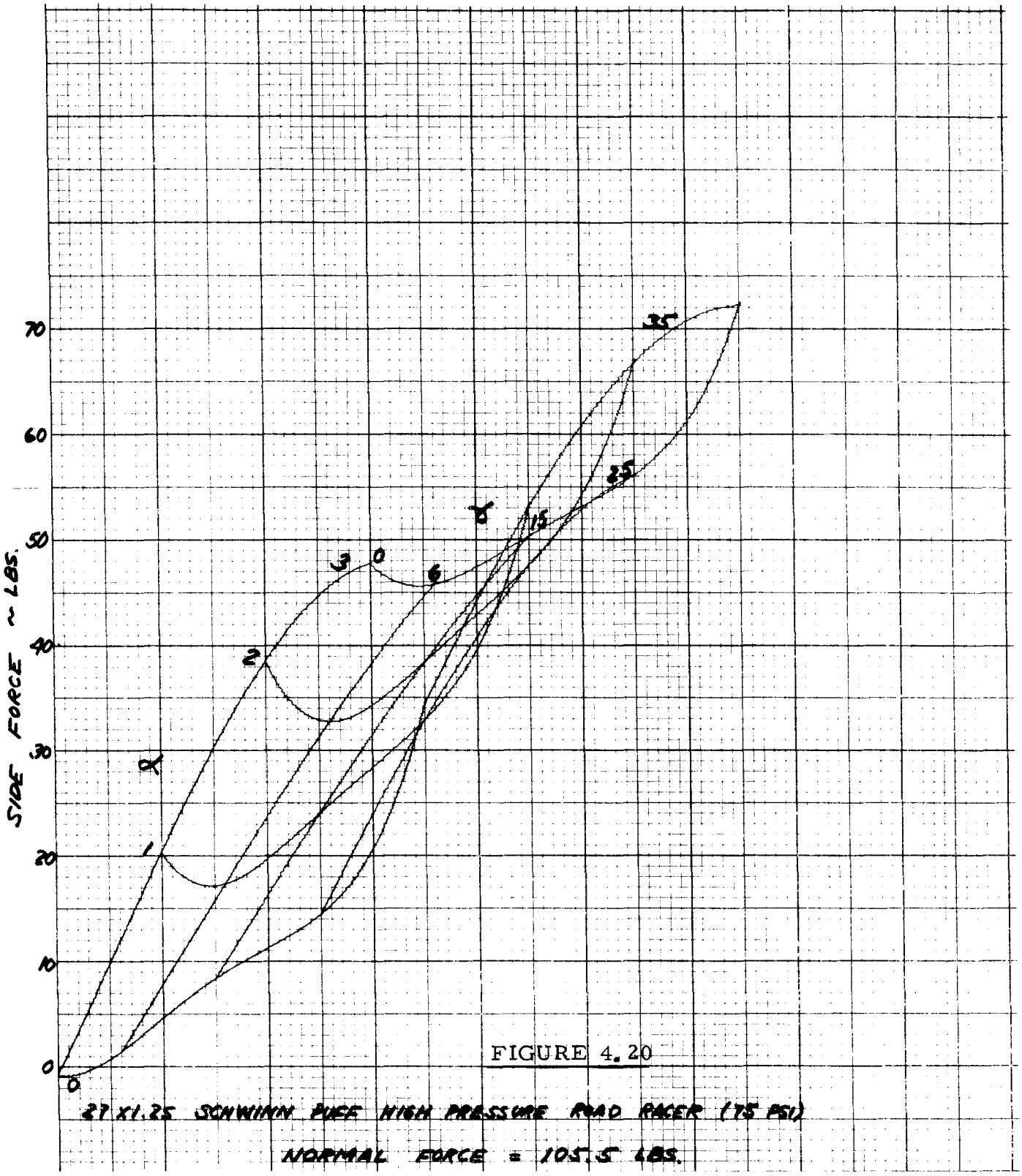

FIGURE 4.20

27 X 1.25 SCHWINN PACE HIGH PRESSURE ROAD RACER (75 PSI)

NORMAL FORCE = 105.5 LBS.

4.3 Physical Characteristics of Typical Rider

Parameter data representing a bicycle rider were developed from computations involving published data for a 5th percentile female anthropometric device. Estimates of the center of gravity and moments of inertia for the device in a riding position were obtained from calculations using the measured mass, inertia and C.G. locations of the basic body components. The roll pitch and yaw moments of inertia of the total rider about its C.G. were determined by summing the appropriate component inertias and their respective mass transfer terms. The center of gravity position of the total rider in the x-z plane was established from mass distribution calculations involving the body components. A conservative estimate of accuracy for the computed parameters is believed to be ten percent.

Results of the analysis are given in Table 4.2. The radial distance from the total body C.G. to the C.G. of a given component was scaled from a schematic (Figure 4.21) of the body oriented in a sitting position. Component dimensions, masses, moments of inertia, and C.G. positions were obtained from Reference 10. The reference describes parametric data with respect to the I_{yy} (pitch) axis and in certain cases component inertias (e.g., upper and lower arms and legs and torso) with respect to the roll and yaw axis were estimated using analytical methods outlined in the reference. The effect on accuracy of these estimates is small since the mass transfer terms dominate in determining the total moment of inertia. The analysis is useful in determining inertia parameters for a rider in other positions and simply requires a different component schematic to determine the appropriate mass transfer terms.

Figure 4.21 RIDER BODY COMPONENT DIMENSIONS AND C.G. LOCATIONS USED TO CALCULATE MOMENTS OF INERTIA

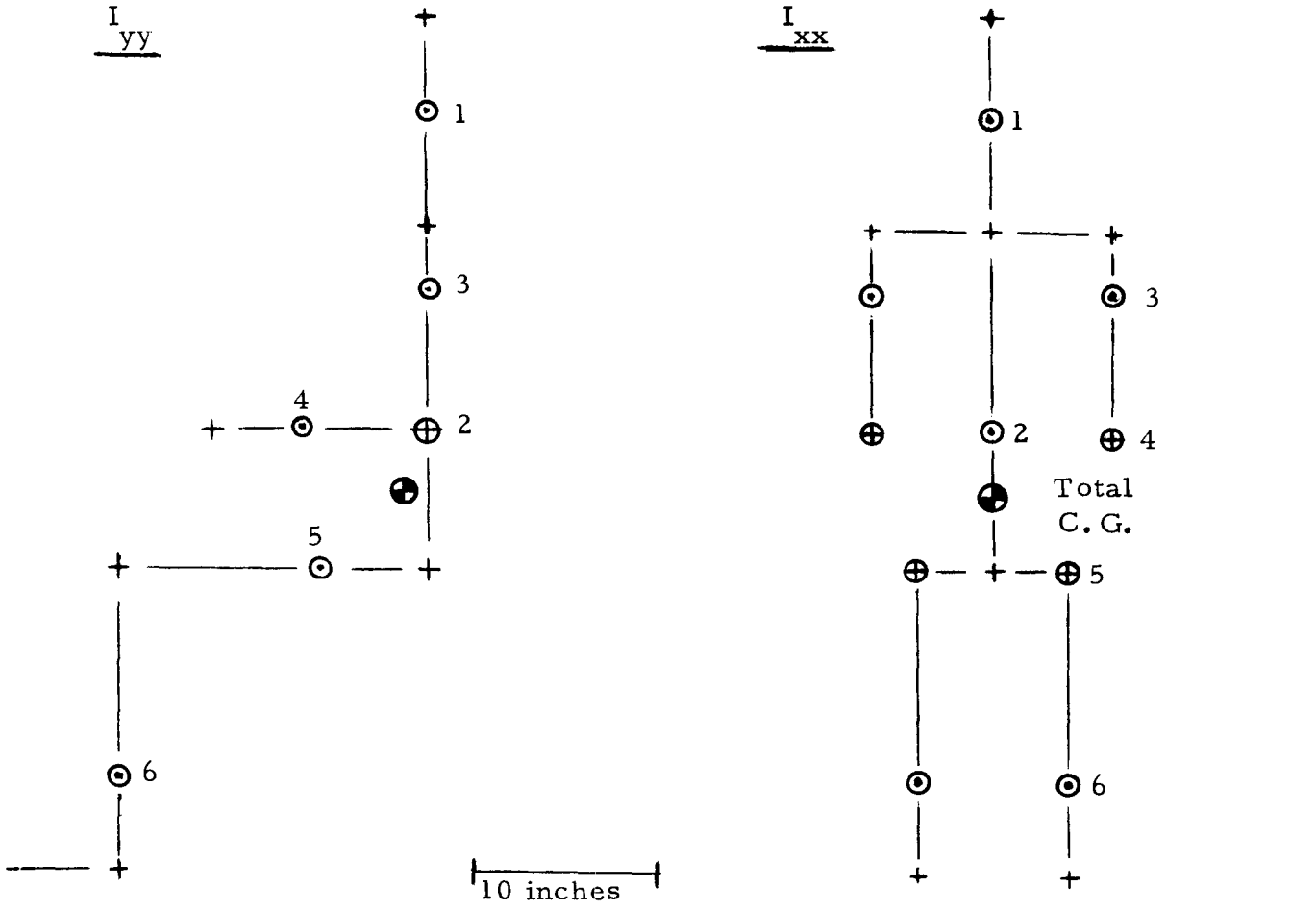

Table 4.2 SUMMARY OF COMPUTED RIDER INERTIA PARAMETERS

Moment of Inertia		I_{xx}			I_{yy}			I_{zz}		
Body Component	Component Mass lb-sec^2/in	I_{CG} lb-in-sec^2	r (in)	$I_{CG} + M_r^2$	I_{CG} lb-in-sec^2	r (in)	$I_{CG} + M_r^2$	I_{CG} lb-in-sec^2	r (in)	$I_{CG} + M_r^2$
Head	0.020	0.162	20.5	8.432	0.162	20.5	8.432	0.162	1.5	0.206
Torso	0.120	1.205	3.4	1.595	1.205	3.5	2.675	0.168	1.5	1.475
Upper Arm (2)	0.016	0.140	12.9	2.150	0.140	11.0	2.030	0.005	6.9	0.747
Lower Arm (2)	0.014	0.004	7.5	0.814	0.164	6.3	0.734	0.164	9.5	1.494
Upper Leg (2)	0.055	0.039	5.8	1.870	0.876	6.0	2.836	0.876	6.0	2.836
Lower Leg & Foot (2)	0.045	1.200	16.1	12.960	1.200	22.0	23.200	0.027	16.0	11.680
				$\Sigma = 27.821$			$\Sigma = 39.907$			$\Sigma = 18.438$

5.0 VALIDATION OF THE COMPUTER SIMULATION BY CORRELATION WITH FULL SCALE EXPERIMENTAL TESTS

A comparison of recorded motion variables (speed, steer angle, lean angle, and lateral acceleration) from full scale experimental maneuvers with corresponding output from the computer simulation program was made to establish the validity of the simulation program. Since a rider control model has not yet been incorporated in the simulation program, relatively simple maneuvers were essential. These maneuvers included steady state circular turning with a rider, and riderless maneuvers with free and forced steer inputs. A simulated maneuver was generated by the computer program using the same bicycle configuration, initial conditions, and steering torque as was measured for a specific experimental test. Comparisons of the motion variables from the experimental and simulated maneuvers are made and discussed in the following section.

5.1 Test Bicycle Instrumentation

The test bicycle was instrumented with: (1) a potentiometer connected to the steer axis for measuring the steer angle, Figure 5.3, (2) a gyroscope mounted on the horizontal frame member to measure the bicycle roll angle, Figure 5.3, (3) an accelerometer mounted beneath the horizontal frame member to measure lateral acceleration, Figure 5.4, (4) a d.c. tach-generator mounted on the rear wheel to measure forward velocity, Figure 5.2. Two 2-channel strip chart recorders and power supplies were mounted in the chase car, Figure 5.5, and operated by the chase car driver. Instrumentation power and data signals were transmitted to and from the bicycle through an eleven conductor fifty foot long cable. The influence of cable mass and drag on bike motion was minimized by

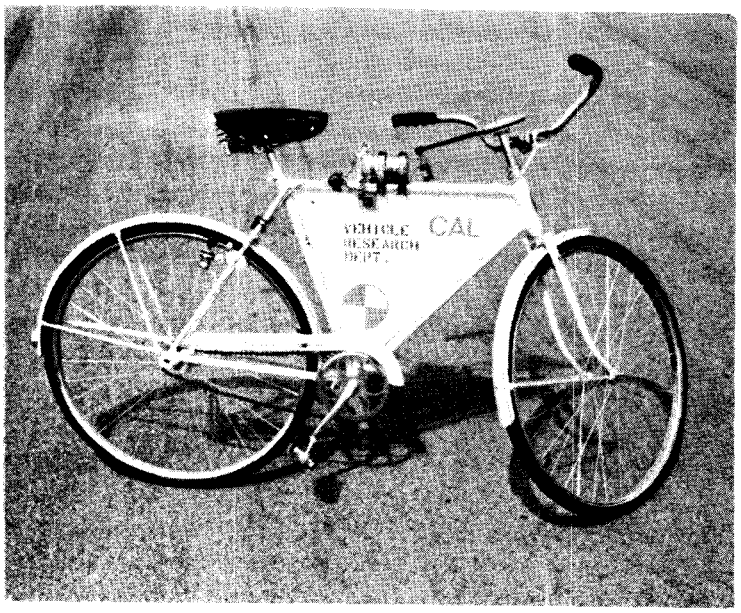

FIGURE 5.1

nstrumented bicycle

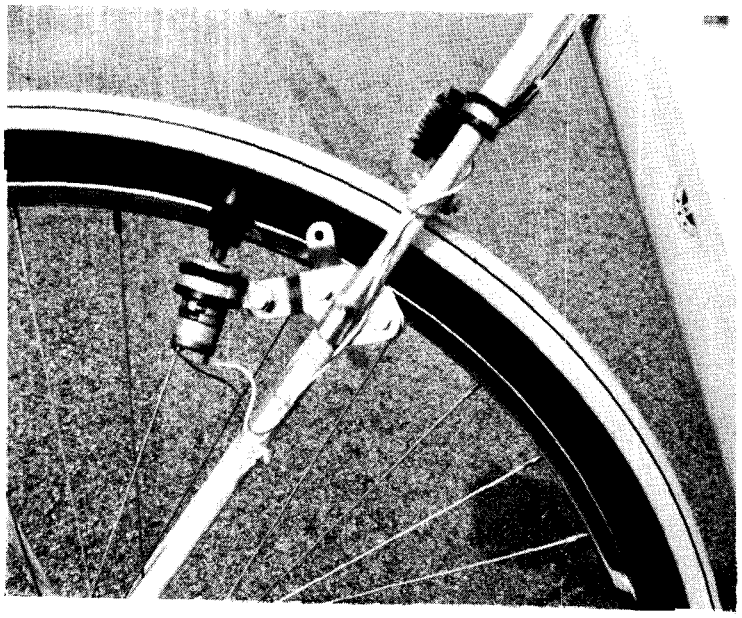

FIGURE 5.2

D.C. tach-generator
for speed measurement

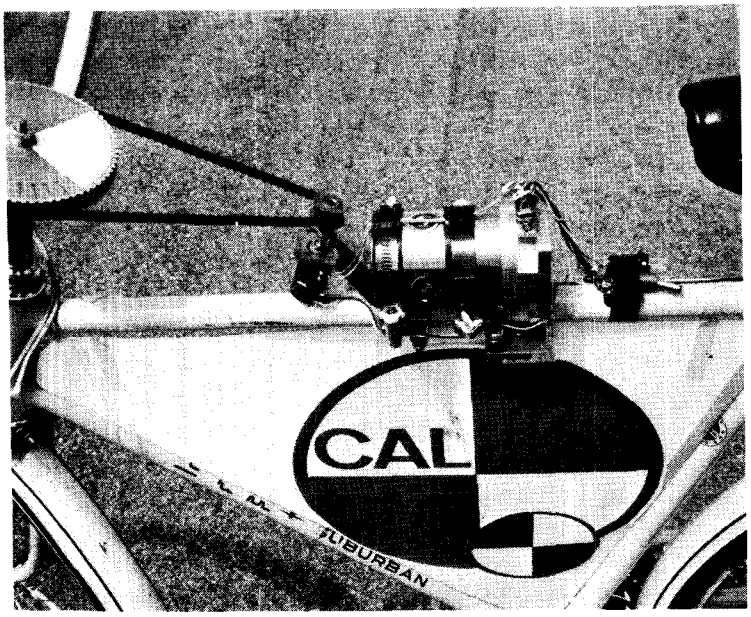

FIGURE 5.3

Roll angle gyro and
steer angle potentiometer

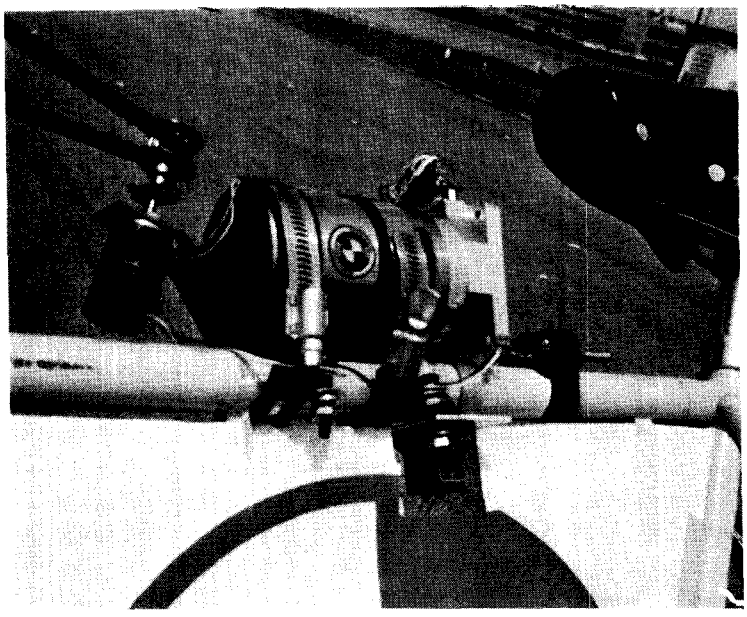

FIGURE 5.4

Lateral accelerometer
(mounted beneath frame
member)

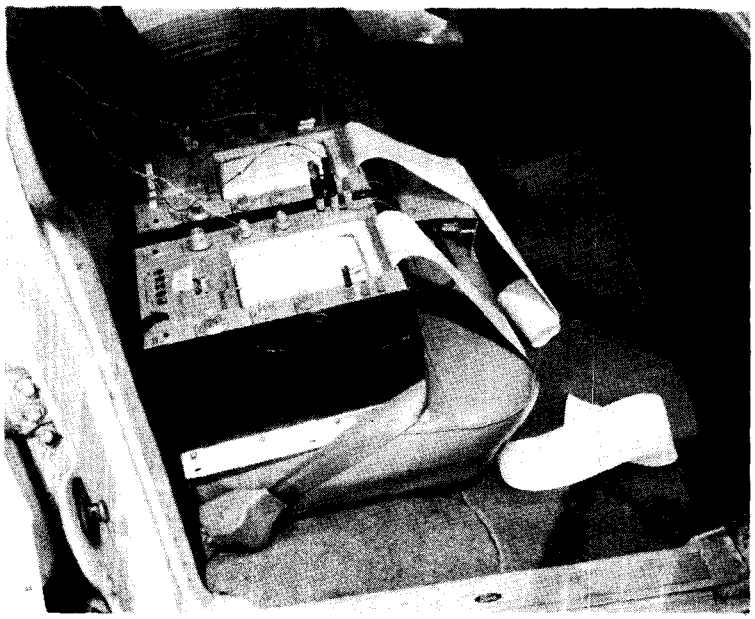

FIGURE 5.5

Two channel strip chart recorders mounted in chase car

fabricating a very flexible cable from light weight teflon-covered wire. The cable was loosely hung from a boom extending laterally from the chase car and connected to the bicycle through a pull-out coupling beneath the rear of the saddle.

Transducers were chosen on the basis of minimum weight as well as sensor range, resolution, and method of installation. As a result of these requirements, potentiometric sensors were chosen. A summary of transducer specifications is given in Table 5.1 and Figure 5.6 shows the location of each sensor as mounted on the test bicycle.

Data signals were conditioned with filters having a corner frequency (-3 db point, first order rolloff) of approximately one Hertz, resulting in an adequate bandwidth for the frequency content of bicycle responses. In addition to the recorded instrument data, movies were taken of most of the full scale experimental tests.

5.2 Full Scale Validation Tests

The following full scale experimental maneuvers were performed with the instrumented bicycle to obtain data for validation of the computer simulation.

(1) Motion of riderless bike with free control. Initial speed was approximately 10 mph. Data was recorded until bicycle fell over. Duration of the free control maneuver was about five seconds, Figures 5.7 and 5.8.

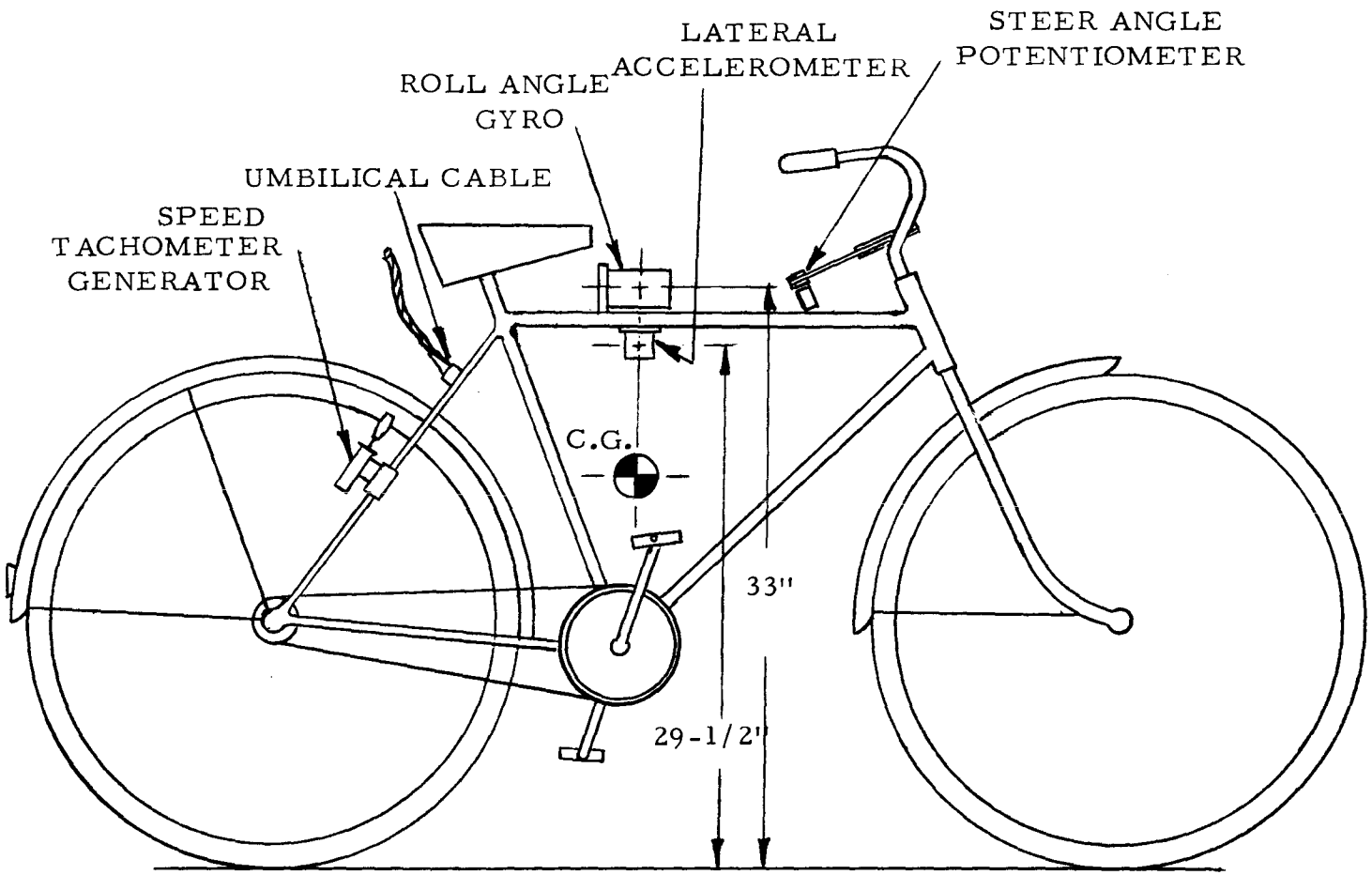

Figure 5.6 LOCATION OF VALIDATION TEST INSTRUMENTATION

Table 5.1

VALIDATION TEST INSTRUMENTATION
SPECIFICATION SUMMARY

Test Variable	Sensor Type	Make, Model	Range	Approximate Accuracy*	Weight (including mount)
Roll Angle	Free Gyro Potentiometric DC/DC	Humphrey, Inc. FG 23-3101-1	$\pm$ 178°	$\pm$ 2%	1.81 lbs.
Steer Angle	Precision 10 Turn Potentiometer W/Timing Belt 7.2:1 Drive	Helipot	$\pm$ 250°	$\pm$ 1%	0.8 lb.
Lateral Acceleration	Linear Accelerometer	Humphrey, Inc. LA 45-0104-1	$\pm$ 5 g	$\pm$ 2%	0.2 lb.
Speed	Precision D.C. Generator W/Friction Drive (36:1) at Rear Wheel		+ 20 mph	$\pm$ 3%	0.5 lb.

Data Acquisition - (2) Brush Mark 220, Model 15-6327-50, Two Channel Direct Write Recorders
Linearity $\pm$ 0.5% Full Scale, Chart Speed Accuracy $\pm$ 0.25%

* Combined effects of linearity, hysteresis, repeatability.

(2) Motion of riderless bicycle when given a nominal 2.24 lb-sec lateral force impulse (C6 Rocket). Initial speed was approximately 10 mph. Duration of this maneuver was about four seconds. This test was performed by pushing the bicycle up to speed in a straight path, then firing a small rocket motor to provide the lateral thrust. The rocket motor was rigidly attached to the bicycle frame approximately one foot above and one foot forward of the total c.g., Figure 5.9.

(3) Motion of riderless bicycle when given a nominal 6.72 lb-in-sec torque impulse (B14 Rocket) about the steer axis. Two runs were made with very good repeatability. The initial speed was about 9 mph and the duration of the run was approximately four seconds. In these tests the rocket motor was attached to the handlebar six inches from the steer axis, Figures 5.10 and 5.11.

(4) Suspended bicycle with a nominal 6.72 lb-in-sec torque impulse (B14 Rocket) about the steer axis. Two tests were made to observe the effect of gyroscopic coupling between the steer and roll degrees of freedom. The bicycle was held or suspended off the ground and a rocket motor was fired to provide the steering torque impulse. One test was made with the front wheel spinning at approximately 12 mph and the second test was made with the front wheel motionless. These tests were recorded on movie film only. The conclusion was that rotating the front wheel had little effect on the resultant steer and roll motions of the bicycle after the rocket blast.

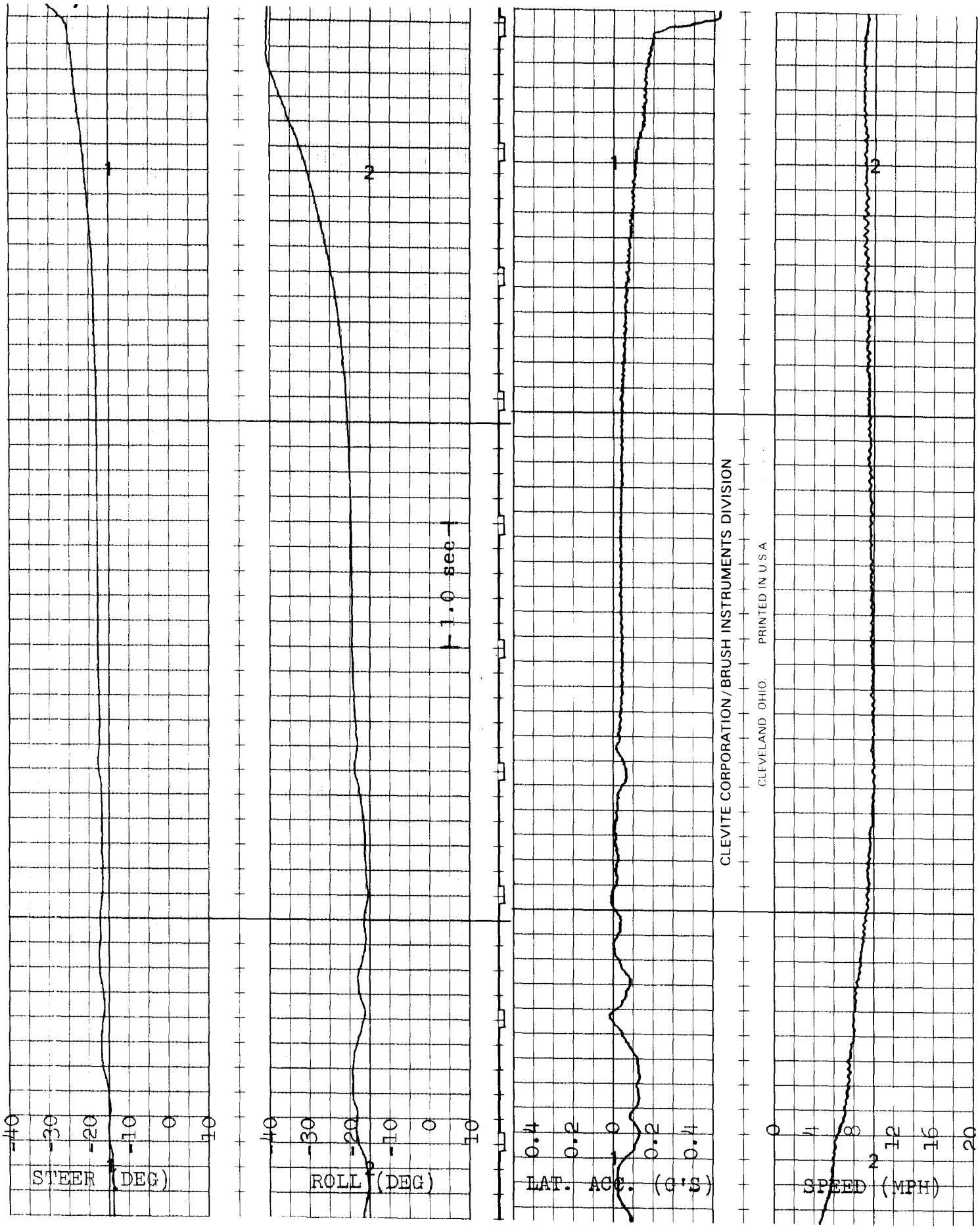

Figure 5.7 FREE CONTROL OF RIDERLESS BICYCLE

Figure 5.8 FREE CONTROL OF RIDERLESS BICYCLE

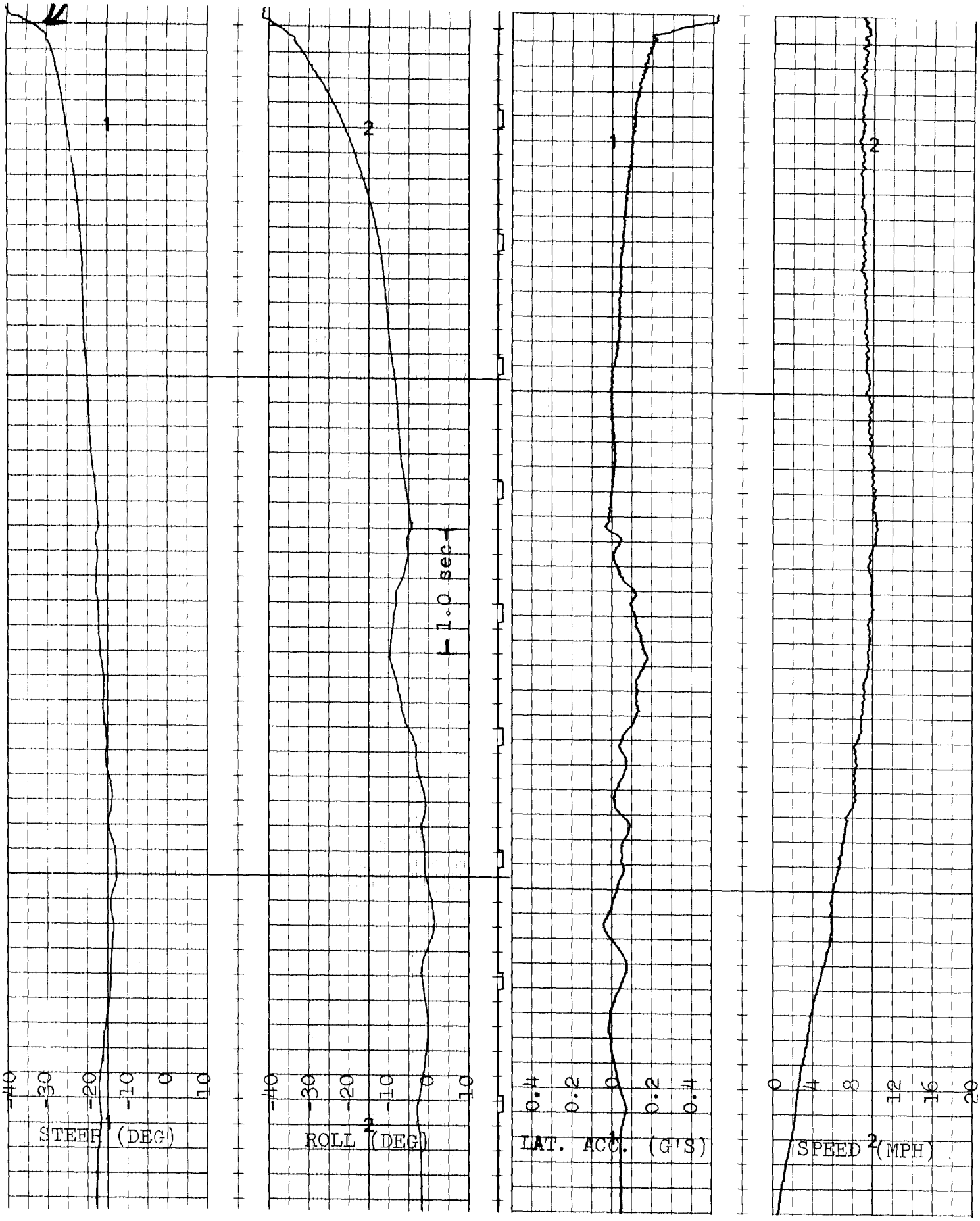

Figure 5.9 RIDERLESS BICYCLE WITH NOMINAL 2.24 LB-SEC LATERAL FORCE IMPULSE

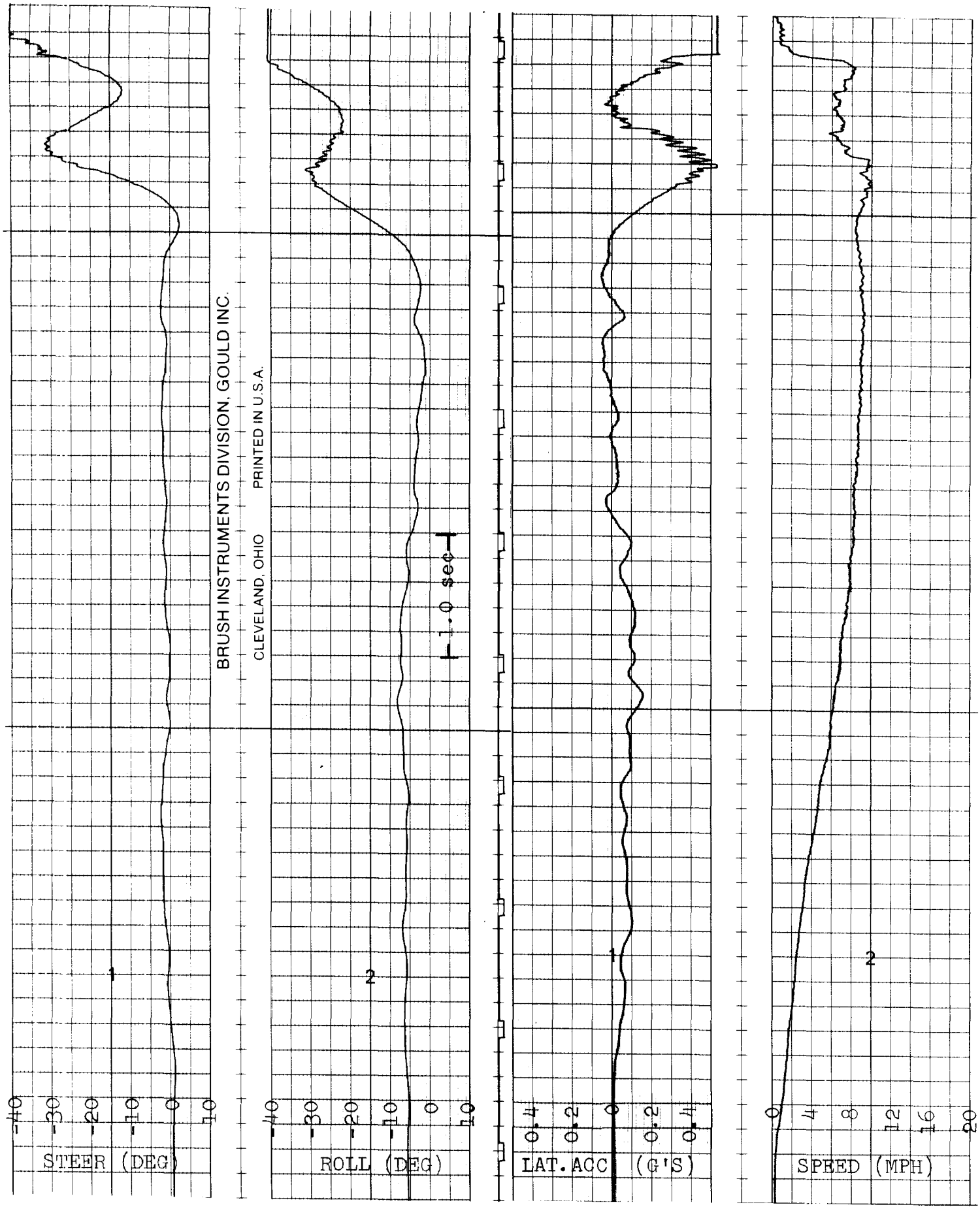

Figure 5.10 RIDERLESS BICYCLE WITH NOMINAL 6.72 LB-IN-SEC STEER TORQUE IMPULSE

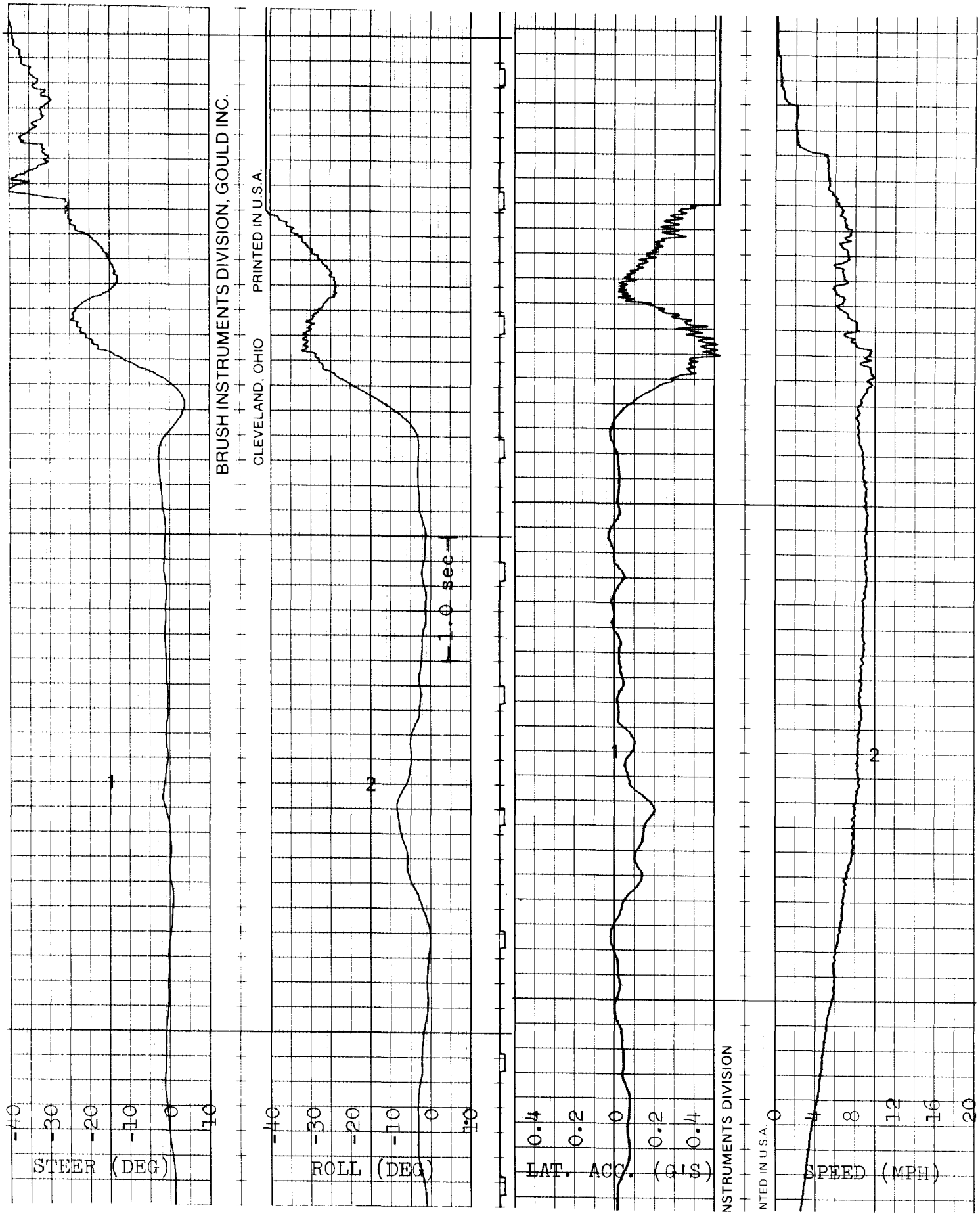

Figure 5.11 RIDERLESS BICYCLE WITH NOMINAL 6.72 LB-IN-SEC STEER TORQUE IMPULSE

(5) Steady state turning of bicycle with rider. Runs were made at speeds of 8, 10, 12, and 14 mph on a forty foot radius circle and on a twenty foot radius circle. These runs represent a range of lateral acceleration from 0.1 g to 0.6 g. Reduced data is presented in numerical form in Table 5.2.

5.3 Rocket Motor Calibration

In order to verify the rocket motor thrust curves published by the manufacturer and to obtain some measure of the variability of the data, time histories of the thrust of two types of rockets were recorded. Three thrust curves were recorded for each type, Figures 5.12 and 5.13. The force output was measured with a high sensitivity fast response strain gage proving ring.

None of the B14 rockets developed a peak thrust of seven pounds indicated by the manufacturer's performance curves. The average impulse of the B14 rockets was approximately 80 percent of the manufacturers rated 1.12 lb-sec impulse. Two of the three C6 rockets tested developed a peak thrust of about 0.5 pound higher than indicated by the manufacturer's performance curves. The steady state thrust of 1.35 pounds for the C6 is exactly that shown by the manufacturer. However, a 0.4 second shorter burning time resulted in the average impulse of the C6 rockets also being only 80% of the nominal 2.24 lb-sec.

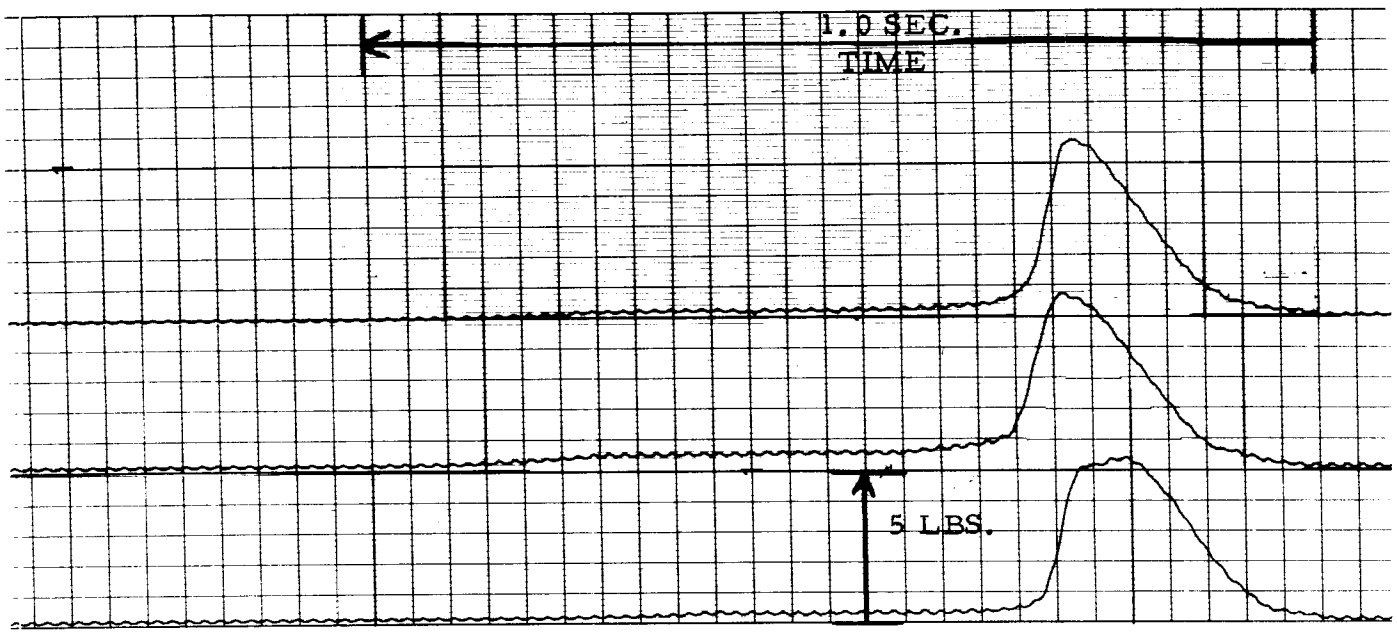

Figure 5.12 THRUST CURVES OF B14 ROCKETS

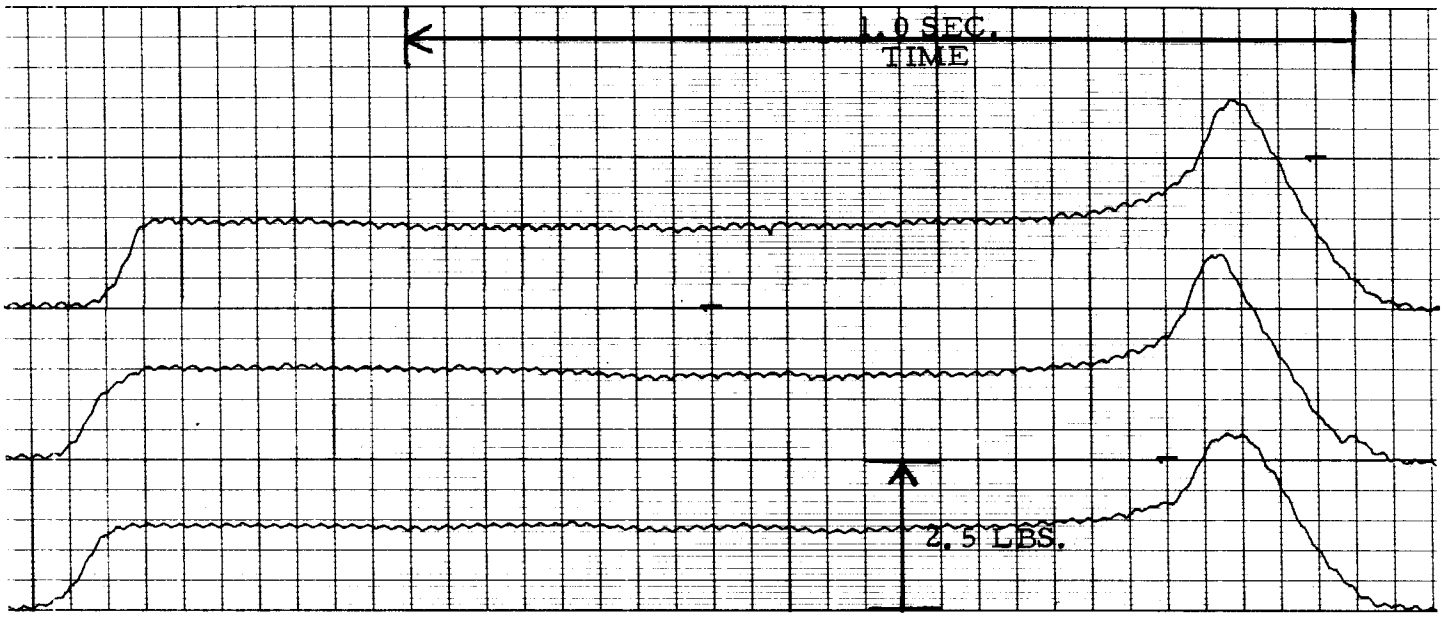

Figure 5.13 THRUST CURVES OF C6 ROCKETS

5.4 Comparison of Computer Simulation with Full Scale Experimental Tests

The time histories of steer and roll angle from the computer simulated validation maneuver agree very well with the data from the two full scale experimental tests, Figure 5.14. The steer torque impulse for the simulated maneuver was 4.5 lb-in-sec. Using the average impulse from the rocket calibration tests, the estimated torque impulse in the full scale tests was 5.4 lb-in-sec, with the rocket mounted 6 inches from the steer axis. A series of simulated maneuvers was made with decreasing values of steering torque impulse. It was found that decreasing the steering torque impulse from 6.7 lb-in-sec (corresponding to the manufacturer's rated impulse) to approximately 4.5 lb-in-sec caused bicycle motion to change from divergent instability to oscillatory instability typical of the full scale maneuver. Steering torque impulses from 4.5 to 3.5 lb-in-sec did not significantly change the motion. Since torques which resist steering motion such as friction in the steering head and tire scrubbing are not explicitly included in the bicycle model, the value of steering torque impulse used in the simulated maneuver is thought to be a good approximation to the full scale experimental tests.

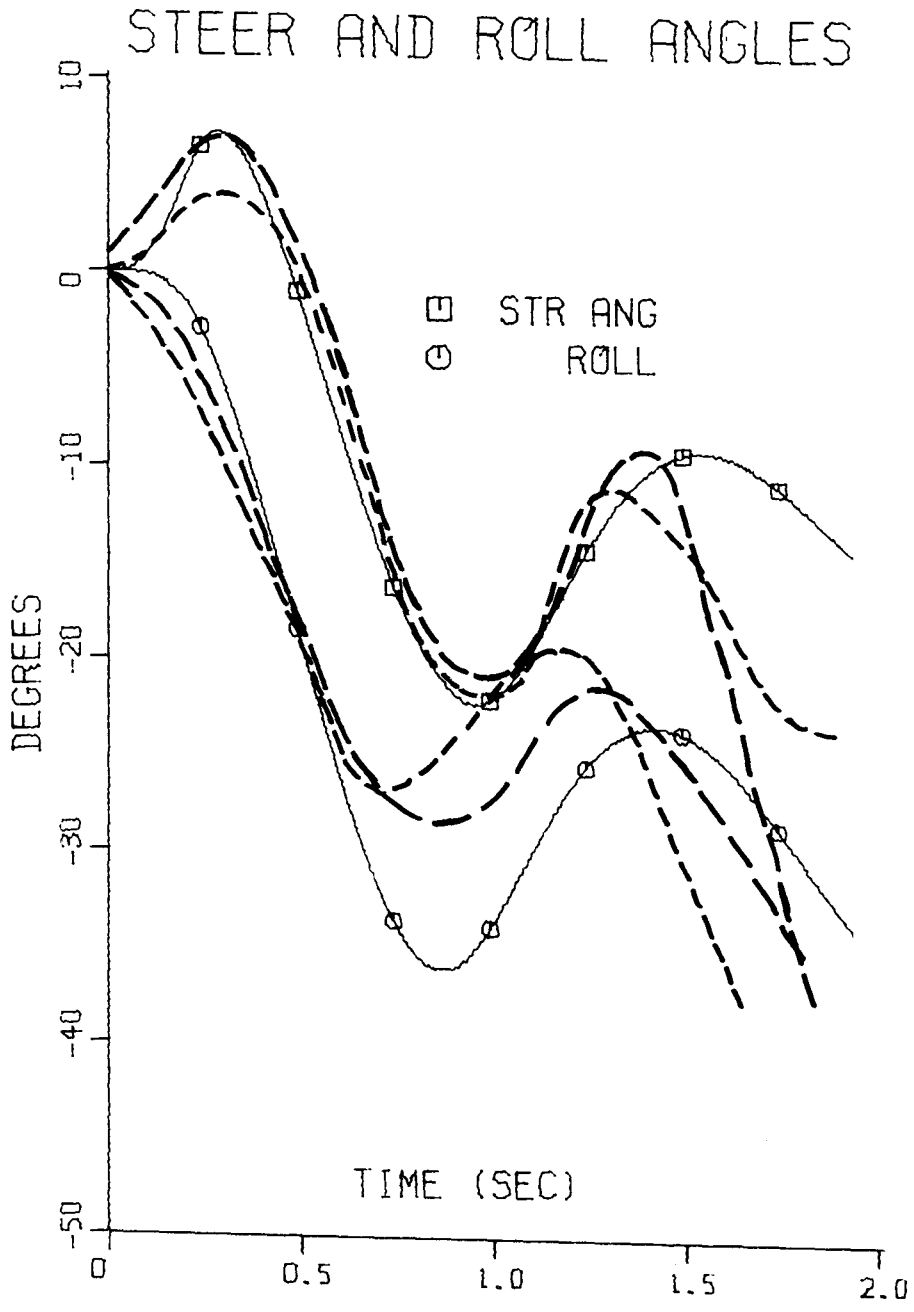

Figure 5.14 COMPARISON OF COMPUTER SIMULATION WITH FULL SCALE EXPERIMENTAL TESTS

6.0 COMPUTER SIMULATION PARAMETER STUDY

A computer simulation study was made to determine the effects on bicycle motion of variations of certain bicycle design parameters. This study consisted of 57 computer simulated bicycle maneuvers. The effects of nine bicycle parameters were studied, each for speeds of 7, 9, and 15 mph.

The simulated maneuver was the steer torque impulse validation maneuver. The configuration of the riderless bicycle as measured with the validation instrumentation and with the Breeze tires was taken as the standard configuration. All simulated maneuvers had a single parameter variation with other data remaining the same as the standard configuration.

For each parameter a value higher and one lower than the standard were run. In some cases the high and low values represented the range of this parameter in current production bicycles. In other cases, arbitrary values of 80% and 120% of the standard were used.

The study also included runs at the three test speeds with data representing the Puff tire and with data representing a rigid "hands-off" rider.

Detailed printed time histories of 36 output variables and plotted time histories for steer angle, roll angle, lateral acceleration, and velocity for each of the 57 simulated maneuvers are contained in additional volumes.

Table 6.1 lists the parameter variations and simulation run numbers, and briefly states the effect on the motion of the bicycle according to the following code.

DU - the motion was Divergently Unstable (indicating that the bicycle fell over immediately).

OU - the motion was Oscillatory Unstable (indicating that the bicycle had both steer and roll oscillations before falling over). The number in parenthesis is the time at which the bicycle finally fell over.

OI - the motion was Oscillatory and it is Inconclusive as to whether the bicycle would have stayed upright or fallen over.

OS - the motion was Oscillatory, however, the bicycle maintained Stability and settled into a steady state turn.

The results of the parameter study show that all maneuvers at 7 mph were divergently unstable and all maneuvers at 15 mph were oscillatory stable regardless of the parameter variations. However, the 15 mph runs do show significant differences in settling time, oscillation frequency, peak amplitude of steer and roll angles, and the steady state value of the steer and roll angles.

The 9 mph runs show the most interesting results since it is at this speed that the parameter variations have the greatest effect on the motion of the bicycle.

The effect of several parameter variations of the bicycle motion at 9 mph are listed below.

a) Reducing the wheelbase from 41.5 inches to 33.2 inches had little effect on the degree of stability, however, increasing the wheelbase to 49.8 inches caused the motion to become divergently unstable.

b) Reducing the total weight from 40.8 pounds to 25.0 pounds reduced the oscillatory motion allowing the bicycle to remain upright. However, increasing the total weight to 55.0 pounds greatly increased the amplitude and reduced the frequency of oscillation.

c) Reducing the total c.g. height from 20.8 inches to 16.6 inches had little effect on the degree of stability. Increasing the c.g. height to 24.9 inches damped the oscillation but caused the bicycle to fall over sooner.

d) Reducing the steer moment of inertia from 1.86 to 1.49 lb-in-sec^2 reduced the tendency to oscillate but caused the bicycle to fall sooner. Increasing the steer moment of inertia to 2.23 greatly increased the amplitude and reduced the frequency of oscillatory motion. The motion had not settled enough by the end of the run (3.0 seconds) to conclude that the bicycle would have remained upright.

e) Reducing caster angle from 21.0 degrees to 15.0 degrees greatly increased the amplitude of oscillation with little effect on frequency. Apparently the motion would have been stable when the oscillation damped out. Increasing the caster angle to 25.0 degrees resulted in increased damping but falling over sooner.

f) Reducing fork offset from 1.87 inches to 0.87 inches increases damping but the bicycle still falls over after about 2.8 seconds. Increasing the fork offset to 2.87 inches greatly increased the amplitude of oscillation and apparently the bicycle would have fallen on the next cycle of the oscillation.

g) Reducing the rolling radius from 13.6 inches to 10.0 inches damped the oscillatory motion and the bicycle was falling with a high roll velocity. Increasing the rolling radius to 14.6 inches significantly changed the motion, increasing the amplitude and reducing the frequency of the steer and roll oscillations. Apparently this increase in rolling radius of one inch tended to stabilize the bicycle motion.

h) The wheel moment of inertia variations had the greatest effect on stability. Reducing the wheel moment of inertia from 1.76 to 1.41 lb-in-sec^2 caused the motion to become divergently unstable. Increasing the wheel moment of inertia to 2.11 lb-in-sec not only damped the oscillatory motion but also caused a significant improvement in stability.

i) Changing from the Breeze tire data to the Puff tire data increased the oscillation amplitude and reduced the frequency with an apparent stabilizing effect on the bicycle motion.

j) The addition of the rigid 102 pound rider (hands-off) caused the bicycle to fall over even at 15 mph. The rate at which the bike fell over with the rider was slower than when riderless and the steer motion was very nonlinear. At 15 mph the roll angle tended to oscillate but fell over after 2.5 seconds.

Table 6.1 BICYCLE PARAMETER STUDY RESULT MATRIX

PARAMETER VARIATION		SPEED		
		7 mph	9 mph	15 mph
Standard Bicycle (Breeze tires)		#2 - DU	#1 - OU (2.6 sec)	#3 - OS
Wheelbase	33.2 in.	#4 - DU	#5 - OU (2.6 sec)	#6 - OS
	49.8 in.	#7 - DU	#8 - DU	#9 - OS
Total Weight	25.0 lb.	#10 - DU	#11 - OS	#12 - OS
	55.0 lb.	#13 - DU	#14 - OI	#15 - OS
Total C.G. Height	16.6 in.	#16 - DU	#17 - OU (3.0 sec)	#18 - OS
	24.9 in.	#19 - DU	#20 - OU (2.8 sec)	#21 - OS
Steer Moment of Inertia	1.49 $lb\text{-}in\text{-}sec^2$	#22 - DU	#23 - OU (2.5 sec)	#24 - OS
	2.23 $lb\text{-}in\text{-}sec^2$	#25 - DU	#26 - OI	#27 - OS
Caster Angle	15.0 deg.	#28 - DU	#29 - OI	#30 - OS
	25.0 deg.	#31 - DU	#32 - OU (2.3 sec)	#33 - OS
Fork Offset	0.87 in.	#34 - DU	#35 - OU (2.8 sec)	#36 - OS
	2.87 in.	#37 - DU	#38 - OI	#39 - OS
Undeflected Rolling Radius	10.0 in.	#40 - DU	#41 - OU (3.0 sec)	#42 - OS
	14.6 in.	#43 - DU	#44 - OI	#45 - OS
Wheel Moment of Inertia	1.41 $lb\text{-}in\text{-}sec^2$	#46 - DU	#47 - DU	#48 - OS
	2.11 $lb\text{-}in\text{-}sec^2$	#49 - DU	#50 - OS	#51 - OS
Standard Bicycle (Puff tires)		#52 - DU	#53 - OS	#54 - OS
Standard Bicycle with 102 pound Rider		#55 - DU	#56 - DU	#57 - OU

7.0 BIBLIOGRAPHY

1. Bower, George S.: " Steering and Stability of Single-Track Vehicles" - The Automobile Engineer, Vol. V, 1915, p. 280-283.

2. Collins, Robert Neil: "A Mathematical Analysis of the Stability of Two-Wheeled Vehicles" - Ph. D. Thesis, University of Wisconsin, 1963.

3. Dohring, E.: "Stability of Single-Track Vehicles" - Forschung Ing. Wes. 21, No. 2, 1955, p. 50-62, translation by Cornell Aeronautical Laboratory, Inc., 1957.

4. Dohring, E.: "Steering Wobble in Single-Track Vehicles" - Automob. techn. z., Vol. 58, No. 10, p. 282-286. (M. I. R. A. Translation No. 62167).

5. Frank, Ernest: "Electrical Measurement Analysis" - McGraw Hill, 1959.

6. Fu, Hiroyasu: "Fundamental Characteristics of Single-Track Vehicles in Steady Turning" - Bulletin of JSME, Vol. 9, No. 34, 1965, p. 284-293.

7. Hanavan, E. P., Jr.: "A Personalized Mathematical Model of the Human Body" - Journal of Spacecraft Vol. 3, No. 3, March 1966, p. 446-448.

8. Kageyama, Katumi, Fu, Hiroyasu, and Kosa, Fumio: "Experimental Study on the Standing Stability of the Motorcycle" - Bulletin of JSME, Vol. 5, No. 17, 1962, p. 202-209.

9. Manning, J. R.: "The Dynamical Stability of Bicycles" - Department of Scientific and Industrial Research, Road Research Laboratory, Note No. RN/1605/JRM, July, 1951.

10. Patten, J.S. and Theiss, C.M.: "Auxiliary Program for Generating Occupant Parameter and Profile Data" - Cornell Aeronautical Laboratory, Technical Report No. VJ-2759-V-1R, January, 1970.

11. Pearsal, R.H.: "The Stability of the Bicycle" - Proc. Inst. Automobile Eng., Vol XVII, 1922, p. 395.

12. Rice, Roy S. and Roland, R. Douglas, Jr.: "An Evaluation of the Performance and Handling Qualities of Bicycles" - Cornell Aeronautical Laboratory, Technical Report No. VJ-2888-K, April 1970.

13. Shames, I.H.: Engineering Mechanics, Vol. II Dynamics, Prentice-Hall, 1966.

14. Singh, Digvijai V.: "Advanced Concepts of the Stability of Two-Wheeled Vehicles - Application of Mathematical Analysis to Actual Vehicles" - Ph. D. Thesis, University of Wisconsin, 1964.

15. Singh, D. V. and Goel, V. K.: "Stability of Rajdoot Scooter" - Paper #710273, SAE Automotive Engineering Congress, January, 1971.

16. Swearingen, J. J. and Young, J. W.: "Determination of Centers of Gravity of Children, Sitting and Standing" - Civil Aeromedical Research Institute, Report No. AM65-23, August 1965.

17. Van Lunteren, A. and Stassen, H. G.: "Annual Report of the Man-Machine Systems Group" - Laboratory for Measurement and Control, Dept. of Mech. Eng., Delft University of Technology, 1970.

18. Van Lunteren, A. and Stassen, H. G.: "Investigations of the Characteristics of a Human Operator Stabilizing a Bicycle Model" - Intern. Symp. on Ergonomics in Machine Design, Prague, 1967.

19. Van Lunteren, A. and Stassen, H. G.: "On-Line Parameter Estimation of the Human Transfer in a Man-Bicycle System" - IVth IFAC Congress, Warsaw, 1969, Paper 70.3.

20. Van Lunteren, A. and Stassen, H. G.: "On the Variance of the Bicycle Rider's Behavior" - 6th Annual Conference on Manual Control, Wright Patterson AFB, Ohio, 1970.

21. Whipple, F.J.W.: "The Stability of the Motion of a Bicycle" - Quarterly Journal of Pure and Applied Math., Vol. 30, No. 120, 1899, p. 312-348.

22. Wilson-Jones, R.A.: "Steering and Stability of Single-Track Vehicles" - Proceedings of the Institution of Mechanical Engineers, Automobile Division, London, 1951-52.

APPENDIX I

Measured and Corrected Side Force Data for Schwinn Breeze and Puff Bicycle Tires

27X1.25 SCHWINN BREEZE SPORTS TOURING (65 PSI)

NORMAL FORCE = 36.4

INCLINATION ANGLE	0.0	10.00	20.00	30.00	40.00
MEASURED SLIP ANGLE	-2.00	-2.00	-2.00	-2.00	-2.00
MEASURED LATERAL FORCE	******	******	-18.00	-14.00	-14.00
CORRECTED SLIP ANGLE	******	******	-1.44	-1.61	-1.66
CORRECTED LATERAL FORCE	******	******	-16.90	-11.60	-10.30
MEASURED SLIP ANGLE	-1.00	-1.00	-1.00	-1.00	-1.00
MEASURED LATERAL FORCE	******	******	-13.00	-10.00	-9.00
CORRECTED SLIP ANGLE	******	******	-0.61	-0.75	-0.83
CORRECTED LATERAL FORCE	******	******	-11.70	-7.40	-5.10
MEASURED SLIP ANGLE	-0.50	-0.50	-0.50	-0.50	-0.50
MEASURED LATERAL FORCE	-12.00	-10.00	-9.50	-8.00	-8.00
CORRECTED SLIP ANGLE	-0.06	-0.17	-0.23	-0.32	-0.37
CORRECTED LATERAL FORCE	-13.20	-9.90	-8.10	-5.30	-4.00
MEASURED SLIP ANGLE	0.0	0.0	0.0	0.0	0.0
MEASURED LATERAL FORCE	-0.30	-7.50	-6.00	-5.00	-4.00
CORRECTED SLIP ANGLE	0.07	0.24	0.15	0.07	-0.00
CORRECTED LATERAL FORCE	-2.00	-7.30	-4.50	-2.20	0.10
MEASURED SLIP ANGLE	0.50	0.50	0.50	0.50	0.50
MEASURED LATERAL FORCE	-4.50	-4.00	-4.00	-3.50	0.0
CORRECTED SLIP ANGLE	0.68	0.62	0.58	0.52	0.36
CORRECTED LATERAL FORCE	-5.50	-3.70	-2.40	-0.60	4.20
MEASURED SLIP ANGLE	1.00	1.00	1.00	1.00	1.00
MEASURED LATERAL FORCE	0.50	1.00	0.0	2.50	5.00
CORRECTED SLIP ANGLE	1.01	0.95	0.94	0.82	0.69
CORRECTED LATERAL FORCE	-0.40	1.40	1.70	5.50	9.30
MEASURED SLIP ANGLE	2.00	2.00	2.00	2.00	2.00
MEASURED LATERAL FORCE	7.00	7.00	7.00	11.00	10.00
CORRECTED SLIP ANGLE	1.79	1.75	1.70	1.53	1.52
CORRECTED LATERAL FORCE	6.30	7.60	8.90	14.20	14.50
MEASURED SLIP ANGLE	3.00	3.00	3.00	3.00	3.00
MEASURED LATERAL FORCE	17.00	16.00	18.50	17.50	17.00
CORRECTED SLIP ANGLE	2.45	2.44	2.31	2.30	2.28
CORRECTED LATERAL FORCE	16.50	16.80	20.60	20.90	21.70
MEASURED SLIP ANGLE	4.00	4.00	4.00	4.00	4.00
MEASURED LATERAL FORCE	18.50	22.00	22.00	21.50	20.00
CORRECTED SLIP ANGLE	3.39	3.23	3.19	3.16	3.17
CORRECTED LATERAL FORCE	18.20	23.00	24.30	25.10	24.90
MEASURED SLIP ANGLE	6.00	6.00	6.00	6.00	6.00
MEASURED LATERAL FORCE	27.00	28.00	25.00	26.00	21.00
CORRECTED SLIP ANGLE	5.10	5.02	5.08	5.00	5.12
CORRECTED LATERAL FORCE	27.10	29.40	27.70	30.00	25.30
MEASURED SLIP ANGLE	8.00	8.00	8.00	8.00	8.00
MEASURED LATERAL FORCE	29.00	29.00	23.00	26.00	24.00
CORRECTED SLIP ANGLE	7.02	6.97	7.13	6.99	7.01
CORRECTED LATERAL FORCE	29.50	30.80	26.10	30.40	29.70
MEASURED SLIP ANGLE	10.00	10.00	10.00	10.00	10.00
MEASURED LATERAL FORCE	******	******	******	23.00	23.00
CORRECTED SLIP ANGLE	******	******	******	9.07	9.03
CORRECTED LATERAL FORCE	******	******	******	27.80	29.10

SLIP ANGLE OFFSET = 1.06

27X1.25 SCHWINN BREEZE SPORTS TOURING (65 PSI)

NORMAL FORCE = 73.4

INCLINATION ANGLE	0.0	10.00	20.00	30.00	40.00
MEASURED SLIP ANGLE	-2.00	-2.00	-2.00	-2.00	-2.00
MEASURED LATERAL FORCE	******	******	-25.00	-19.00	-13.00
CORRECTED SLIP ANGLE	******	******	-1.16	-1.44	-1.67
CORRECTED LATERAL FORCE	******	******	-25.30	-16.82	-10.00
MEASURED SLIP ANGLE	-1.00	-1.00	-1.00	-1.00	-1.00
MEASURED LATERAL FORCE	******	******	-16.50	-11.50	-8.50
CORRECTED SLIP ANGLE	******	******	-0.45	-0.66	-0.82
CORRECTED LATERAL FORCE	******	******	-16.60	-10.13	-5.30
MEASURED SLIP ANGLE	-0.50	-0.50	-0.50	-0.50	-0.50
MEASURED LATERAL FORCE	-15.50	-13.00	-12.00	-8.00	-4.00
CORRECTED SLIP ANGLE	0.08	-0.03	-0.10	-0.28	-0.48
CORRECTED LATERAL FORCE	-17.40	-14.12	-12.00	-6.52	-0.70
MEASURED SLIP ANGLE	0.0	0.0	0.0	0.0	0.0
MEASURED LATERAL FORCE	-11.50	-7.50	-8.00	-6.00	1.00
CORRECTED SLIP ANGLE	0.44	0.28	0.26	0.15	-0.15
CORRECTED LATERAL FORCE	-13.30	-8.52	-7.90	-4.42	4.40
MEASURED SLIP ANGLE	0.50	0.50	0.50	0.50	0.50
MEASURED LATERAL FORCE	-6.00	-2.50	-5.00	2.00	7.00
CORRECTED SLIP ANGLE	0.76	0.61	0.66	0.38	0.15
CORRECTED LATERAL FORCE	-7.70	-3.42	-4.80	3.68	10.50
MEASURED SLIP ANGLE	1.00	1.00	1.00	1.00	1.00
MEASURED LATERAL FORCE	1.00	3.00	2.00	6.00	11.00
CORRECTED SLIP ANGLE	1.02	0.93	0.92	0.74	0.51
CORRECTED LATERAL FORCE	-0.60	2.18	2.30	7.78	14.60
MEASURED SLIP ANGLE	2.00	2.00	2.00	2.00	2.00
MEASURED LATERAL FORCE	9.00	12.00	9.50	15.50	20.00
CORRECTED SLIP ANGLE	1.75	1.62	1.67	1.38	1.21
CORRECTED LATERAL FORCE	7.60	11.38	10.00	18.47	23.80
MEASURED SLIP ANGLE	3.00	3.00	3.00	3.00	3.00
MEASURED LATERAL FORCE	20.50	23.50	23.00	27.50	30.00
CORRECTED SLIP ANGLE	2.36	2.23	2.21	2.01	1.87
CORRECTED LATERAL FORCE	19.30	23.07	23.70	27.67	34.00
MEASURED SLIP ANGLE	4.00	4.00	4.00	4.00	4.00
MEASURED LATERAL FORCE	27.50	33.50	35.00	36.50	37.00
CORRECTED SLIP ANGLE	3.12	2.89	2.80	2.71	2.63
CORRECTED LATERAL FORCE	26.50	33.27	35.90	38.98	41.20
MEASURED SLIP ANGLE	6.00	6.00	6.00	6.00	6.00
MEASURED LATERAL FORCE	43.00	44.00	47.00	50.00	46.00
CORRECTED SLIP ANGLE	4.59	4.53	4.35	4.24	4.32
CORRECTED LATERAL FORCE	42.40	44.17	48.30	52.77	50.60
MEASURED SLIP ANGLE	8.00	8.00	8.00	8.00	8.00
MEASURED LATERAL FORCE	52.00	54.00	56.00	53.00	51.00
CORRECTED SLIP ANGLE	6.28	6.18	6.08	6.13	6.14
CORRECTED LATERAL FORCE	51.80	54.57	57.70	56.17	56.00
MEASURED SLIP ANGLE	10.00	10.00	10.00	10.00	10.00
MEASURED LATERAL FORCE	******	******	******	55.00	51.00
CORRECTED SLIP ANGLE	******	******	******	8.05	8.12
CORRECTED LATERAL FORCE	******	******	******	58.57	56.40

SLIP ANGLE OFFSET = 1.07

27X1.25 SCHWINN BREEZE SPORTS TOURING (65 PSI)

NORMAL FORCE =105.5

INCLINATION ANGLE	0.0	10.00	20.00	30.00	40.00
MEASURED SLIP ANGLE	-2.00	-2.00	-2.00	-2.00	-2.00
MEASURED LATERAL FORCE	******	******	-26.00	-19.00	-11.00
CORRECTED SLIP ANGLE	******	******	-1.08	-1.37	-1.71
CORRECTED LATERAL FORCE	******	******	-27.70	-19.05	-8.70
MEASURED SLIP ANGLE	-1.00	-1.00	-1.00	-1.00	-1.00
MEASURED LATERAL FORCE	******	******	-18.50	-12.00	-4.00
CORRECTED SLIP ANGLE	******	******	-0.33	-0.61	-0.95
CORRECTED LATERAL FORCE	******	******	-20.00	-11.85	-1.50
MEASURED SLIP ANGLE	-0.50	-0.50	-0.50	-0.50	-0.50
MEASURED LATERAL FORCE	-17.00	-15.00	-13.00	-6.50	0.0
CORRECTED SLIP ANGLE	0.15	0.09	-0.02	-0.29	-0.59
CORRECTED LATERAL FORCE	-19.60	-17.35	-14.40	-6.25	2.60
MEASURED SLIP ANGLE	0.0	0.0	0.0	0.0	0.0
MEASURED LATERAL FORCE	-13.50	-11.00	-10.00	-6.00	7.50
CORRECTED SLIP ANGLE	0.53	0.44	0.38	0.19	-0.34
CORRECTED LATERAL FORCE	-16.00	-13.25	-11.30	-5.65	10.20
MEASURED SLIP ANGLE	0.50	0.50	0.50	0.50	0.50
MEASURED LATERAL FORCE	-7.00	-3.00	-1.00	3.00	14.00
CORRECTED SLIP ANGLE	0.81	0.67	0.57	0.39	-0.06
CORRECTED LATERAL FORCE	-9.40	-5.15	-2.20	3.45	16.90
MEASURED SLIP ANGLE	1.00	1.00	1.00	1.00	1.00
MEASURED LATERAL FORCE	1.50	3.00	4.00	13.00	19.00
CORRECTED SLIP ANGLE	1.03	0.97	0.90	0.55	0.27
CORRECTED LATERAL FORCE	-0.90	0.95	2.90	13.55	21.90
MEASURED SLIP ANGLE	2.00	2.00	2.00	2.00	2.00
MEASURED LATERAL FORCE	9.00	13.00	16.00	24.50	27.00
CORRECTED SLIP ANGLE	1.77	1.63	1.50	1.15	1.00
CORRECTED LATERAL FORCE	6.90	11.15	15.10	25.25	30.10
MEASURED SLIP ANGLE	3.00	3.00	3.00	3.00	3.00
MEASURED LATERAL FORCE	23.50	27.00	29.00	35.00	38.00
CORRECTED SLIP ANGLE	2.28	2.16	2.06	1.80	1.59
CORRECTED LATERAL FORCE	21.60	25.35	28.30	35.95	42.30
MEASURED SLIP ANGLE	4.00	4.00	4.00	4.00	4.00
MEASURED LATERAL FORCE	31.00	38.00	41.50	47.00	49.00
CORRECTED SLIP ANGLE	3.02	2.79	2.63	2.40	2.25
CORRECTED LATERAL FORCE	29.30	36.55	41.00	48.15	52.50
MEASURED SLIP ANGLE	6.00	6.00	6.00	6.00	6.00
MEASURED LATERAL FORCE	50.50	56.00	62.00	66.00	67.00
CORRECTED SLIP ANGLE	4.36	4.17	3.94	3.75	3.81
CORRECTED LATERAL FORCE	49.20	54.95	61.90	67.55	65.00
MEASURED SLIP ANGLE	8.00	8.00	8.00	8.00	8.00
MEASURED LATERAL FORCE	67.50	72.00	76.00	79.00	77.00
CORRECTED SLIP ANGLE	5.78	5.62	5.46	5.30	5.29
CORRECTED LATERAL FORCE	66.60	71.35	76.30	80.95	81.30
MEASURED SLIP ANGLE	10.00	10.00	10.00	10.00	10.00
MEASURED LATERAL FORCE	******	******	******	81.00	80.00
CORRECTED SLIP ANGLE	******	******	******	7.22	7.19
CORRECTED LATERAL FORCE	******	******	******	83.35	84.70

SLIP ANGLE OFFSET = 1.10

27X1.25 SCHWINN PUFF HIGH PRESSURE ROAD RACER (75 PSI)

NORMAL FORCE = 36.4

INCLINATION ANGLE	0.0	6.00	15.00	25.00	35.00
MEASURED SLIP ANGLE	-2.00	-2.00	-2.00	-2.00	-2.00
MEASURED LATERAL FORCE	-14.50	-16.00	-13.00	-16.00	-18.00
CORRECTED SLIP ANGLE	-1.47	-1.44	-1.58	-1.53	-1.50
CORRECTED LATERAL FORCE	-16.00	-16.72	-12.55	-14.25	-14.95
MEASURED SLIP ANGLE	-1.00	-1.00	-1.00	-1.00	-1.00
MEASURED LATERAL FORCE	-10.50	-11.00	-9.00	-11.00	-13.00
CORRECTED SLIP ANGLE	-0.61	-0.62	-0.72	-0.70	-0.68
CORRECTED LATERAL FORCE	-11.80	-11.52	-8.35	-9.05	-9.75
MEASURED SLIP ANGLE	-0.50	-0.50	-0.50	-0.50	-0.50
MEASURED LATERAL FORCE	-8.00	-7.00	-8.00	-8.00	-9.00
CORRECTED SLIP ANGLE	-0.19	-0.25	-0.26	-0.30	-0.31
CORRECTED LATERAL FORCE	-9.20	-7.42	-7.25	-5.95	-5.65
MEASURED SLIP ANGLE	0.0	0.0	0.0	0.0	0.0
MEASURED LATERAL FORCE	-4.00	-4.50	-4.00	-4.00	-6.00
CORRECTED SLIP ANGLE	0.17	0.16	0.10	0.06	0.08
CORRECTED LATERAL FORCE	-5.10	-4.82	-3.15	-1.85	-2.55
MEASURED SLIP ANGLE	0.50	0.50	0.50	0.50	0.50
MEASURED LATERAL FORCE	-1.50	-2.00	0.0	-1.50	1.00
CORRECTED SLIP ANGLE	0.58	0.57	0.47	0.48	0.35
CORRECTED LATERAL FORCE	-2.50	-2.22	0.95	0.75	4.55
MEASURED SLIP ANGLE	1.00	1.00	1.00	1.00	1.00
MEASURED LATERAL FORCE	1.00	2.00	3.00	1.00	4.00
CORRECTED SLIP ANGLE	1.00	0.94	0.87	0.89	0.75
CORRECTED LATERAL FORCE	0.10	1.88	4.05	3.35	7.65
MEASURED SLIP ANGLE	2.00	2.00	2.00	2.00	2.00
MEASURED LATERAL FORCE	9.00	8.00	7.00	8.00	12.00
CORRECTED SLIP ANGLE	1.72	1.73	1.73	1.65	1.47
CORRECTED LATERAL FORCE	8.30	8.08	8.25	10.55	15.85
MEASURED SLIP ANGLE	3.00	3.00	3.00	3.00	3.00
MEASURED LATERAL FORCE	14.00	14.00	14.00	12.00	20.00
CORRECTED SLIP ANGLE	2.55	2.52	2.49	2.51	2.20
CORRECTED LATERAL FORCE	13.50	14.28	15.45	14.75	24.05
MEASURED SLIP ANGLE	4.00	4.00	4.00	4.00	4.00
MEASURED LATERAL FORCE	20.00	19.00	18.00	15.00	22.00
CORRECTED SLIP ANGLE	3.34	3.35	3.35	3.40	3.13
CORRECTED LATERAL FORCE	19.70	19.48	19.65	17.95	26.25
MEASURED SLIP ANGLE	6.00	6.00	6.00	6.00	6.00
MEASURED LATERAL FORCE	29.00	23.00	24.00	19.00	23.00
CORRECTED SLIP ANGLE	5.03	5.20	5.13	5.26	5.08
CORRECTED LATERAL FORCE	29.10	23.88	26.05	22.35	27.65

SLIP ANGLE OFFSET = 0.98

27X1.25 SCHWINN PUFF HIGH PRESSURE ROAD RACER (75 PSI)

NORMAL FORCE = 73.4

INCLINATION ANGLE	0.0	6.00	15.00	25.00	35.00
MEASURED SLIP ANGLE	-2.00	-2.00	-2.00	-2.00	-2.00
MEASURED LATERAL FORCE	-21.00	-20.50	-18.00	-21.00	-18.00
CORRECTED SLIP ANGLE	-1.23	-1.26	-1.37	-1.31	-1.47
CORRECTED LATERAL FORCE	-23.20	-22.28	-18.91	-20.61	-15.96
MEASURED SLIP ANGLE	-1.00	-1.00	-1.00	-1.00	-1.00
MEASURED LATERAL FORCE	-16.00	-16.00	-11.00	-13.00	-11.00
CORRECTED SLIP ANGLE	-0.40	-0.41	-0.61	-0.59	-0.71
CORRECTED LATERAL FORCE	-18.00	-17.58	-11.71	-12.41	-9.76
MEASURED SLIP ANGLE	-0.50	-0.50	-0.50	-0.50	-0.50
MEASURED LATERAL FORCE	-12.00	-10.50	-8.00	-9.00	-4.00
CORRECTED SLIP ANGLE	-0.04	-0.10	-0.21	-0.22	-0.44
CORRECTED LATERAL FORCE	-13.90	-11.98	-8.61	-9.31	-1.66
MEASURED SLIP ANGLE	0.0	0.0	0.0	0.0	0.0
MEASURED LATERAL FORCE	-8.00	-5.50	-3.50	-3.50	-2.00
CORRECTED SLIP ANGLE	0.33	0.23	0.13	0.09	-0.01
CORRECTED LATERAL FORCE	-9.80	-6.88	-4.01	-2.71	0.44
MEASURED SLIP ANGLE	0.50	0.50	0.50	0.50	0.50
MEASURED LATERAL FORCE	-2.00	0.0	1.50	1.00	7.00
CORRECTED SLIP ANGLE	0.62	0.54	0.46	0.44	0.18
CORRECTED LATERAL FORCE	-3.70	-1.28	1.09	1.89	9.54
MEASURED SLIP ANGLE	1.00	1.00	1.00	1.00	1.00
MEASURED LATERAL FORCE	2.00	6.00	7.00	5.50	12.00
CORRECTED SLIP ANGLE	0.99	0.84	0.78	0.78	0.51
CORRECTED LATERAL FORCE	0.40	4.82	6.69	6.49	14.64
MEASURED SLIP ANGLE	2.00	2.00	2.00	2.00	2.00
MEASURED LATERAL FORCE	10.00	13.00	14.00	15.00	22.00
CORRECTED SLIP ANGLE	1.71	1.60	1.54	1.46	1.17
CORRECTED LATERAL FORCE	8.60	12.02	13.89	16.19	24.84
MEASURED SLIP ANGLE	3.00	3.00	3.00	3.00	3.00
MEASURED LATERAL FORCE	22.00	21.00	22.00	25.50	34.00
CORRECTED SLIP ANGLE	2.31	2.33	2.26	2.10	1.77
CORRECTED LATERAL FORCE	20.80	20.22	22.09	26.89	37.04
MEASURED SLIP ANGLE	4.00	4.00	4.00	4.00	4.00
MEASURED LATERAL FORCE	30.00	29.50	29.00	30.00	41.50
CORRECTED SLIP ANGLE	3.03	3.04	3.02	2.95	2.51
CORRECTED LATERAL FORCE	29.00	28.92	29.29	31.59	44.74
MEASURED SLIP ANGLE	6.00	6.00	6.00	6.00	6.00
MEASURED LATERAL FORCE	44.00	41.00	41.00	39.00	47.00
CORRECTED SLIP ANGLE	4.55	4.64	4.61	4.63	4.31
CORRECTED LATERAL FORCE	43.40	40.82	41.69	40.99	50.64

SLIP ANGLE OFFSET = 0.95

27X1.25 SCHWINN PUFF HIGH PRESSURE ROAD RACER (75 PSI)

NORMAL FORCE =105.5

INCLINATION ANGLE	0.0	6.00	15.00	25.00	35.00
MEASURED SLIP ANGLE	-2.00	-2.00	-2.00	-2.00	-2.00
MEASURED LATERAL FORCE	-25.00	-22.50	-21.00	-23.00	-15.00
CORRECTED SLIP ANGLE	-1.07	-1.16	-1.22	-1.20	-1.53
CORRECTED LATERAL FORCE	-27.90	-25.33	-23.26	-23.96	-13.96
MEASURED SLIP ANGLE	-1.00	-1.00	-1.00	-1.00	-1.00
MEASURED LATERAL FORCE	-19.00	-16.00	-12.50	-13.00	-5.00
CORRECTED SLIP ANGLE	-0.28	-0.38	-0.51	-0.54	-0.87
CORRECTED LATERAL FORCE	-21.70	-18.63	-14.56	-13.76	-3.76
MEASURED SLIP ANGLE	-0.50	-0.50	-0.50	-0.50	-0.50
MEASURED LATERAL FORCE	-14.50	-11.00	-9.00	-8.50	3.00
CORRECTED SLIP ANGLE	0.07	-0.05	-0.13	-0.10	-0.64
CORRECTED LATERAL FORCE	-17.10	-13.53	-10.96	-9.16	4.34
MEASURED SLIP ANGLE	0.0	0.0	0.0	0.0	0.0
MEASURED LATERAL FORCE	-9.00	-7.00	-3.00	-1.00	6.00
CORRECTED SLIP ANGLE	0.38	0.31	0.16	0.05	-0.25
CORRECTED LATERAL FORCE	-11.50	-9.43	-4.86	-1.56	7.44
MEASURED SLIP ANGLE	0.50	0.50	0.50	0.50	0.50
MEASURED LATERAL FORCE	-3.00	-4.00	3.00	6.00	12.00
CORRECTED SLIP ANGLE	0.68	0.71	0.46	0.32	0.05
CORRECTED LATERAL FORCE	-5.40	-6.33	1.24	5.54	13.54
MEASURED SLIP ANGLE	1.00	1.00	1.00	1.00	1.00
MEASURED LATERAL FORCE	3.00	6.50	10.50	9.00	22.00
CORRECTED SLIP ANGLE	0.98	0.86	0.71	0.71	0.21
CORRECTED LATERAL FORCE	0.70	4.27	8.84	8.64	23.64
MEASURED SLIP ANGLE	2.00	2.00	2.00	2.00	2.00
MEASURED LATERAL FORCE	13.00	15.50	17.00	20.50	30.00
CORRECTED SLIP ANGLE	1.64	1.55	1.48	1.32	0.94
CORRECTED LATERAL FORCE	10.90	13.47	15.54	20.34	31.84
MEASURED SLIP ANGLE	3.00	3.00	3.00	3.00	3.00
MEASURED LATERAL FORCE	28.00	26.00	28.00	32.50	45.00
CORRECTED SLIP ANGLE	2.13	2.19	2.11	1.92	1.43
CORRECTED LATERAL FORCE	26.10	24.17	26.74	32.54	47.04
MEASURED SLIP ANGLE	4.00	4.00	4.00	4.00	4.00
MEASURED LATERAL FORCE	38.00	31.00	37.00	43.00	53.00
CORRECTED SLIP ANGLE	2.79	3.02	2.80	2.56	2.16
CORRECTED LATERAL FORCE	36.30	29.37	35.94	43.24	55.24
MEASURED SLIP ANGLE	6.00	6.00	6.00	6.00	6.00
MEASURED LATERAL FORCE	48.50	52.00	54.00	56.00	69.00
CORRECTED SLIP ANGLE	4.43	4.31	4.22	4.11	3.61
CORRECTED LATERAL FORCE	47.20	50.77	53.34	56.64	71.64

SLIP ANGLE OFFSET = 0.94